



Universitat Autònoma de Barcelona

**Study of the transport
mechanism of the
melibiose permease from
*Escherichia coli***

Li-Ying Wang



Universitat Autònoma de Barcelona

**Study of the transport
mechanism of the
melibiose permease from
*Escherichia coli***

**Memòria presentada per na Li-Ying Wang
Per optar al grau de Doctor.**

**Els treballs presentats han estat dirigits pels
Drs. Esteve Padrós i Morell i Josep Bartomeu Cladera Cerdà,
i realitzats en la Unitat de Biofísica
del Departament de Bioquímica i de Biologia
Molecular i el Centre d'Estudis en Biofísica (CEB)
de la Universitat Autònoma de Barcelona**

Vist i plau dels directors de la tesi:

Dr. Esteve Padrós i Morell

Dr. Josep Bartomeu Cladera Cerdà

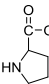
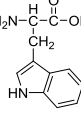
Table of contents

| | |
|---|----|
| 1 INTRODUCTION | 1 |
| 1.1 Membrane proteins are important for life | 1 |
| 1.2 The cell membrane..... | 1 |
| 1.3 Membrane transport proteins | 3 |
| 1.4 Major facilitator superfamily | 4 |
| 1.5 Melibiose permease | 7 |
| 1.5.1 Topological Models of MelB _{EC} | 9 |
| 1.5.2 2D and 3D structure of melibiose permease | 10 |
| 1.6 Transport mechanism | 11 |
| 1.6.1 General mechanisms of sugar transport..... | 13 |
| 1.6.2 Hypothesis for the transport mechanisms of melibiose permease | 16 |
| 1.7 Crystallization and structure determination | 18 |
| 1.8 Biophysical studies of MelB..... | 20 |
| 1.8.1 Förster Resonance Energy Transfer (FRET)..... | 21 |
| 1.8.2 Fourier Transform Infrared (FTIR) spectroscopy..... | 22 |
| 1.9 Molecular dynamics simulations | 25 |
| 2 OBJECTIVES | 35 |
| 3 MATERIALS AND METHODS | 37 |
| 3.1 Materials | 37 |
| 3.1.1 Reagents..... | 37 |
| 3.1.2 Kits..... | 38 |
| 3.1.3 Instruments..... | 38 |
| 3.1.4 Buffers..... | 39 |
| 3.2 Methods..... | 42 |
| 3.2.1 Obtaining the mutant proteins and the Cless protein | 42 |
| 3.2.2 Preparation of vesicles | 52 |

| | |
|---|-----|
| 3.2.3 Fourier transform infrared spectroscopy (FTIR) | 54 |
| 3.2.4 Förster resonance energy transfer spectroscopy (FRET) | 65 |
| 3.2.5 X-ray crystallography | 67 |
| 3.2.6 Molecular dynamics simulation | 68 |
| 4 RESULTS AND DISCUSSION | 75 |
| 4.1 Analysis of the conserved residues in loop 7-8/end of helix VII | 75 |
| 4.2 Cysteine-scanning mutagenesis of loop 7-8/end of helix VII | 76 |
| 4.3 Fluorescence results | 78 |
| 4.3.1 FRET in proteoliposomes | 78 |
| 4.3.2 FRET of Inside Out (ISO) vesicles | 83 |
| 4.3.3 Conclusions from the fluorescence results | 86 |
| 4.4 The infrared difference spectra | 87 |
| 4.4.1 General features of the infrared difference spectra | 87 |
| 4.4.2 Conserved amino acids in loop 7-8 | 88 |
| 4.4.3 Charged amino acids in loop 7-8: D264C and D266C | 94 |
| 4.4.4 The unconserved aromatic amino acid in loop 7-8: F268C | 99 |
| 4.5 Molecular dynamics | 105 |
| 4.5.1 Minimization and Equilibration | 105 |
| 4.5.2 Molecular Dynamics of wild type MelB _{EC} | 106 |
| 4.5.3 Molecular Dynamics of MelB mutated at conserved amino acids in loop 7-8/end of helix VII | 110 |
| 4.5.4 Conclusions from the molecular dynamics results | 112 |
| 4.6 Crystallization studies of MelB R149C mutant | 114 |
| 5 GENERAL DISCUSSION | 117 |
| APPENDIX | 129 |

ABBREVIATIONS

Amino Acids

| | | | | | | | |
|-------|--|-------|--|-------|---|-------|---|
| A Ala | $\begin{array}{c} \text{H} \\ \\ \text{H}_2\text{N}-\text{C}-\text{C}-\text{OH} \\ \\ \text{CH}_3 \end{array}$ | G Gly | $\begin{array}{c} \text{H} \\ \\ \text{H}_2\text{N}-\text{C}-\text{C}-\text{OH} \\ \\ \text{H} \end{array}$ | M Met | $\begin{array}{c} \text{H} \\ \\ \text{H}_2\text{N}-\text{C}-\text{C}-\text{OH} \\ \\ \text{CH}_2 \\ \\ \text{CH}_2 \\ \\ \text{S} \\ \\ \text{CH}_3 \end{array}$ | S Ser | $\begin{array}{c} \text{H} \\ \\ \text{H}_2\text{N}-\text{C}-\text{C}-\text{OH} \\ \\ \text{CH}_2 \\ \\ \text{OH} \end{array}$ |
| C Cys | $\begin{array}{c} \text{H} \\ \\ \text{H}_2\text{N}-\text{C}-\text{C}-\text{OH} \\ \\ \text{CH}_2 \\ \\ \text{SH} \end{array}$ | H His | $\begin{array}{c} \text{H} \\ \\ \text{H}_2\text{N}-\text{C}-\text{C}-\text{OH} \\ \\ \text{CH}_2 \\ \\ \text{N} \\ \\ \text{NH} \end{array}$ | N Asn | $\begin{array}{c} \text{H} \\ \\ \text{H}_2\text{N}-\text{C}-\text{C}-\text{OH} \\ \\ \text{CH}_2 \\ \\ \text{C}=\text{O} \\ \\ \text{NH}_2 \end{array}$ | T Thr | $\begin{array}{c} \text{H} \\ \\ \text{H}_2\text{N}-\text{C}-\text{C}-\text{OH} \\ \\ \text{HC}-\text{OH} \\ \\ \text{CH}_3 \end{array}$ |
| D Asp | $\begin{array}{c} \text{H} \\ \\ \text{H}_2\text{N}-\text{C}-\text{C}-\text{OH} \\ \\ \text{CH}_2 \\ \\ \text{C}=\text{O} \\ \\ \text{OH} \end{array}$ | I Ile | $\begin{array}{c} \text{H} \\ \\ \text{H}_2\text{N}-\text{C}-\text{C}-\text{OH} \\ \\ \text{HC}-\text{CH}_3 \\ \\ \text{CH}_2 \\ \\ \text{CH}_3 \end{array}$ | P Pro |  | V Val | $\begin{array}{c} \text{H} \\ \\ \text{H}_2\text{N}-\text{C}-\text{C}-\text{OH} \\ \\ \text{HC}-\text{CH}_3 \\ \\ \text{CH}_3 \end{array}$ |
| E Glu | $\begin{array}{c} \text{H} \\ \\ \text{H}_2\text{N}-\text{C}-\text{C}-\text{OH} \\ \\ \text{CH}_2 \\ \\ \text{CH}_2 \\ \\ \text{C}=\text{O} \\ \\ \text{OH} \end{array}$ | K Lys | $\begin{array}{c} \text{H} \\ \\ \text{H}_2\text{N}-\text{C}-\text{C}-\text{OH} \\ \\ \text{CH}_2 \\ \\ \text{CH}_2 \\ \\ \text{CH}_2 \\ \\ \text{CH}_2 \\ \\ \text{NH}_2 \end{array}$ | Q Gln | $\begin{array}{c} \text{H} \\ \\ \text{H}_2\text{N}-\text{C}-\text{C}-\text{OH} \\ \\ \text{CH}_2 \\ \\ \text{CH}_2 \\ \\ \text{C}=\text{O} \\ \\ \text{NH}_2 \end{array}$ | W Trp |  |
| F Phe | $\begin{array}{c} \text{H} \\ \\ \text{H}_2\text{N}-\text{C}-\text{C}-\text{OH} \\ \\ \text{CH}_2 \\ \\ \text{C}_6\text{H}_5 \end{array}$ | L Leu | $\begin{array}{c} \text{H} \\ \\ \text{H}_2\text{N}-\text{C}-\text{C}-\text{OH} \\ \\ \text{CH}_2 \\ \\ \text{HC}-\text{CH}_3 \\ \\ \text{CH}_3 \end{array}$ | R Arg | $\begin{array}{c} \text{H} \\ \\ \text{H}_2\text{N}-\text{C}-\text{C}-\text{OH} \\ \\ \text{CH}_2 \\ \\ \text{CH}_2 \\ \\ \text{CH}_2 \\ \\ \text{NH} \\ \\ \text{C}=\text{NH} \\ \\ \text{NH}_2 \end{array}$ | Y Tyr | $\begin{array}{c} \text{H} \\ \\ \text{H}_2\text{N}-\text{C}-\text{C}-\text{OH} \\ \\ \text{CH}_2 \\ \\ \text{C}_6\text{H}_4 \\ \\ \text{OH} \end{array}$ |

General abbreviations

| | |
|--------------------------------|---|
| λ_{em} | emission wavelength |
| λ_{ex} | excitation wavelength |
| ABC | ATP-binding cassette superfamily |
| Abs | absorbance |
| AdiC | L-arginine/agmatine antiporter from <i>E. coli</i> |
| AEBSF | 4-(2-Aminoethyl) benzenesulfonyl fluoride hydrochloride |
| APS | ammonium persulfate |
| ATR-FTIR | attenuated total reflection-Fourier transform infrared |
| BSA | bovine serum albumin |
| C ₁₂ E ₈ | dodecyl octaethylene glycol ether |
| C ₁₂ E ₉ | dodecyl nonaethylene glycol ether |
| CMC | The critical micelle concentration |
| Cymal-5 | 5-cyclohexyl-1-pentyl- β -D-maltoside |

| | |
|--------------------|---|
| Cymal-6 | 6-cyclohexyl-1-hexyl- β -D-maltoside |
| Cless | the mutant protein without cysteines |
| DDM | n-Dodecyl β -D-maltoside |
| DM | Decyl β -D-maltopyranoside |
| DMSO | dimethyl sulfoxide |
| D ² G | dns ² -S-Gal,2'-(N-dansyl)-aminoethyl-1-thio-D-galactopyranoside |
| DTT | 1, 4-dithio-threitol |
| EDTA | ethylenediaminetetraacetic acid |
| FRET | Förster resonance energy transfer |
| GPCRs | G protein coupled receptors |
| GPH | glycoside-pentoside-hexuronide:cationsymporter family |
| M | mg/mL |
| IMV | inverted membrane vesicles |
| IR _{diff} | Infrared difference |
| ISO | Inside-out |
| KPi | potassium phosphate buffer |
| lactose | 4-O- β -galactopyranosyl-D-glucose |
| LacY | lactose permease of <i>Escherichia coli</i> |
| LAPAO | (3-lauryl-starch)-N, N'-(dimethylamino) propylamine oxide |
| LB | Luria Broth |
| Mel | melibiose; 6-O- α -D-galactopyranosyl-D-glucose |
| MelB | melibiose permease from <i>Escherichia coli</i> |
| MelB _{EC} | melibiose permease from <i>Escherichia coli</i> |
| MelB _{KP} | melibiose permease from <i>Klebsiella pneumoniae</i> |
| MelB _{SY} | melibiose permease from <i>Salmonella typhimurium</i> |
| MDS | Molecular dynamics simulation |
| MFS | major facilitator superfamily |
| MW | molecular weight |
| NEM | N-ethylmaleimide |
| OG | n-octyl- β -D-glucoside |
| PCR | polymerase chain reaction |
| PDB | Protein Data Bank |
| PEG | polyethylene glycol |

| | |
|----------------|---|
| PL | Proteoliposomes |
| R ² | the correlation coefficient |
| SDS-PAGE | sodium dodecyl sulfate polyacrylamide gel electrophoresis |
| TCDB | transporter classification database |
| TM | transmembrane |
| UDM | Undecyl- β -d-maltoside |
| α -NPG | p-nitrophenyl α -D-galactopiranoside |

1 INTRODUCTION

1.1 Membrane proteins are important for life

About 60% of approved drug targets are membrane proteins, down to ~40% when experimental targets are added.¹ As an example, we can focus on diabetes. As we all know, diabetes is a group of metabolic diseases causing high levels of blood sugar. Based on the information from the international diabetes federation, we know that the number of people with diabetes may increase to 592 million by 2035. Diabetes caused 4.9 million deaths in 2014, and that means every 7 seconds a person with diabetes dies.² From the WHO web site we know that it was one of the 10 leading causes of death in the world in 2012, and it occupied 2.7 % of all deaths in the world in that year. [<http://www.who.int/mediacentre/factsheets/fs310/en/>] So it is very important to find out the mechanism by which the sugar passes the cell membranes and then explore the drug target.

1.2 The cell membrane

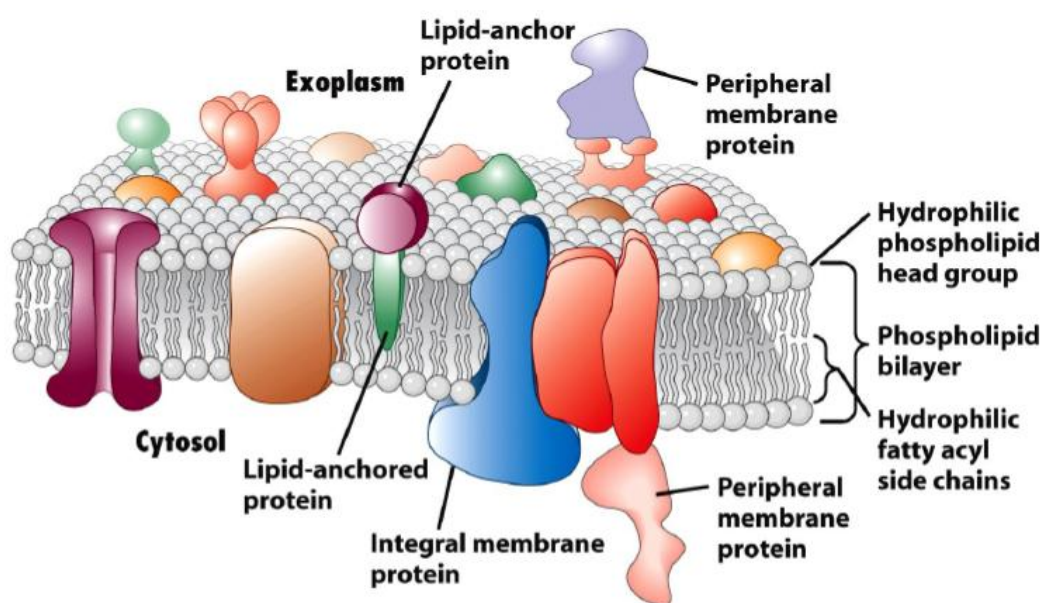


Figure 1.1 Fluid mosaic model of biomembranes.³

The membrane of the cell is very important for keeping the cell structure and function. The basic architecture of the biomembrane is a phospholipid bilayer which contains several proteins. From the model of the biomembrane in Figure 1.1, we can infer that most of the functions of the membrane are based on the membrane proteins.

In all cells, the membrane forms a permeability barrier that separates the cytoplasm from the exterior environment. Since every living cell must acquire raw materials for biosynthesis and for energy production from its surroundings, and must release the byproducts of metabolism to its environment, the compounds need to cross the membrane.⁴ There are several ways (or mechanisms) for the transport of substances between the periplasmic side and cytoplasmic side of the membrane (Figure 1.2): simple diffusion through the bilayer or channels driven by a concentration gradient; facilitated diffusion which move the substrates from high to low concentration through a binding process with membrane protein carriers (i.e. membrane protein transporters); active transport by means of a protein transporter with a specific binding site that undergoes a change in affinity driven by energy released by an exergonic process, such as ATP hydrolysis (primary active transport), ions moving down its concentration gradient (secondary active transport), usually against concentration gradient.⁵ The study of the genome-wide sequence data from eubacterial, archaean, and eukaryotic organisms shows that 20~30% of the genes encode membrane proteins.⁶ Since biological membranes are in general highly impermeable to molecules, for a compound such a sugar to enter the cell, it needs the help of the membrane protein. Integral membrane proteins, lipid-anchored membrane proteins and peripheral membrane proteins are the three categories of membrane proteins.⁷

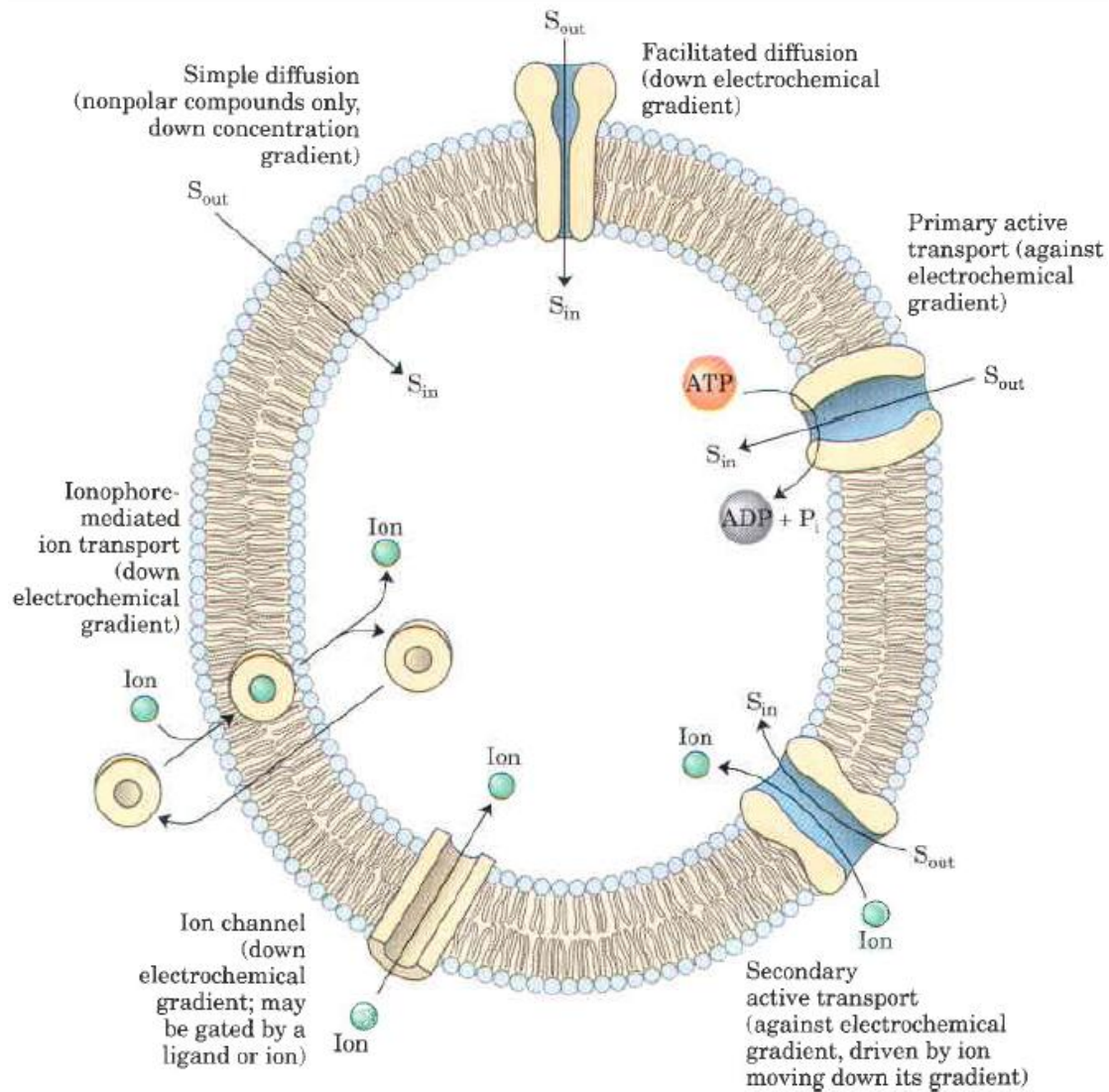


Figure 1.2 Summary of transport types.⁴

1.3 Membrane transport proteins

Membrane Transport Proteins are classified in three classes: ATP-powered pumps, which transport ions and various small molecules against their concentration gradients by using ATP; channels, which transport water, specific ions, or hydrophilic small molecules across membranes down their electrochemical gradient or their concentration very quickly; and finally the transporters, which move a wide variety of ions and molecules across cell membranes very slowly. There are 3 type of transporters (Figure 1.3): uniporters, which transport a single type of molecule down its concentration gradient; symporters, which catalyze the movement of one molecule

against its concentration, driven by the movement of one or more ions down an electrochemical gradient in the same directions; and antiporters, which catalyze the movement of one molecule against its concentration, driven by the movement of one or more ions down an electrochemical gradient in the opposite directions.⁷

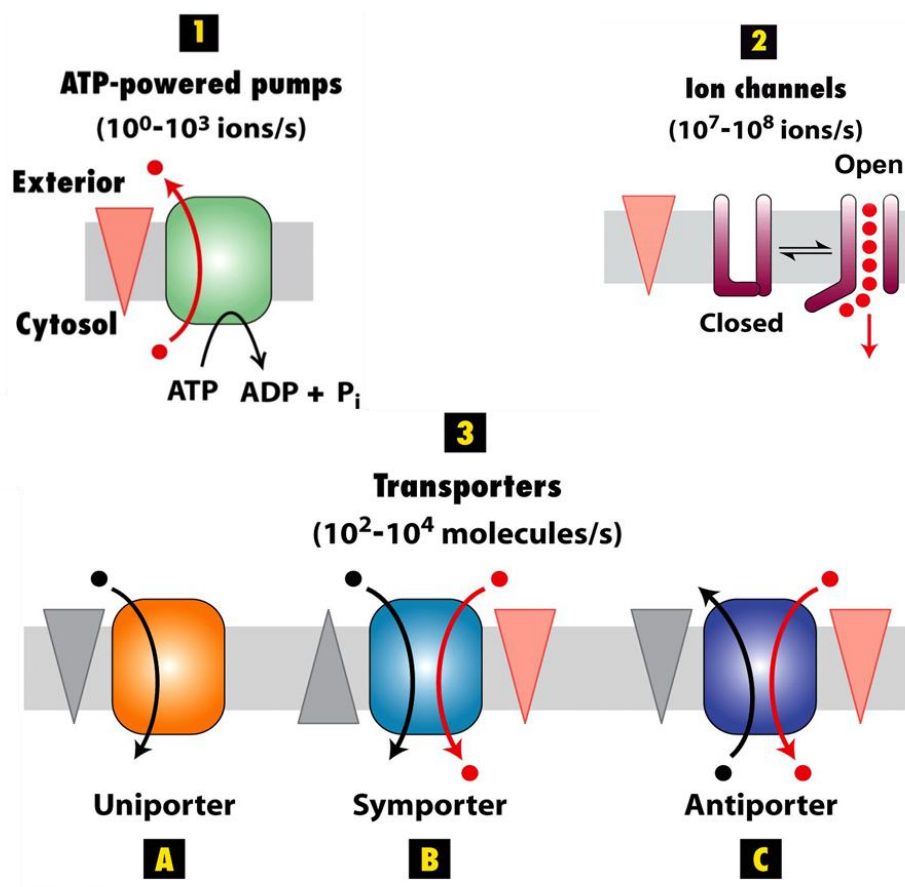


Figure 1.3 Membrane transport proteins. Gradients are indicated by triangles with the tip pointing toward lower concentration, electrical potential, or both. (1-3) The three major types of transport proteins. Red circles represent specific ions (or water); black circles represent specific small molecules or ions driven by movement of one or more ions down an electrochemical gradient (red circles). According to ⁷

1.4 Major facilitator superfamily

The transporter classification database⁸ includes all 56 superfamilies of different membrane protein transporters. The major facilitator superfamily is the largest known superfamily of secondary carriers. In 2012, this superfamily had 74 subfamilies of

diverse characteristics. The table below shows the main sub family of the MFS family.⁹

Table 1.1 The members of the MFS family (<http://www.tcdb.org/superfamily.php>)

| TC N. | MFS family |
|---------|--|
| 2.A.1 | The Major Facilitator Superfamily (MFS) |
| 2.A.2 | The Glycoside-Pentoside-Hexuronide (GPH):Cation Symporter Family |
| 2.A.12 | The ATP:ADP Antiporter (AAA) Family |
| 2.A.17 | The Proton-dependent Oligopeptide Transporter (POT/PTR) Family |
| 2.A.48 | The Reduced Folate Carrier (RFC) Family |
| 2.A.60 | The Organo Anion Transporter (OAT) Family |
| 2.A.71 | The Folate-Biopterin Transporter (FBT) Family |
| 9.B.111 | The 6TMS Lysyl tRNA synthetase (LysS) Family |

The most frequent topological type of these MFS permeases is that almost all proteins share an architecture of 12 transmembrane segments. They arose from a single 3-transmembrane segment structure that duplicated to give a 6-TMS unit that in its turn duplicated to a 12-TMS protein (Figure 1.4).¹⁰⁻¹²

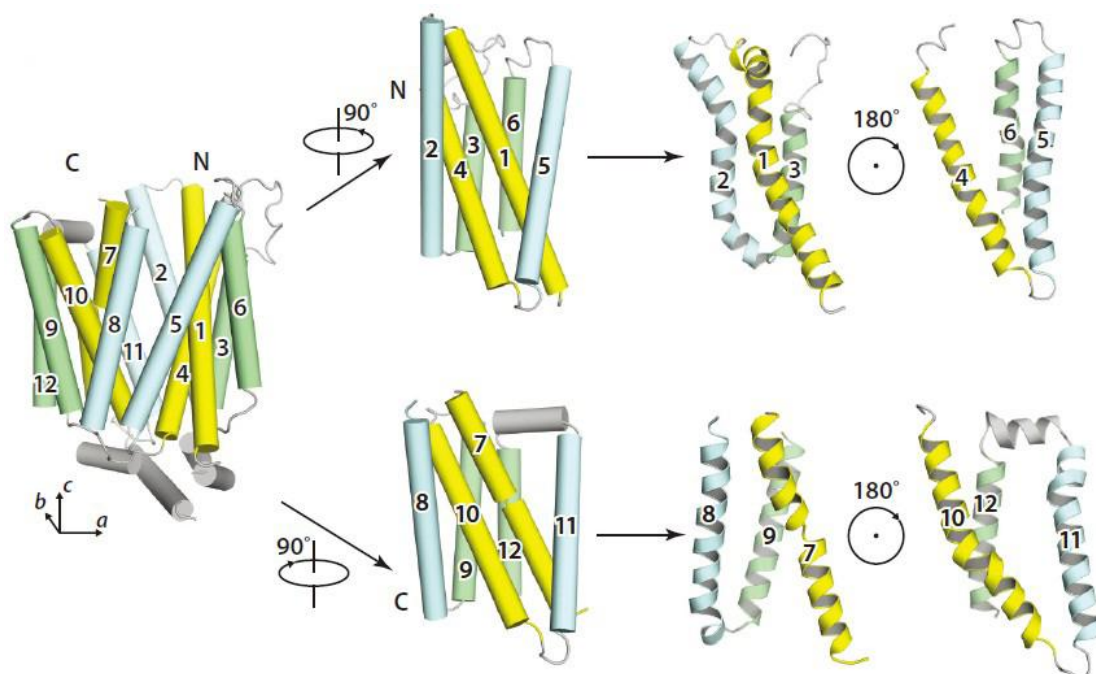


Figure 1.4 A canonical MFS fold. The 12-TM structure in an MFS fold contains two discretely folded domains, the N and C domains, which are related by an approximate 180° rotation around axis c (defined at the bottom of the panel). Each domain consists of two inverted

3-TM repeats. The corresponding helices in each of these units have the same color.¹²

Table 1.2 MFS proteins of known structure

| Protein | Function | Organism | PDB code | Resolution limit (Å) | Year of publication |
|--------------------|---------------------------------------|-----------------------------------|------------------------------------|----------------------|---------------------|
| LacY | Lactose: proton symporter | <i>Escherichia coli</i> | 1PV6, 1PV7, 2CFP, 2CFQ, 2V8N, 2Y5Y | 2.95 | 2003 |
| GlpT | Glycerol-3-phosphate: Pi antiporter | <i>Escherichia coli</i> | 1PW4 | 3.3 | 2003 |
| EmrD | Multidrug transporter | <i>Escherichia coli</i> | 2GFP | 3.5 | 2006 |
| FucP | L-Fucose: proton symporter | <i>Escherichia coli</i> | 3O7Q, 3O7P | 3.1 | 2009 |
| PepT _{so} | Peptide: proton symporter | <i>Shewanella oneidensis</i> | 2XUT | 3.6 | 2011 |
| PepT _{st} | Peptide: proton symporter | <i>Streptococcus thermophilus</i> | 4APS | 3.3 | 2012 |
| XylE | D-Xylose: proton symporter | <i>Escherichia coli</i> | 4GBY, 4GBZ, 4GC0 | 2.6 | 2012 |
| XylE | D-Xylose: proton symporter | <i>Escherichia coli</i> | 4JA3, 4JA4 | 3.8 | 2013 |
| GlcP | Glucose: H ⁺ symporter | <i>Staphylococcus epidermidis</i> | 4LDS | 3.2 | 2013 |
| PepT _{gk} | Peptide: proton symporter | <i>Geobacillus kaustophilus</i> | 4IKV, 4IKW, 4IKX, 4IKY, 4IKZ | 1.9 | 2013 |
| PiPT | Phosphate: proton symporter | <i>Piriformospora indica</i> | 4J05 | 2.9 | 2013 |
| NarU | Nitrate: nitrite antiporter | <i>Escherichia coli</i> | 4IU9, 4IU8 | 3.01 | 2013 |
| NarK | Nitrate: nitrite antiporter | <i>Escherichia coli</i> | 4JR9, 4JRE | 2.6 | 2013 |
| YajR | Drug efflux transporter | <i>Escherichia coli</i> | 3WDO | 3.15 | 2013 |
| LacY | Lactose: proton symporter | <i>Escherichia coli</i> | 4OAA | 3.5 | 2014 |
| MelB | Na ⁺ : melibiose symporter | <i>Salmonella typhimurium</i> | 4M64 | 3.35 | 2014 |
| XylE | D-Xylose: proton symporter | <i>Escherichia coli</i> | 4QIQ | 3.51 | 2014 |

| | | | | | |
|--------------------|-----------------------------|------------------------------|------------------|------|------|
| PepT _{so} | Peptide: proton symporter | <i>Shewanella oneidensis</i> | 4TPH, 4TPG, 4TPJ | 3.15 | 2014 |
| YbgH | Peptide: proton symporter | <i>Escherichia coli</i> | 4Q65 | 3.4 | 2014 |
| NRT _{1.1} | Nitrate: proton symporter | <i>Arabidopsis thaliana</i> | 4CL4(5A2N), 4CL5 | 3.7 | 2014 |
| NRT _{1.1} | Nitrate: proton symporter | <i>Arabidopsis thaliana</i> | 4OH3 | 3.25 | 2014 |
| GLUT1 | glucose transporter | <i>Homo sapiens</i> | 4PYP | 3.17 | 2014 |
| PepT _{so} | Peptide: proton symporter | <i>Shewanella oneidensis</i> | 4UVM | 3 | 2015 |
| PepT _{so} | Peptide: proton symporter | <i>Shewanella oneidensis</i> | 4XNJ, 4XNI | 2.3 | 2015 |
| NarK | Nitrate: nitrite antiporter | <i>Escherichia coli</i> | 4U4V, 4U4T, 4U4W | 2.35 | 2015 |

1.5 Melibiose permease

Melibiose permease is one of the GPH family members (<http://www.tcdb.org/search/result.php?tc=2.A.2.7>) in the TCDB list whose 3D structure has been described¹³.

The generalized transport reaction catalyzed by the GPH: cation symporter family is:

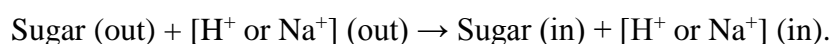


Table 1.3 Cation selectivity of members of the GPH family¹⁴

| Substrate | α -galactosides | β -galactosides | | Monosaccharides | α/β -glucuronides |
|--------------------|--|---|-----------------------------------|---|------------------------------|
| | melibiose | TMG | lactose | D-galactose | |
| MelB _{EC} | H ⁺ , Na ⁺ , Li ⁺ | Na ⁺ , Li ⁺ , (H ⁺) | Na ⁺ , Li ⁺ | H ⁺ , Na ⁺ , (Li ⁺) | ND |
| MelB _{SY} | Na ⁺ , Li ⁺ | Na ⁺ , Li ⁺ | ND | ND | ND |
| MelB _{KP} | H ⁺ | H ⁺ , Li ⁺ | Li ⁺ | ND | ND |
| LacS _{ST} | H ⁺ | H ⁺ | H ⁺ | H ⁺ | ND |
| GusB _{EC} | NT | NT | NT | NT | H ⁺ |

MelB, 6-*O*- α -galactopyranosyl-*D*-glucose; TMG, methyl- β -*D*-thiogalactopyranoside; lactose, 4-*O*- β -galactopyranosyl-*D*-glucose; ND, not determined; NT, not transported. Cations between brackets mean that the activation by them is very poor. MelB_{EC}, melibiose permease *Escherichia coli*; MelB_{SY}, melibiose permease of *Salmonella typhimurium*; MelB_{KP}, melibiose permease from *Klebsiella pneumoniae*; LacS_{ST}, lactose permease of *Streptococcus thermophilus*; GusB_{EC}, glucuronide transporter of *Escherichia coli*.

The GPH protein couples the uphill transport of the sugar towards the cell interior with the downhill electrochemical ion gradient of Na^+ , Li^+ or H^+ . The cation selectivity of the members of GPH family is listed in Table 1.3.

Table 1.4 Cation specificity for sugar substrates of MelB_{EC}¹⁶

| Sugar substrate | cation specificity | Structure | |
|------------------------|---------------------------------------|------------------------------|--|
| β -galactosides | lactose | Na^+ | |
| | L-arabinose- β -D-galactoside | Na^+ | |
| | D-fructose- β -D-galactoside | Na^+ | |
| | o-nitrophenyl- β -D-galactoside | Na^+ | |
| | p-nitrophenyl- β -D-galactoside | Na^+ | |
| α -galactosides | raffinose | H^+ , Na^+ | |
| | melibiose | H^+ , Na^+ | |
| | p-nitrophenyl- α -galactoside | H^+ , Na^+ | |
| monosaccharides | D-galactose | H^+ , Na^+ | |
| | D-fucose | Na^+ | |
| | L-arabinose | Na^+ | |
| | D-galactosamine | Na^+ | |

The MelB_{EC} transporter can use H⁺, Na⁺ (Table 1.4) or Li⁺ to transport, while other transporters show different cation specificity for sugar uptake.^{15, 16}

1.5.1 Topological Models of MelB_{EC}

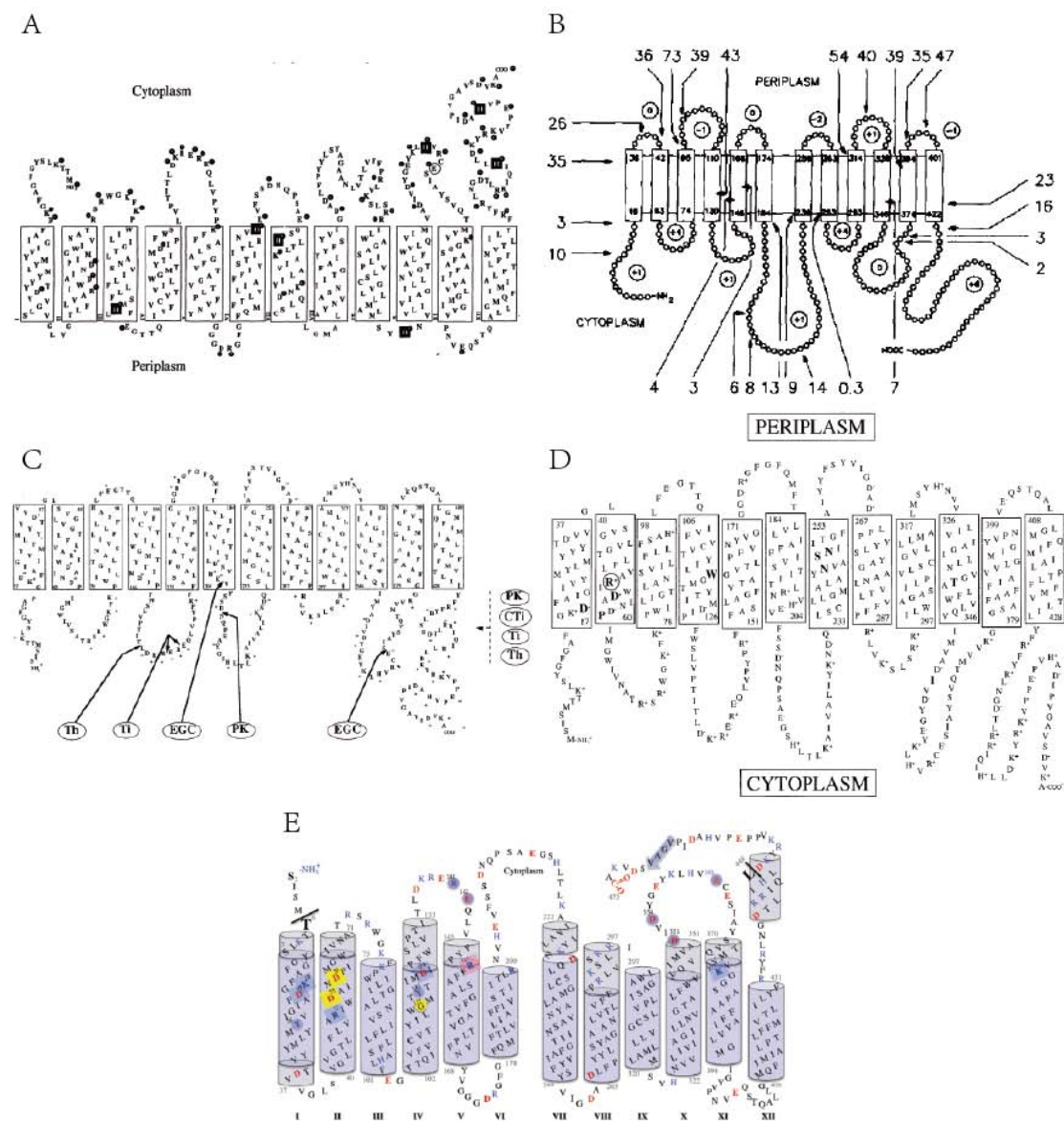


Figure 1.5 Some topological structure models of the melibiose permease. A in 1990²⁰; B in 1992²¹; C in 1996-7^{22, 23}; D in 1999²⁴; E in 2009²⁵.

The melibiose carrier was first found out in *Escherichia coli*.¹⁷ Later on, it was

found in *Salmonella typhimurium* cells.¹⁸ This MelB_{ST} was able to accumulate methyl 1-thio- β -D-galactopyranoside (TMG) against a concentration gradient.¹⁹ In the following years, people were trying to find out the structure of the MelB protein. The first MelB topology model was established in 1990.²⁰ Two years later, Botfield developed a topology model of the melibiose carrier from both hydropathy analysis and alkaline phosphatase fusion data.²¹ Pourcher *et al* and Gwizdek *et al* revised this model with assumptions based again on alkaline phosphatase activity and protease digestion respectively.^{22, 23} After two more years the old topology model was adapted²⁴ and following the development of computer science, a 3D structure model was built in 2009.²⁵

1.5.2 2D and 3D structure of melibiose permease

Before the resolution of the crystal structure using X-rays, electron crystallography was used to examine the structure²⁶. Despite the relatively low resolution (8 Å), the MelB monomer had a size of $\sim 49\text{Å} \times 37\text{Å}$ and could host the 12 predicted transmembrane α -helices in the projection map from 2D crystals (Figure 1.6A). After three years, a three-dimensional structure of MelB at 10Å resolution in the membrane plane with cryo-electron microscopy from two-dimensional crystals showed a heart-shaped molecule composed of two domains with a large central cavity between them (Figure 1.6B).²⁷ A breakthrough was finally achieved in 2014, with the first crystal structure of MelB of *Salmonella typhimurium* at a resolution of 3.35 Å.¹³ The four molecules in each asymmetric unit exhibit two conformations, the outward partially occluded state conformation and the outward inactive state conformation (Figure 1.6C). Remarkably, residues at positions Asp-55/Asp-59/Asp-124 and Tyr-120/Thr-121/Thr-373 form a trigonal bipyramid geometry, as a potential cation binding site. Notably, replacing any of the residues at position 55, 59, 124, or 121 with cysteine led to altered cation selectivity^{13, 28, 29}, backing the concept of the geometry described above as a cation binding site^{13, 29}.

The structures of MelB_{ST} provide a way for understanding the coupling and alternating-access mechanism of the MelB_{EC} ion symporter.

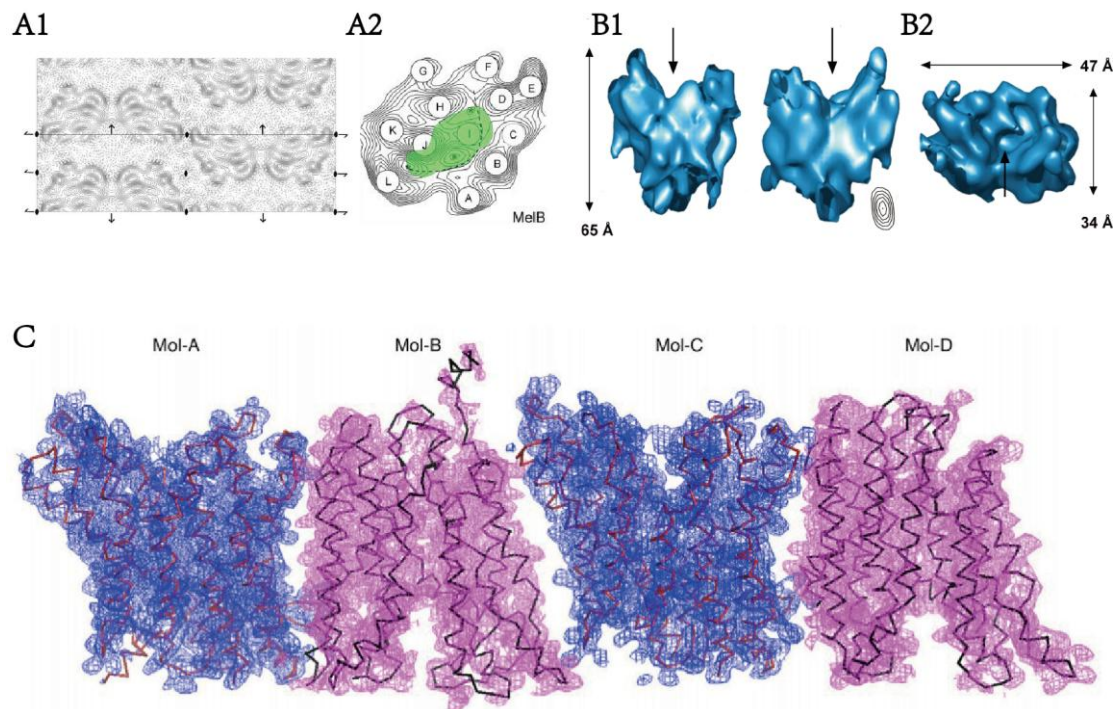


Figure 1.6 A) 2D projection map of MelB_{EC};²⁶ B) 3D cryo-EM images of MelB_{EC};²⁷ C) The 2Fo-Fc maps of four molecules of MelB_{ST}.¹³

1.6 Transport mechanism

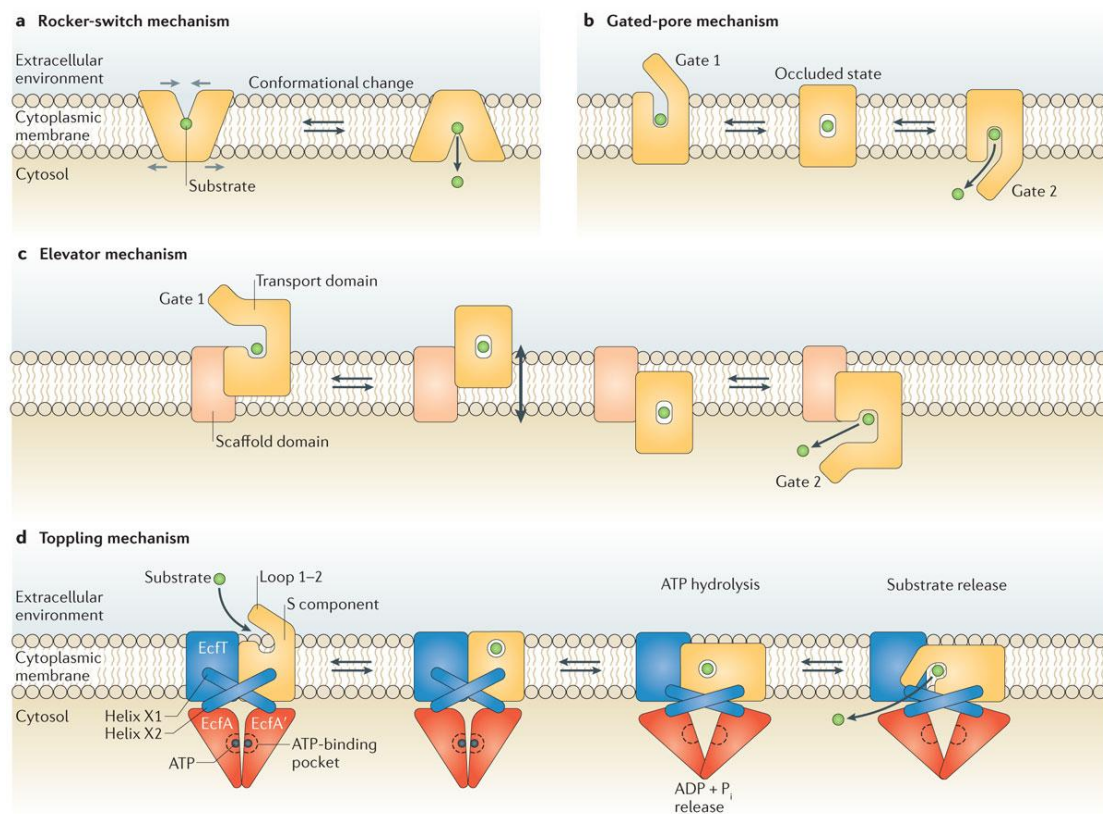
In the alternating access mechanism, protein-mediated substrate transport across membranes requires that access to the solute-binding site alternates between the periplasmic side and cytoplasmic side of the membrane. This alternating access mechanism was proposed more than half a century ago³⁰, long before the first structure of a membrane protein was solved³¹. Four models for transport have been suggested - the rocker-switch mechanism, the gated-pore mechanism, the elevator mechanism and the toppling mechanism (Figure 1.7 a-d).^{32, 33} The basic principles of these four models are briefly discussed below:

In the rocker-switch mechanism (Figure 1.7a), the substrate binds to a site in the protein that is located close to the midway of the membrane. A swiveling movement

around a hinge region at the substrate-binding site (light grey arrows) alternates access between the periplasmic side and cytoplasmic sides of the membrane, allowing substrates to release.³³

In the gated-pore mechanism (Figure 1.7b), the substrate-binding site is located in the center of the membrane and alternating access is implemented by using two gates. An occluded intermediate state exists when both gates are closed.³³

In the elevator mechanism (Figure 1.7c), two gates control access to the binding site, and the protein region that has bound the substrate undertakes a translational movement in the membrane when it is in an occluded state. An elevator domain is needed to facilitate the lift-type movement of the transport domain.³³



Nature Reviews | Microbiology

Figure 1.7 Models for alternating-access mechanisms of transport. a) Rocker-switch mechanism. b) Gated-pore mechanism. c) Elevator mechanism. d) Toppling mechanism.³³

The toppling mechanism (Figure 1.7d) would be similar to the elevator mechanism, except that it is proposed to orient instead of lift the S component so that

its substrate-binding site faces the extracellular environment. In the example, the hydrolysis of ATP and release of inorganic phosphate (Pi) and ADP lead to toppling of the S component and the substrate-binding site becomes oriented towards the cytoplasmic side.³³

Based on recent structural data from several secondary transport proteins, theoretical energy profiles were described for a series of different conformational states during coupled transport (Figure 1.8).³⁴ This explains why the number of well-resolved 3D structures of membrane transporters is still rather limited. At the same time provides some concepts for understanding the transport mechanism.

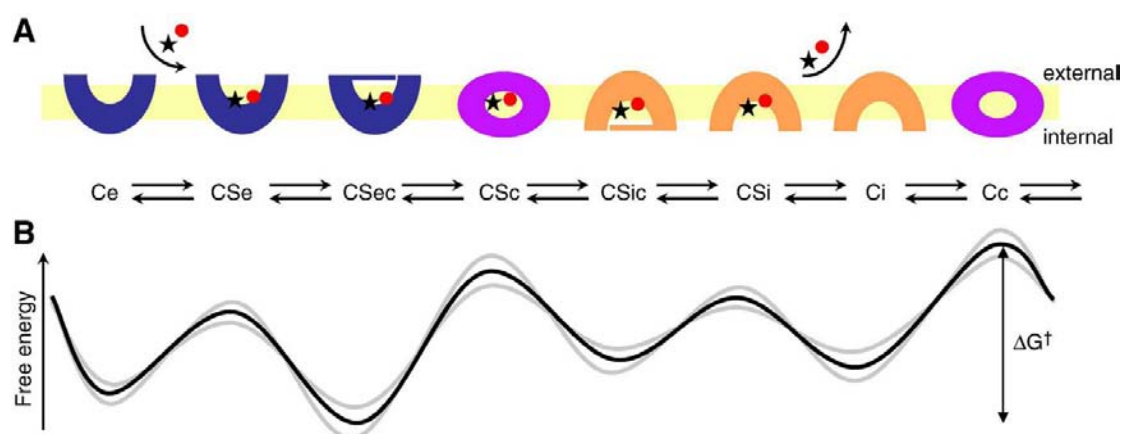


Figure 1.8 A series of different conformational states during coupled transport. (A) Substrates (S, star and red circle) bind to an externally open carrier conformation (Ce), forming a transient substrate-bound state CSe, which transforms to an occluded substrate-bound state still facing the external side of the membrane (CSec). Switching from CSec to an inward-facing, occluded substrate-bound state CSic passes through a fully occluded, probably transient, substrate-bound intermediate state, CSc. Substrates are then released from a transient substrate-bound inward-facing open conformation (CSi) and the carrier can switch back from inward open (Ci) to outward open (Ce) state via a fully occluded, intermediate state Cc in the case of symport (see text for details). (B) Theoretical energy profile (black) of different carrier states during catalysis, indicating minima at the gated substrate-bound states, and a putative rate-limiting barrier for the re-conversion of the empty carrier. Note that the barriers and minima will vary for different transporters: alternate situations are represented by additional profiles in gray.³⁴

1.6.1 General mechanisms of sugar transport

LacY (lactose permease of *Escherichia coli*), a lactose/ H⁺ symporter, is a

paradigm for the major facilitator superfamily (MFS) of membrane transport proteins.³⁵ Its transport mechanism is well studied as shown in Figure 1.9.³⁶ The key characteristics of the ordered mechanism are summarized by Madej *et al*³⁶ as follows: (1) Lactose/H⁺ symport in the uphill or downhill energetic modes is just the same reaction. The difference is in the downhill symport process: deprotonation is the rate-limiting step in the downhill process, but it is no longer limiting in the uphill process: and either dissociation of sugar or a conformational change that leads to deprotonation becomes limiting. (2) Sugar-binding and dissociation, are the driving force for alternating access, but not $\Delta\tilde{\mu}_{\text{H}^+}$. (3) LacY has to be protonated to bind sugar. (4) Galactoside binds by an induced-fitting mechanism, which powers transition to an occluded state. (5) Sugar dissociates first. (6) Upon sugar dissociation, there is a conformational change leading to deprotonation of LacY.

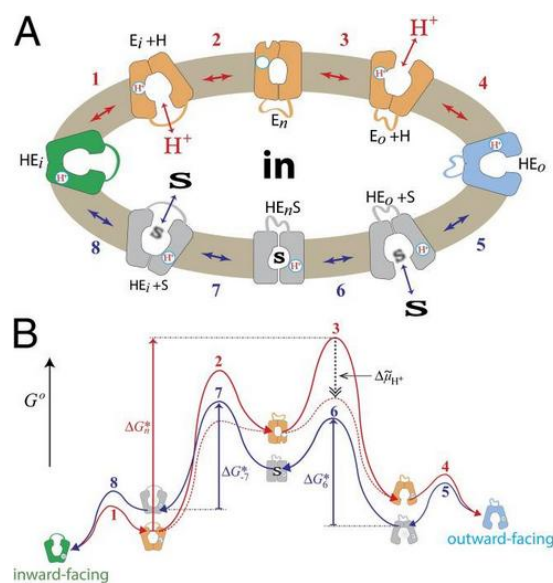


Figure 1.9 Transport cycle of MFS symporter. (A) Overview of the postulated steps in the transport model. Inward-facing (green) and outward-facing (blue) conformations are separated by the apo-intermediate conformations (orange) or by the occluded-intermediate conformations (gray). Steps are numbered consecutively: 1: Opening of the H⁺ site; 2: Deprotonation to inside and reorientation to the apo-intermediate with a central cavity closed to either side of the membrane; 3: Opening of the outward-facing cavity and reprotonation from the outside; 4: Formation of outward-open, substrate-free conformation; 5 and 6: Substrate binding and induced fitting to the occluded conformation; 7: Opening of the inward-facing cavity and release of the sugar; 8: Formation of the protonated, substrate-free conformation. (B) Hypothetical energy profile for the transport cycle. The colors of the lines correspond to parts of the transport reaction

equivalent to A.³⁶

Four different Na⁺ cotransporter crystal structures have been solved in different conformations (see Figure 1.10). These cotransporters have been solved in the outward open (C2), outward occluded (C3), and inward facing (C5) conformations for the nucleobase cotransporter Mhp1³⁷; an outward occluded (C3) conformation for the leucine cotransporter LeuT³⁸; an intermediate conformation between C3 and C4 for BetP³⁹; an inward occluded and inward open conformations (C4, C5) for vSGLT1^{40, 41}. As yet, there are no structures of these proteins in the C1 or C6 conformations. From those crystal structures, Wright *et al* proposed a six state model for the SGLTs Na⁺ cotransporter (Figure 1.10).⁴²

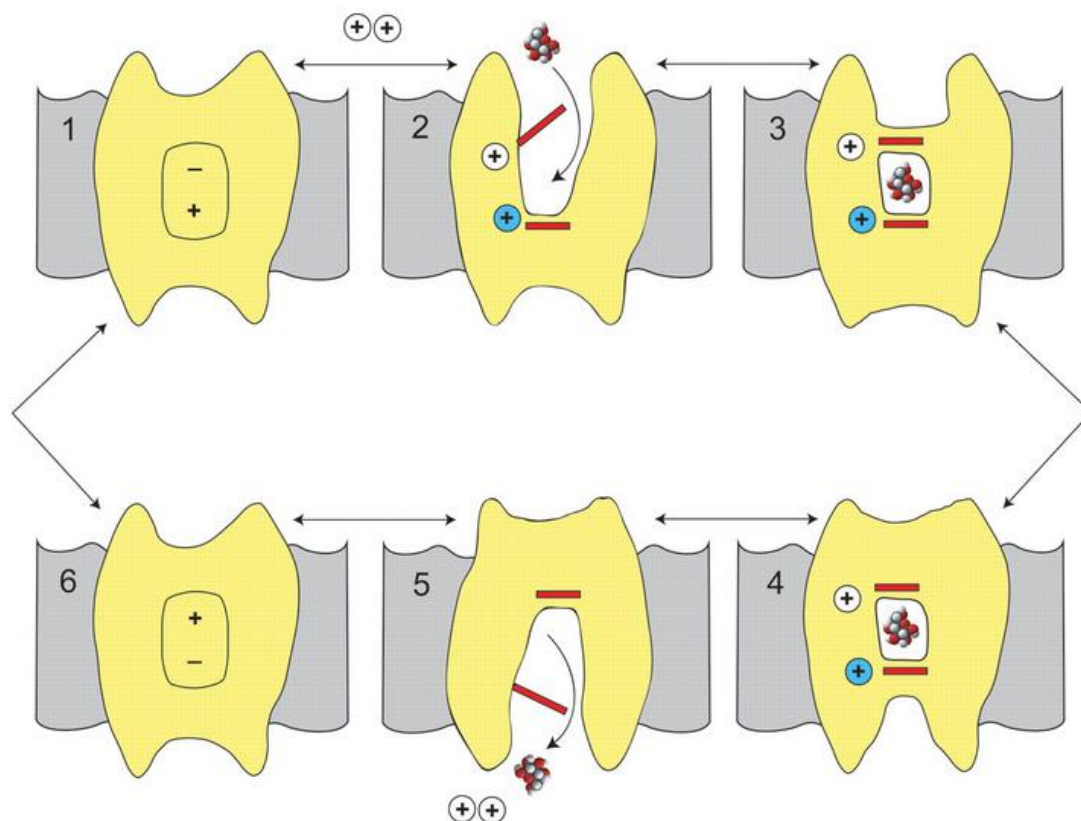


Figure 1.10 A 6-state model of SGLTs to integrate the kinetic and structural data. Na⁺ binds first to the outside to open the outside gate (C2) permitting outside sugar to bind and be trapped in the binding site (C3). This is followed by a conformational change from an outward occluded (C3) to an inward occluded (C4) state. Upon opening the inward gate (C5), the Na⁺ and sugar are released into the cell interior. There is a paucity of experiments addressing the order of the ligand dissociation at the cytosolic surface. The transport cycle is completed by the change in conformation from the inward facing ligand-free (C6) to the outward facing ligand free (C1) states. Structures corresponding to C2 and C3 have been obtained for Mhp1, C3 for LeuT, and C4 for

vSGLT.⁴²

1.6.2 Hypothesis for the transport mechanisms of melibiose permease

The melibiose permease faces the same situation as other sugar cotransporters in the sense that it doesn't have crystal structures in all the conformations. So hypothesis for the transport mechanisms of the melibiose permease need to be based not only on the known crystal structure from the MFS family, but also on the biochemistry and biophysics studies.

Two kinetic models were proposed by León *et al* and Yousef *et al* in 2009 (Figure 1.11). They suggested that sugar translocation occurs via the alternating access mechanism. In this mechanism, the empty MelB presents a conformational dynamic behavior between inward-facing and outward-facing orientations (C_o , C_i and step 6). The subsequent binding of cation (C_oNa and step 1) and sugar (C_oName1 and step 2) will induce the conformational changes from outward-facing to inward-facing (C_oName1 , C^*Name1 , C_iName1 and step 3), then the substrates binding sites are faced to cytoplasmic medium. Sugar (C_iName1 and step 4) and cation (C_i and step 5) will subsequently leave MelB, and then the empty MelB returns to the initial state (C_o , C_i and step 6).^{25, 43}

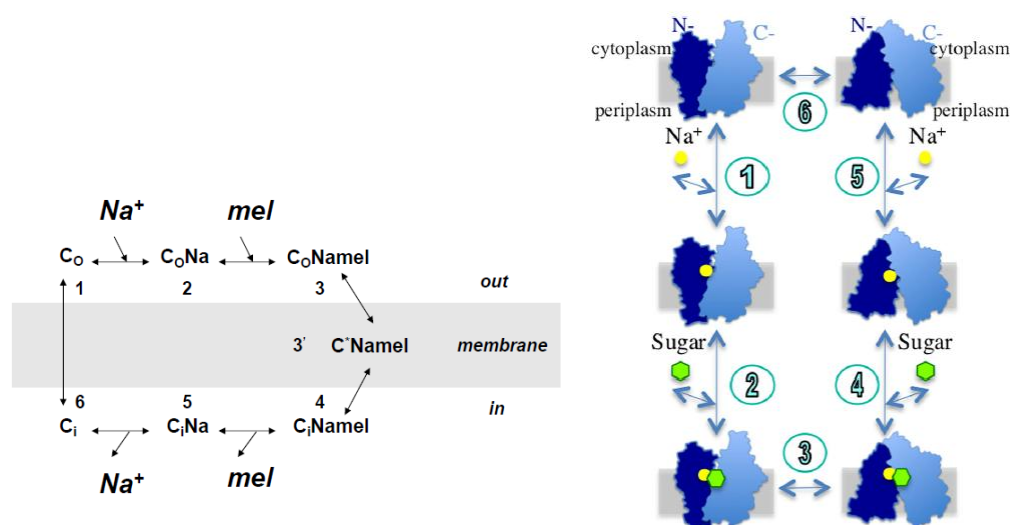


Figure 1.11 Left: Kinetic model of Na^+ -sugar cotransport by MelB in physiological orientation. The C_o , C^* and C_i indicate MelB states with an outward-facing, occluded or inward-facing

conformation, respectively. Starting from C_o (empty carrier), binding of Na^+ and then melibiose successively drives the outward-facing transporter into the C_oNa and C_oName1 states (5). The outward-facing to inward-facing carrier reorientation towards the cytoplasm ($C_oName1 \leftrightarrow C_iName1$) is proposed to include an intermediate occluded state (C^*Name1). After sequential release of melibiose ($C_iName1 \leftrightarrow C_iNa$) and Na^+ ($C_iNa \leftrightarrow C_i$) into the inner compartment (3), MelB cycling ends by a return of the empty carrier towards the outer membrane surface ($C_i \leftrightarrow C_o$).⁴³ Right: A kinetic scheme of the efflux mode of galactoside/ Na^+ symport for MelB. A cross section of the membrane is shown as a gray rectangle.²⁵

In 2014, Ethayathulla *et al* published the first crystal structure of MelB with two different conformations: partially outward occluded state conformation and the outward inactive state conformation (4M64-A¹³ and 4M64-B¹³). They propose a mechanism after combining the information from their study with the solved crystal structure of full inward open conformation for PepT (2XUT⁴⁴), LacY (2V8N⁴⁵, 1PV7⁴⁶) and GlpT (1PW4⁴⁷); inward partial open conformation for NarU (4IU8-B⁴⁸) and XylE (4JA4⁴⁹); inward partially occluded conformation for XylE (4JA3⁴⁹) and NarU (4IU8-A⁴⁸); inward occluded conformation for NarK (4JR9⁵⁰, 4JRE⁵⁰) and PiPT (4J05⁵¹); intermediate conformation between inward and outward for EmrD (2GFP⁵²); outward occluded conformation for XylE (4GBY⁵³); and full outward conformation for FucP (3O7Q⁵⁴). The simplified scheme for MelB transport mechanism is shown in Figure 1.12. The melibiose efflux includes eight states following the black arrow's direction: [1] Inward Na^+ -bound state. Binding of a Na^+ to the cation-binding site induces an increase in sugar affinity. [2] Inward Na^+ -bound and melibiose-bound state. [3] Occluded Na^+ -bound and melibiose-bound state. [4] Outward Na^+ -bound and melibiose-bound state. [5] Outward melibiose-released state. [6] Outward Na^+ -released state. [7] Occluded-empty state. Formation of the unloaded intermediate state occluded on both sides. [8] Inward-empty state. When the cavity is open to the cytoplasmic side, the next transport cycle begins.¹³

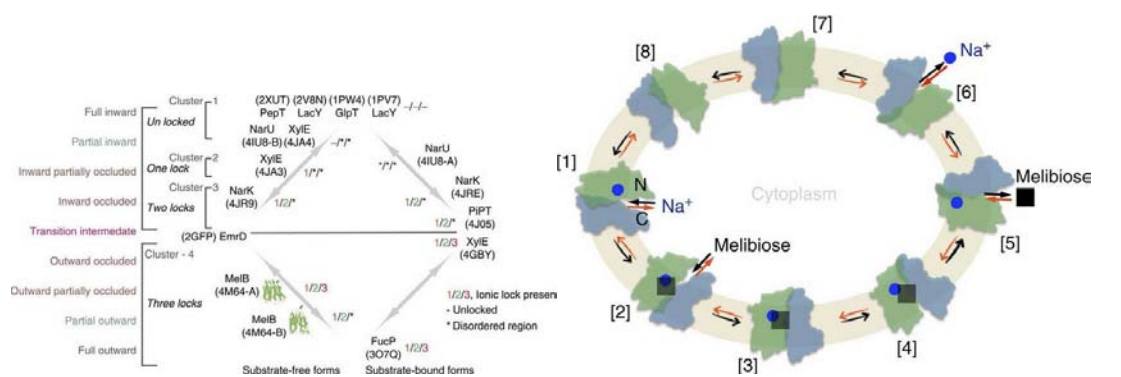


Figure 1.12 Left: Clusters of MFS permeases in different conformations. Structures were categorized into clusters according to their conformational state. *, Disordered region in structure; -, at an unlocked state; 1/2/3, the presence of lock-1, lock-2 or lock-3. PDB ID is shown for each structure. Right: Scheme for Na⁺/melibiose symport. [1–8], Kinetic steps in the overall transport cycle. The green colour-filled cycle represents the cell inner membrane. Na⁺, blue circles; melibiose, black squares. N, the N-terminal domain in green colour; C, the C-terminal domain in blue color. Melibiose influx down a sugar concentration gradient starts at step [6] and proceeds via the red arrows around the circle, and melibiose efflux down a sugar concentration gradient starts at [1] and proceeds via the black arrows around the circle. Active transport of melibiose against a concentration gradient proceeds from step [6] via the red arrows as the melibiose influx.¹³

1.7 Crystallization and structure determination

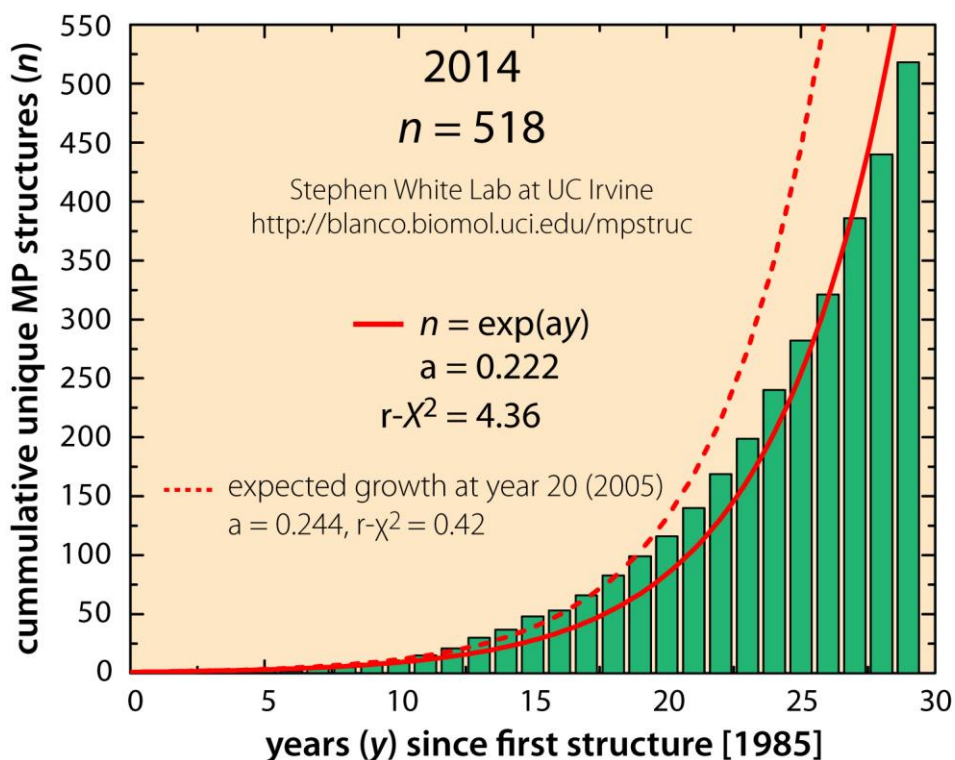


Figure 1.13 The growth rate of successfully solved unique membrane protein structures.

(Membrane Proteins of Known Structure; <http://blanco.biomol.uci.edu/mpstruc/>)

When the first membrane protein crystal structure was determined, crystallization of a membrane protein was widely perceived as extremely arduous. Now, that perception has changed drastically, and the process is nearly regarded as routine.⁵⁵ The progress of the membrane protein structural biology has been tracked on Stephen White's website (<http://blanco.biomol.uci.edu/mpstruc/>). The growth rate of successfully solved unique membrane protein structures is presented in Figure 1.13. A statistics of crystallization methods used for new structure reported from 2012 to mid-2014 in different types of membrane proteins is shown in table 1.5. It means the majority of structures currently being determined utilize direct crystallization of protein–detergent complexes, suggesting that this approach should be tried first for most new membrane-protein targets.⁵⁵

Table 1.5 Crystallization methods used for new structure reports from 2012 to mid-2014.⁵⁵

| Protein class | <i>Crystallized using bicelles</i> | <i>Crystallized using lipidic mesophase</i> | <i>Crystallized as protein-detergent complex</i> | <i>total No. identified</i> |
|----------------------|------------------------------------|---|--|-----------------------------|
| <i>monotopic</i> | 1 | 0 | 11 | 12 |
| <i>beta barrel</i> | 3 | 2 | 22 | 27 |
| <i>alpha (total)</i> | 8 | 39 | 145 | 192 |

There are three basic types of three-dimensional membrane protein crystals (Figure 1.14): Type I crystals consist of ordered stacks of two-dimensional crystals, which are present in a bilayer; In type II three-dimensional crystals, the hydrophobic surface of membrane proteins is covered by a detergent micelle. Stable crystal contacts are made between the hydrophilic surfaces of the protein; in a modification of type II (type II b), tightly and specifically bound antibody fragments add a hydrophilic domain to the complex. This surface expansion provides additional sites for crystal contacts and space for the detergent micelle.⁵⁶

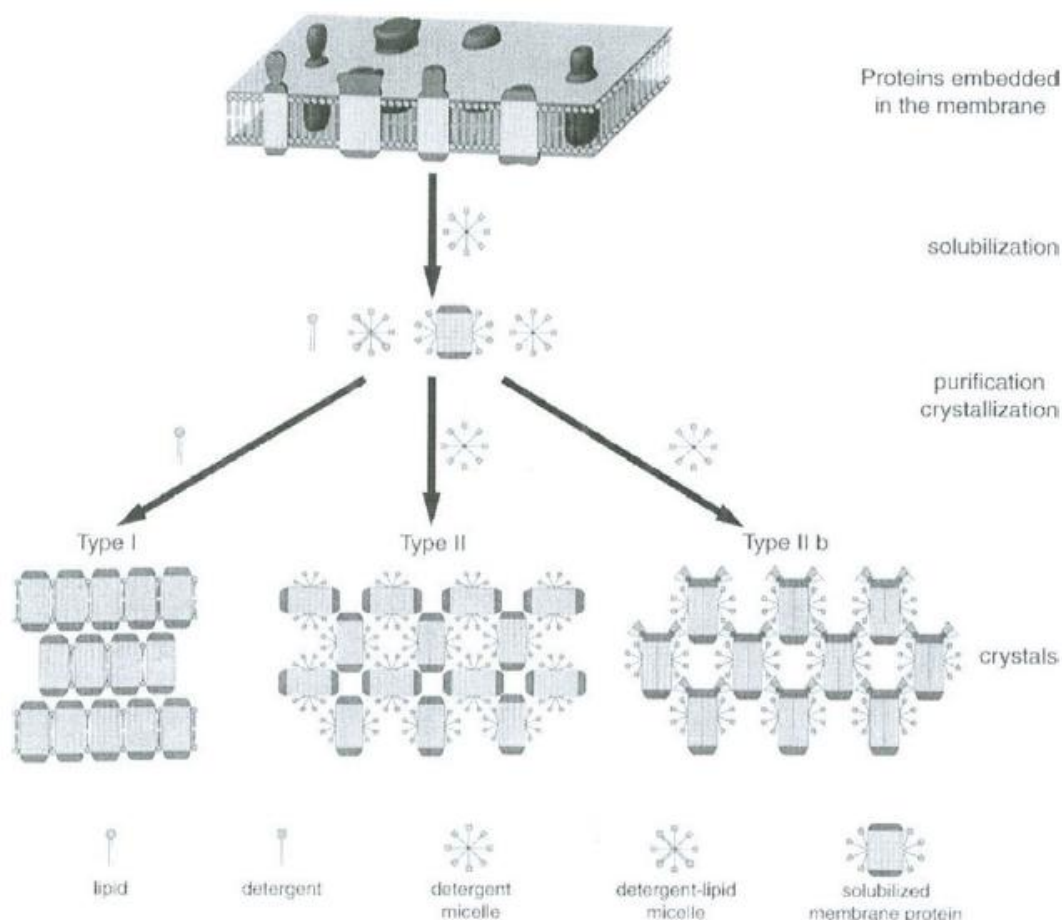


Figure 1.14 Basic types of three-dimensional membrane protein crystals. Type I crystals consist of ordered stacks of two-dimensional crystals, which are present in a bilayer. In the detergent solubilized state the hydrophobic surface of membrane proteins is covered by a micelle. This membrane protein-detergent complexes form so-called type II three-dimensional crystals. Stable crystal contacts are made between the hydrophilic surfaces of the protein. In a modification of type II (type II b), tightly and specifically bound antibody fragments add a hydrophilic domain to the complex. This surface expansion provides additional sites for crystal contacts and space for the detergent micelle.⁵⁶

Membrane proteins crystallized in type I was used for structure determination by electron microscopy. Several structures of membrane proteins at medium resolution ($\sim 5 - 10 \text{ \AA}$) have already been obtained. But higher resolution can be obtained by X-ray crystallography using type II (or type II b) crystals.⁵⁶

1.8 Biophysical studies of MeIB

1.8.1 Förster Resonance Energy Transfer (FRET)

The galactosyl analog 2'-(N-dansyl)-aminoethyl-1-thio-D-galactopyranoside (D^2G), which can bind to MelB, but cannot be transported, is an artificial ligand of the melibiose permease.^{57, 58} This fluorescent probe was invented to test binding abilities in the MelB transporter. It was used for vesicles as well as for proteoliposomes of the MelB transporter. The emitted fluorescence of D^2G can be recorded by exciting the intrinsic tryptophans at 295 nm and examining the FRET. Like melibiose, the binding affinity of D^2G was increased when sodium was added. This result also supports the idea that D^2G and melibiose were using the same binding site. The fluorescence emission maximum of the D^2G bound to MelB is around 460 nm. The intensity of the D^2G fluorescence at 460 nm is relatively small in sodium-free medium (Figure 1.15). The fluorescence signal was highly increased when sodium was added. The signal of D^2G bound to MelB recorded in sodium medium is blue shifted around 25 nm from that recorded in the absence of NaCl, suggesting a hydrophobic environment surrounding the fluorescent probe.⁵⁸

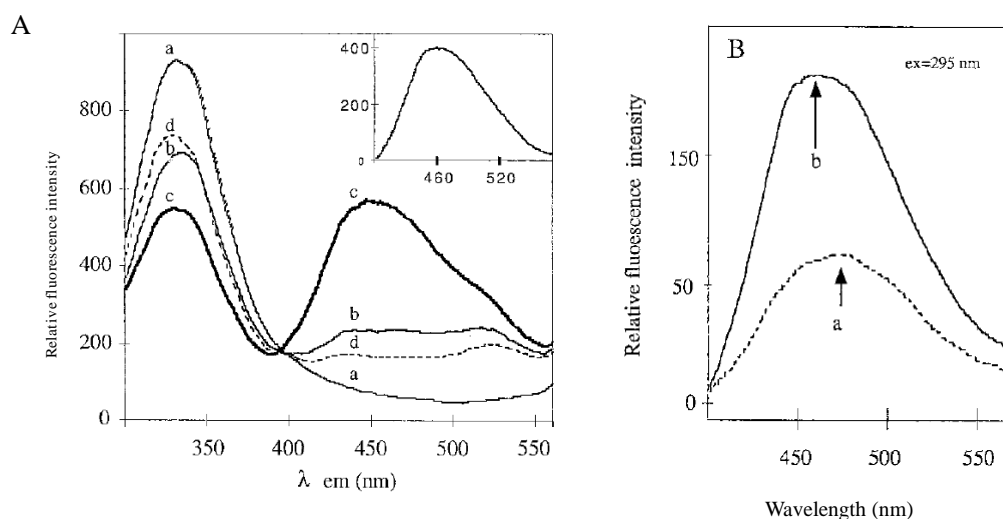


Figure 1.15 A: FRET of the melibiose permease wild type protein, a: only protein, b: MelB with 15 μ M D^2G , c: MelB with 15 μ M D^2G with 10 mM NaCl, d: MelB with 15 μ M D^2G , 10 mM NaCl and 150 mM melibiose – competitive replacement of D^2G . **B:** Effect of NaCl on the spectral properties of D^2G bound to MelB by illuminating at 295 nm. a: in the absence of NaCl; b: after the addition of NaCl.

1.8.2 Fourier Transform Infrared (FTIR) spectroscopy

FTIR spectroscopy is a well-established biophysical technique for the examination of protein secondary structure and structural changes⁵⁹. Identification of protein secondary structure components and their relative proportion in the overall structure can be derived from an analysis of the protein absorption due to the vibration in the amide I and II bands.⁶⁰

Moreover, the effect of substituting D for H atoms in the protein signal provides an additional insight into the protein backbone to the aqueous solvent.⁶¹ Data from FTIR spectroscopy revealed the secondary structure composition of the MelB transporter. The protein consisted of α -helices, β -sheets, 3_{10} -helices and unordered domains (Table 1.6). The fact that the secondary structure of MelB is constituted by α -helices is in agreement with the 12 transmembrane helices.¹³ Sodium and melibiose induced conformational changes in MelB can be detected by infrared spectroscopy in the region of amide I and amide II.⁶²

Table 1.6 Secondary structure composition and assignments of MelB_{EC}

| H ₂ O | | | D ₂ O | | |
|---------------------------------|---------|---------------------------------|---------------------------------|---------|--|
| Wavenumber* (cm ⁻¹) | % area* | Assignment | Wavenumber* (cm ⁻¹) | % area* | Assignment |
| 1683 | 17 | Rev. turns | 1683 | 16 | Rev. turns |
| | | | 1678 | | |
| | | | 1671 | | |
| | | | 1665 | | |
| 1660 | 49 | α , unordered | 1660 | 42 | α |
| 1653 | | | 1653 | | |
| 1647 | 12 | 3_{10} , open loops, α | 1646 | 13 | unordered, α |
| 1640 | | | 1638 | 29 | β -sheets, 3_{10} , open loops |
| 1634 | 20 | β -sheets | 1629 | | |
| 1628 | | | | | |

*The values were rounded off to the nearest integer

Attenuated total reflection Fourier transform infrared spectroscopy is one of the most powerful methods. ATR difference spectroscopy permits the study of the transport mechanism of substances with membrane proteins by the alternating perfusion of a substrate-containing buffer and the reference buffer.^{29, 43, 63, 64} A stable protein film on to the top of the germanium ATR crystal is required.⁶⁵

The MelB mutant was constructed with Cless permease used as the molecular background. León *et al* checked the similarity of the substrate-induced difference spectra of the Cless and the WT permeases. The results showed that the main parts of the difference spectra (Figure 1.16, 1.17, 1.18) are very similar, albeit not entirely identical, and yield comparable information on fully active MelB permeases.⁴³ Hence, Cless has a limited impact on changes due to sodium binding or melibiose interaction in the presence of sodium or proton. Spectra deconvolution by the maximum entropy method⁶⁶ was applied to resolve overlapped bands of the difference spectra. It reveals that the Cless' peaks are similar to the wild-type transporter (Figure 1.16, 1.17, 1.18). For the sodium-induced difference spectrum of Cless, the peaks in the 1660-1651 cm^{-1} interval (amide I) and around 1540 cm^{-1} (amide II) are assigned to α -helix structures. The detected peaks at 1741/1726 cm^{-1} and 1403/1384 cm^{-1} are assigned to the vibration of the protonated and deprotonated carboxylic acids, respectively.⁶⁵

The melibiose-induced spectra in the presence of the proton or the sodium are very different from the sodium-elicited IR difference spectra in shape and intensity. Since the melibiose molecular is bigger than the sodium ion, this suggests that melibiose induces greater conformational changes than binding of cation alone. Peaks related to α -helix structures are detected at 1668, 1659 and 1653 cm^{-1} . The β -structure peaks are at 1688, 1680, 1672, 1643 and 1633 cm^{-1} .⁶⁷

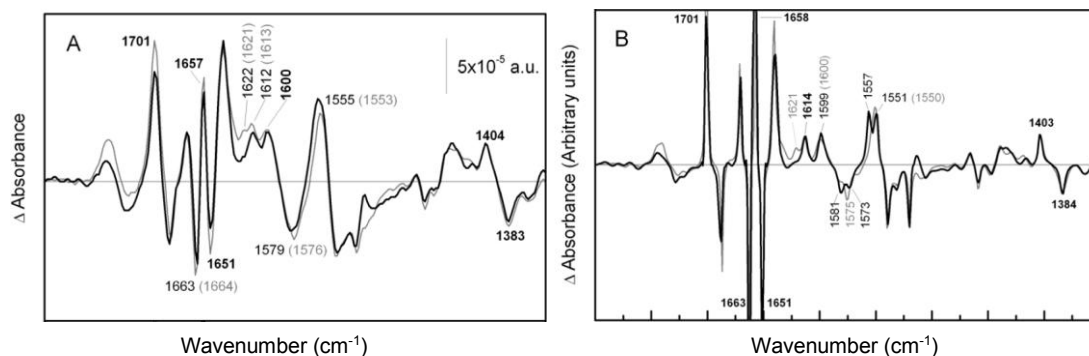


Figure 1.16 Comparison of Na⁺-induced difference spectra of Cless and WT permeases.⁴³ (A) (solid line) difference spectrum of Cless in 20 mM MES, 100 mM KCl, 10 mM NaCl, pH 6,6 minus Cless in 20 mM MES, 110 mM KCl, pH 6,6; (shaded line) difference spectrum of WT under the same conditions. (B) deconvoluted of the spectra shown in A.

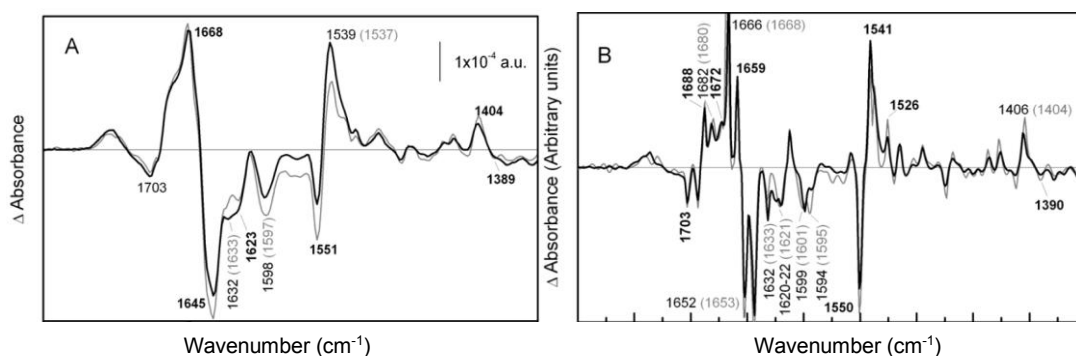


Figure 1.17 Comparison of melibiose-induced difference spectra of Cless and WT permeases in the presence of Na⁺.⁴³ (A) (solid line) difference spectrum of Cless in 20 mM MES, 100 mM KCl, 10 mM NaCl, 10 mM melibiose, pH 6.6 minus Cless in 20 mM MES, 100 mM KCl, 10 mM NaCl, pH 6.6; (shaded line) difference spectrum of WT under the same conditions. (B) deconvoluted of the spectra shown in A.

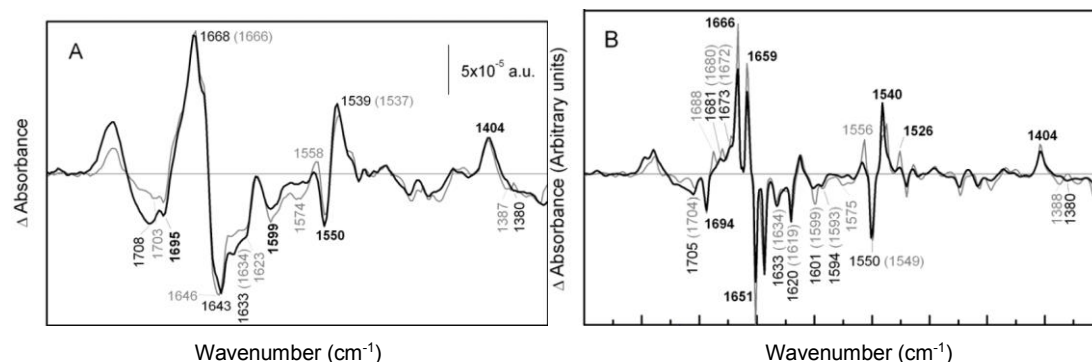


Figure 1.18 Comparison of melibiose-induced difference spectra of Cless and WT permeases, in the presence of H⁺.⁴³ (A) (solid line) difference spectrum of Cless in 20 mM MES, 100 mM KCl, 50 mM melibiose, pH 6.6 minus Cless in 20 mM MES, 100 mM KCl, pH 6.6; (shaded line) difference spectrum of WT under the same conditions. (B) deconvoluted of the spectra shown in A.

1.9 Molecular dynamics simulations

The lack of complete knowledge of the biochemical properties and the detailed structure of membrane transporters makes it difficult to deeply understand the transporter mechanism. In recent years, the availability of 2D and 3D structures obtained by X-ray and EM crystallography^{13, 26, 27}, as well as contributions from computational and theoretical approaches²⁹, has greatly enhanced our understanding of melibiose permease. Despite these advancements, the resolved 3D structures¹³ of MelB transporters are still not enough for a deeper understanding of the movement of the substrates. Moreover, transport is not a static process, so the molecular dynamics simulations may be able to provide the dynamic aspects of the transport process.

Molecular dynamics simulations are largely based on classical mechanics and statistical mechanics theories.⁶⁸ In a typical atomistic MD simulation, interactions are calculated between atoms using a set of parameters that define a potential energy function, representing a “force field”.⁶⁹

Various force fields (AMBER⁷⁰, CHARMM⁷¹, OPLS⁷² and so on.) are available for biomolecular simulations, with minor differences in parameters of their potential energy functions. A typical potential energy function for biomolecular simulations, E , includes terms that describe bonded (bonds, bond angles, dihedral angles, etc.) and nonbonded (van der Waals and electrostatic) interactions:

$$E_{\text{bonded}} = E_{\text{bond}} + E_{\text{angle}} + E_{\text{dihedral}}$$

$$E_{\text{nonbonded}} = E_{\text{vdW}} + E_{\text{elec}}$$

$$E_{\text{total}} = E_{\text{bonded}} + E_{\text{nonbonded}}$$

Various software is also available, such as ACEMD, NAMD, GROMOS, ect. Detailed information is in Materials and methods part.

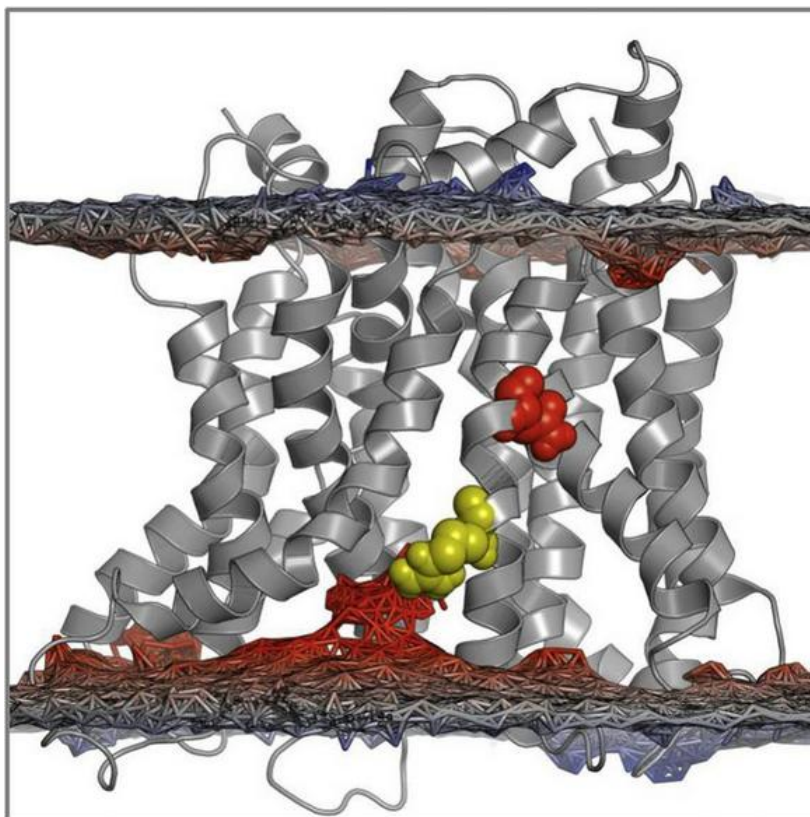


Figure 1.19 Coarse-grained molecular dynamic simulation of MelB_{ST} according to Stansfeld *et al*⁷³. Asn-58 is in red color, Arg-52 is in yellow color.

For MelB_{ST}, there is a simulation result published, using Coarse-grained molecular dynamics (CGMD) simulations. The CGMD simulations enable insertion of membrane proteins into explicit models of lipid bilayers. Figure 1.19 shows the MelB_{ST} inserted into the lipid bilayer with some highlighted residues.⁷³

Moreover, in our group previous work²⁹ showed an interesting result in the molecular dynamics simulations of MelB_{EC} (Figure 1.20). The Lys-377 was attracted by Asp-59 and Asp-55 during the MD simulations in the absence of sodium, and kept a stable distance with Tyr-120 and Asp-124. But when the Asp-59 was protonated, the Lys-377 was interacting with Asp-55 and away from Tyr-120 instead of standstill (Figure 1.21). When the sodium was positioned in the middle of Asp-55, Asp-59, Tyr120, Asp124 and Lys-377, the Na⁺ binding site appeared (Figure 1.22).

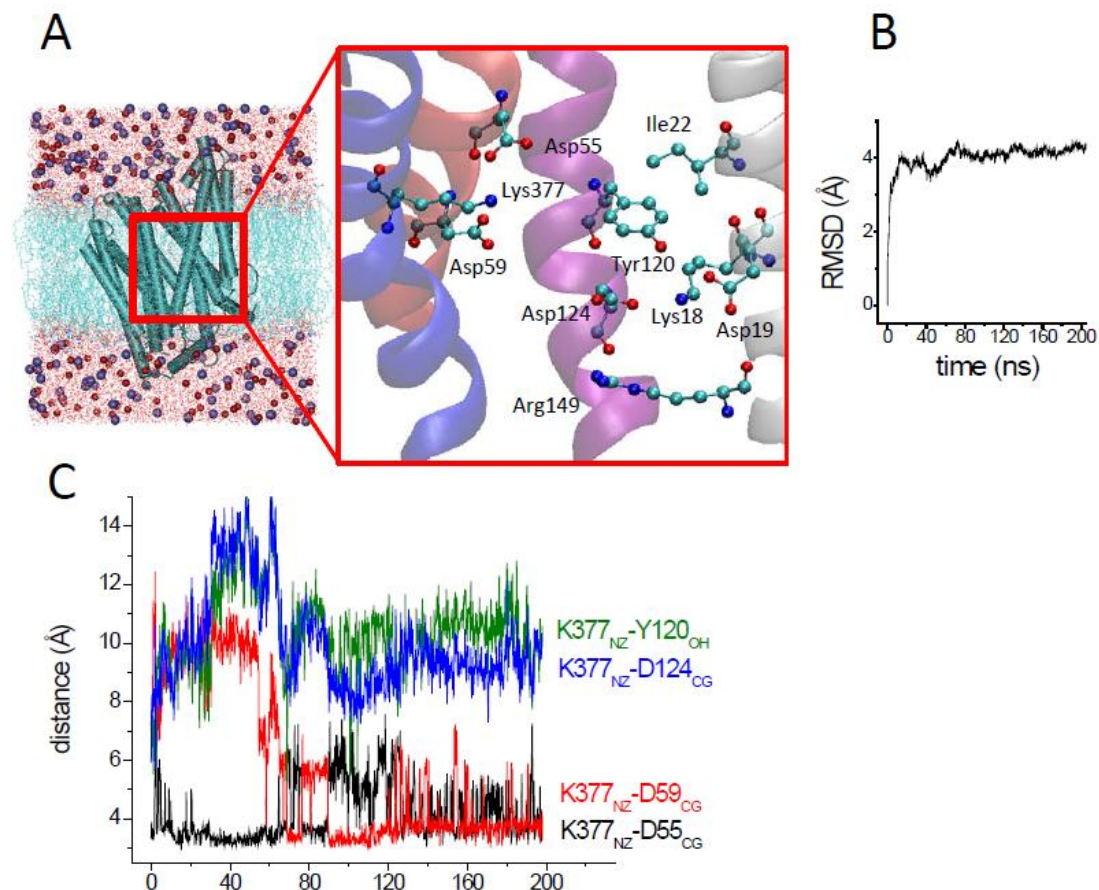


Figure 1.20 Molecular dynamics of MelB_{EC}. (A) The simulated system after equilibration for 200 ps. The expanded figure shows a snapshot of the proposed cation binding site environment, after 200 ns simulation. The protein is shown in cartoon representation (blue), with the cytoplasmic side at the bottom. The POPE bilayer (light blue) and the waters (red) are drawn in lines. Na⁺ (blue) and Cl⁻ (red) are drawn in van der Waals representation. The MelB_{ST-A} crystal structure 4M64 (6) was mutated in all amino acids corresponding to those of MelB, briefly minimized and included in a bilayer of POPE with layers of water molecules and NaCl 0.3 M were finally added (see Methods). The figure was generated with VMD software (25). (B) Drift from the initial structure as measured by the RMSD of backbone C α atoms. (C) Time course of the specified distances, indicative of the location of the NZ atom of K377 interacting with the CG atom of D55 and D59 but distant from the OH atom of Y120 or the CG atom of D124.²⁹

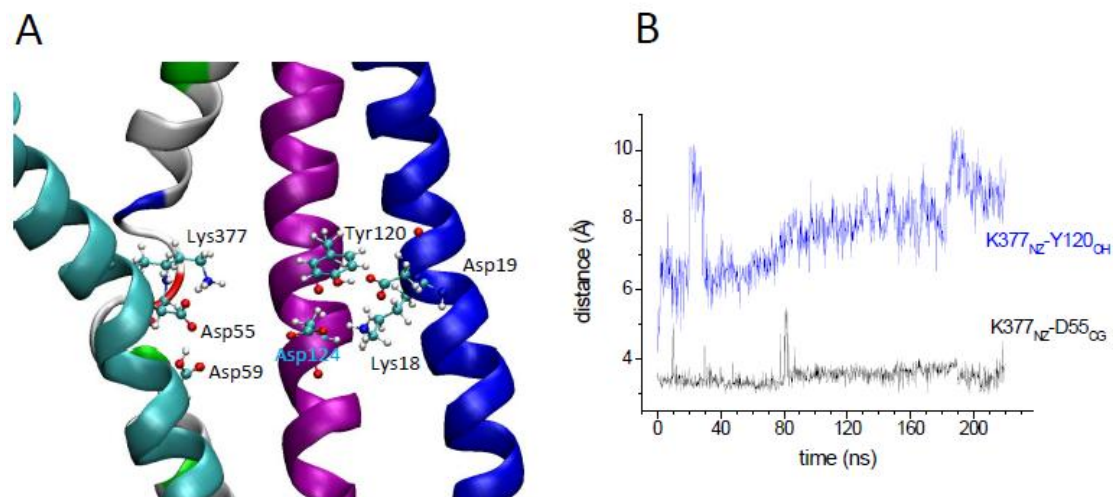


Figure 1.21 Simulation of MelB with D59 protonated. (A) Snapshot of the substrate's binding sites region of MelB with D59 protonated, after 220 ns simulation. (B) Time course of the distances between the NZ atom of K377 and the CG atom of D55 or the OH atom of Y120.²⁹

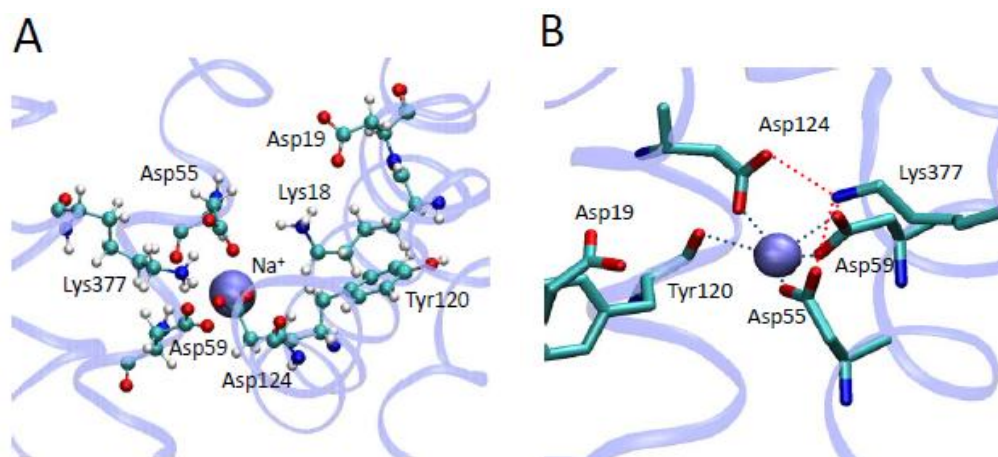


Figure 1.22 Organization of the Na⁺ binding site. (A) Snapshot of the proposed binding site environment of MelB with a Na⁺ positioned initially in between D55 and D59, after 330 ns of simulation. (B) Detail of the Na⁺ binding site showing the ligands from the protein.²⁹

REFERENCES

1. Yildirim, M. A., Goh, K. I., Cusick, M. E., Barabasi, A. L., and Vidal, M. (2007) Drug-target network, *Nature biotechnology* 25, 1119-1126.
2. Shi, Y., and Hu, F. B. (2014) The global implications of diabetes and cancer, *Lancet* 383, 1947-1948.
3. Lodish, Berk, Kaiser, Bretscher, Ploegh, Amon, and Scott (2008) *Molecular cell biology*, Sixth ed.
4. Nelson, D. L. (2008) *Lehninger Principles of Biochemistry*, 5th ed., SARA TENNEY, New York.
5. Karp, G. (2010) *Cell and Molecular Biology-Concepts and Experiments*.Gerald.Karp, 6th ed., wiley.
6. Wallin, E., and von Heijne, G. (1998) Genome-wide analysis of integral membrane proteins from eubacterial, archaean, and eukaryotic organisms, *Protein Science* 7, 1029-1038.
7. Lodish, Berk, Kaiser, Bretscher, Ploegh, Amon, and Scott (2013) *Molecular cell biology*, Seventh ed.
8. Saier, M. H., Jr., Reddy, V. S., Tamang, D. G., and Vastermark, A. (2014) The transporter classification database, *Nucleic acids research* 42, D251-258.
9. Reddy, V. S., Shlykov, M. A., Castillo, R., Sun, E. I., and Saier, M. H., Jr. (2012) The major facilitator superfamily (MFS) revisited, *The FEBS journal* 279, 2022-2035.
10. Yan, N. (2013) Structural advances for the major facilitator superfamily (MFS) transporters, *Trends in biochemical sciences* 38, 151-159.
11. Shi, Y. (2013) Common folds and transport mechanisms of secondary active transporters, *Annual review of biophysics* 42, 51-72.
12. Yan, N. (2015) Structural Biology of the Major Facilitator Superfamily Transporters, *Annual review of biophysics* 44, 257-283.
13. Ethayathulla, A. S., Yousef, M. S., Amin, A., Leblanc, G., Kaback, H. R., and Guan, L. (2014) Structure-based mechanism for Na(+)/melibiose symport by MelB, *Nature communications* 5, 3009.
14. Poolman, B., Knol, J., van der Does, C., Henderson, P. J., Liang, W. J., Leblanc, G., Pourcher, T., and Mus-Veteau, I. (1996) Cation and sugar selectivity determinants in a novel family of transport proteins, *Molecular microbiology* 19, 911-922.
15. Chaptal, V., Kwon, S., Sawaya, M. R., Guan, L., Kaback, H. R., and Abramson, J. (2011) Crystal structure of lactose permease in complex with an affinity inactivator yields unique insight into sugar recognition, *Proceedings of the National Academy of Sciences of the United States of America* 108, 9361-9366.
16. Wilson, D. M., and Wilson, T. H. (1987) Cation specificity for sugar substrates of the melibiose carrier in Escherichia coli, *Biochimica et biophysica acta* 904, 191-200.
17. Pardee, A. B. (1957) An inducible mechanism for accumulation of melibiose in Escherichia coli, *Journal of bacteriology* 73, 376-385.
18. Stock, J., and Roseman, S. (1971) A sodium-dependent sugar co-transport system in bacteria, *Biochemical and biophysical research communications* 44, 132-138.
19. Tokuda, H., and Kaback, H. R. (1977) Sodium-dependent methyl 1-thio-beta-D-galactopyranoside transport in membrane vesicles isolated from Salmonella typhimurium, *Biochemistry* 16, 2130-2136.

20. Pourcher, T., Bassilana, M., Sarkar, H. K., Kaback, H. R., and Leblanc, G. (1990) The melibiose/Na⁺ symporter of *Escherichia coli*: kinetic and molecular properties, *Philosophical transactions of the Royal Society of London. Series B, Biological sciences* 326, 411-423.
21. Botfield, M. C., Naguchi, K., Tsuchiya, T., and Wilson, T. H. (1992) Membrane topology of the melibiose carrier of *Escherichia coli*, *The Journal of biological chemistry* 267, 1818-1822.
22. Pourcher, T., Bibi, E., Kaback, H. R., and Leblanc, G. (1996) Membrane topology of the melibiose permease of *Escherichia coli* studied by melB-phoA fusion analysis, *Biochemistry* 35, 4161-4168.
23. Gwizdek, C., Leblanc, G., and Bassilana, M. (1997) Proteolytic mapping and substrate protection of the *Escherichia coli* melibiose permease, *Biochemistry* 36, 8522-8529.
24. Franco, P. J., and Wilson, T. H. (1999) Arg-52 in the melibiose carrier of *Escherichia coli* is important for cation-coupled sugar transport and participates in an intrahelical salt bridge, *Journal of bacteriology* 181, 6377-6386.
25. Yousef, M. S., and Guan, L. (2009) A 3D structure model of the melibiose permease of *Escherichia coli* represents a distinctive fold for Na⁺ symporters, *Proceedings of the National Academy of Sciences of the United States of America* 106, 15291-15296.
26. Hacksell, I., Rigaud, J. L., Purhonen, P., Pourcher, T., Hebert, H., and Leblanc, G. (2002) Projection structure at 8 Å resolution of the melibiose permease, an Na-sugar co-transporter from *Escherichia coli*, *The EMBO journal* 21, 3569-3574.
27. Purhonen, P., Lundback, A. K., Lemonnier, R., Leblanc, G., and Hebert, H. (2005) Three-dimensional structure of the sugar symporter melibiose permease from cryo-electron microscopy, *Journal of structural biology* 152, 76-83.
28. Granell, M., Leon, X., Leblanc, G., Padros, E., and Lorenz-Fonfria Victor, A. (2010) Structural insights into the activation mechanism of melibiose permease by sodium binding, *Proceedings of the National Academy of Sciences of the United States of America* 107, 22078-22083.
29. Fuerst, O., Lin, Y., Granell, M., Leblanc, G., Padros, E., Lorenz-Fonfria, V. A., and Cladera, J. (2015) The Melibiose Transporter of *Escherichia coli*: CRITICAL CONTRIBUTION OF LYS-377 TO THE STRUCTURAL ORGANIZATION OF THE INTERACTING SUBSTRATE BINDING SITES, *The Journal of biological chemistry* 290, 16261-16271.
30. Mitchell, P. (1957) A general theory of membrane transport from studies of bacteria, *Nature* 180, 134-136.
31. Deisenhofer, J., Epp, O., Miki, K., Huber, R., and Michel, H. (1985) Structure of the Protein Subunits in the Photosynthetic Reaction Center of *Rhodospseudomonas-Viridis* at 3Å Resolution, *Nature* 318, 618-624.
32. Forrest, L. R., and Rudnick, G. (2009) The rocking bundle: a mechanism for ion-coupled solute flux by symmetrical transporters, *Physiology* 24, 377-386.
33. Slotboom, D. J. (2014) Structural and mechanistic insights into prokaryotic energy-coupling factor transporters, *Nat Rev Microbiol* 12, 79-87.
34. Forrest, L. R., Kramer, R., and Ziegler, C. (2011) The structural basis of secondary active transport mechanisms, *Biochimica et biophysica acta* 1807, 167-188.
35. Kaback, H. R., Smirnova, I., Kasho, V., Nie, Y., and Zhou, Y. (2011) The alternating access transport mechanism in LacY, *The Journal of membrane biology* 239, 85-93.
36. Madej, M. G., Sun, L., Yan, N., and Kaback, H. R. (2014) Functional architecture of MFS D-glucose transporters, *Proceedings of the National Academy of Sciences of the United States*

- of America III*, E719-727.
37. Shimamura, T., Weyand, S., Beckstein, O., Rutherford, N. G., Hadden, J. M., Sharples, D., Sansom, M. S., Iwata, S., Henderson, P. J., and Cameron, A. D. (2010) Molecular basis of alternating access membrane transport by the sodium-hydantoin transporter Mhp1, *Science* 328, 470-473.
 38. Yamashita, A., Singh, S. K., Kawate, T., Jin, Y., and Gouaux, E. (2005) Crystal structure of a bacterial homologue of Na⁺/Cl⁻-dependent neurotransmitter transporters, *Nature* 437, 215-223.
 39. Ressler, S., Terwisscha van Scheltinga, A. C., Vonrhein, C., Ott, V., and Ziegler, C. (2009) Molecular basis of transport and regulation in the Na(+)/betaine symporter BetP, *Nature* 458, 47-52.
 40. Faham, S., Watanabe, A., Besserer, G. M., Cascio, D., Specht, A., Hirayama, B. A., Wright, E. M., and Abramson, J. (2008) The crystal structure of a sodium galactose transporter reveals mechanistic insights into Na⁺/sugar symport, *Science* 321, 810-814.
 41. Watanabe, A., Choe, S., Chaptal, V., Rosenberg, J. M., Wright, E. M., Grabe, M., and Abramson, J. (2010) The mechanism of sodium and substrate release from the binding pocket of vSGLT, *Nature* 468, 988-991.
 42. Wright, E. M., Loo, D. D., and Hirayama, B. A. (2011) Biology of human sodium glucose transporters, *Physiological reviews* 91, 733-794.
 43. Leon, X., Leblanc, G., and Padros, E. (2009) Alteration of sugar-induced conformational changes of the melibiose permease by mutating Arg141 in loop 4-5, *Biophys. J.* 96, 4877-4886.
 44. Newstead, S., Drew, D., Cameron, A. D., Postis, V. L., Xia, X., Fowler, P. W., Ingram, J. C., Carpenter, E. P., Sansom, M. S., McPherson, M. J., Baldwin, S. A., and Iwata, S. (2011) Crystal structure of a prokaryotic homologue of the mammalian oligopeptide-proton symporters, PepT1 and PepT2, *The EMBO journal* 30, 417-426.
 45. Guan, L., Mirza, O., Verner, G., Iwata, S., and Kaback, H. R. (2007) Structural determination of wild-type lactose permease, *Proceedings of the National Academy of Sciences of the United States of America* 104, 15294-15298.
 46. Abramson, J., Smirnova, I., Kasho, V., Verner, G., Kaback, H. R., and Iwata, S. (2003) Structure and mechanism of the lactose permease of *Escherichia coli*, *Science* 301, 610-615.
 47. Huang, Y., Lemieux, M. J., Song, J., Auer, M., and Wang, D. N. (2003) Structure and mechanism of the glycerol-3-phosphate transporter from *Escherichia coli*, *Science* 301, 616-620.
 48. Yan, H., Huang, W., Yan, C., Gong, X., Jiang, S., Zhao, Y., Wang, J., and Shi, Y. (2013) Structure and mechanism of a nitrate transporter, *Cell reports* 3, 716-723.
 49. Quistgaard, E. M., Low, C., Moberg, P., Tresaugues, L., and Nordlund, P. (2013) Structural basis for substrate transport in the GLUT-homology family of monosaccharide transporters, *Nature structural & molecular biology* 20, 766-768.
 50. Zheng, H., Wisedchaisri, G., and Gonen, T. (2013) Crystal structure of a nitrate/nitrite exchanger, *Nature* 497, 647-651.
 51. Pedersen, B. P., Kumar, H., Waight, A. B., Risenmay, A. J., Roe-Zurz, Z., Chau, B. H., Schlessinger, A., Bonomi, M., Harries, W., Sali, A., Johri, A. K., and Stroud, R. M. (2013) Crystal structure of a eukaryotic phosphate transporter, *Nature* 496, 533-536.
 52. Yin, Y., He, X., Szewczyk, P., Nguyen, T., and Chang, G. (2006) Structure of the multidrug

- transporter EmrD from *Escherichia coli*, *Science* 312, 741-744.
53. Sun, L., Zeng, X., Yan, C., Sun, X., Gong, X., Rao, Y., and Yan, N. (2012) Crystal structure of a bacterial homologue of glucose transporters GLUT1-4, *Nature* 490, 361-366.
54. Dang, S., Sun, L., Huang, Y., Lu, F., Liu, Y., Gong, H., Wang, J., and Yan, N. (2010) Structure of a fucose transporter in an outward-open conformation, *Nature* 467, 734-738.
55. Loll, P. J. (2014) Membrane proteins, detergents and crystals: what is the state of the art?, *Acta crystallographica. Section F, Structural biology communications* 70, 1576-1583.
56. Hunte, C., and Michel, H. (2003) 7 - Membrane Protein Crystallization, In *Membrane Protein Purification and Crystallization (Second Edition)* (Hunte, C., Jagow, G. V., and Schægger, H., Eds.), pp 143-160, Academic Press, San Diego.
57. Cordat, E., Mus-Veteau, I., and Leblanc, G. (1998) Structural studies of the melibiose permease of *Escherichia coli* by fluorescence resonance energy transfer. II. Identification of the tryptophan residues acting as energy donors, *The Journal of biological chemistry* 273, 33198-33202.
58. Maehrel, C., Cordat, E., Mus-Veteau, I., and Leblanc, G. (1998) Structural studies of the melibiose permease of *Escherichia coli* by fluorescence resonance energy transfer. I. Evidence for ion-induced conformational change, *The Journal of biological chemistry* 273, 33192-33197.
59. Barth, A. (2007) Infrared spectroscopy of proteins, *Bba-Bioenergetics* 1767, 1073-1101.
60. Goormaghtigh, E., Raussens, V., and Ruyschaert, J. M. (1999) Attenuated total reflection infrared spectroscopy of proteins and lipids in biological membranes, *Bba-Rev Biomembranes* 1422, 105-185.
61. Dave, N., Troullier, A., Mus-Veteau, I., Dunach, M., Leblanc, G., and Padros, E. (2000) Secondary structure components and properties of the melibiose permease from *Escherichia coli*: a fourier transform infrared spectroscopy analysis, *Biophysical journal* 79, 747-755.
62. Dave, N., Lorenz-Fonfria, V. A., Villaverde, J., Lemonnier, R., Leblanc, G., and Padros, E. (2002) Study of amide-proton exchange of *Escherichia coli* melibiose permease by attenuated total reflection-fourier transform infrared spectroscopy - Evidence of structure modulation by substrate binding, *Journal of Biological Chemistry* 277, 3380-3387.
63. Lorenz-Fonfria, V. A., Leon, X., and Padros, E. (2012) Studying substrate binding to reconstituted secondary transporters by attenuated total reflection infrared difference spectroscopy, *Methods in molecular biology* 914, 107-126.
64. Lin, Y., Fuerst, O., Granell, M., Leblanc, G., Lorenz-Fonfria, V., and Padros, E. (2013) The substitution of Arg149 with Cys fixes the melibiose transporter in an inward-open conformation, *Biochimica et biophysica acta* 1828, 1690-1699.
65. Leon, X., Lorenz-Fonfria, V. A., Lemonnier, R., Leblanc, G., and Padros, E. (2005) Substrate-induced conformational changes of melibiose permease from *Escherichia coli* studied by infrared difference spectroscopy, *Biochemistry* 44, 3506-3514.
66. Lorenz-Fonfria, V. A., and Padros, E. (2005) Maximum entropy deconvolution of infrared spectra: Use of a novel entropy expression without sign restriction, *Applied Spectroscopy* 59, 474-486.
67. León Madrenas, X. (2006) Estudi dels canvis estructurals de la permeasa de melibiosa d'*Escherichia coli* induïts per la unió dels substrats, In *Departament de Bioquímica i Biologia Molecular*, Universitat Autònoma de Barcelona.

68. Allen, M. P., and Tildesley, D. J. (1987) *Computer simulation of liquids*, Clarendon Press; Oxford University Press, Oxford England New York.
69. Shaikh, S. A., Li, J., Enkavi, G., Wen, P. C., Huang, Z., and Tajkhorshid, E. (2013) Visualizing functional motions of membrane transporters with molecular dynamics simulations, *Biochemistry* 52, 569-587.
70. Case, D. A., Cheatham, T. E., 3rd, Darden, T., Gohlke, H., Luo, R., Merz, K. M., Jr., Onufriev, A., Simmerling, C., Wang, B., and Woods, R. J. (2005) The Amber biomolecular simulation programs, *Journal of computational chemistry* 26, 1668-1688.
71. MacKerell, A. D., Bashford, D., Bellott, M., Dunbrack, R. L., Evanseck, J. D., Field, M. J., Fischer, S., Gao, J., Guo, H., Ha, S., Joseph-McCarthy, D., Kuchnir, L., Kuczera, K., Lau, F. T. K., Mattos, C., Michnick, S., Ngo, T., Nguyen, D. T., Prodhom, B., Reiher, W. E., Roux, B., Schlenkrich, M., Smith, J. C., Stote, R., Straub, J., Watanabe, M., Wiorkiewicz-Kuczera, J., Yin, D., and Karplus, M. (1998) All-atom empirical potential for molecular modeling and dynamics studies of proteins, *J Phys Chem B* 102, 3586-3616.
72. Kaminski, G. A., Friesner, R. A., Tirado-Rives, J., and Jorgensen, W. L. (2001) Evaluation and Reparametrization of the OPLS-AA Force Field for Proteins via Comparison with Accurate Quantum Chemical Calculations on Peptides†, *The Journal of Physical Chemistry B* 105, 6474-6487.
73. Stansfeld, P. J., Goose, J. E., Caffrey, M., Carpenter, E. P., Parker, J. L., Newstead, S., and Sansom, M. S. (2015) MemProtMD: Automated Insertion of Membrane Protein Structures into Explicit Lipid Membranes, *Structure* 23, 1350-1361.

2 OBJECTIVES

The *E. coli* melibiose permease is a member of the GPH membrane protein family, which can transport cations and sugars through biological membranes. This transporter has a strong hydrophobic character and a hypothetical secondary structure, which consists of 12 transmembrane helices. Although nowadays an important corpus of information is being gathered on the molecular structure of the sugar and cation binding sites and the molecular dynamics of the residues implicated during transport, little is still known on the importance of other parts of the protein, such as the inter-helical loops, for the transport mechanism. The main objective of the present work was to study the importance of loop 7-8 and the end part of helix VII for the function (sugar transport) of MelB_{EC}. This general objective was planned to be achieved through the following specific objectives:

1. Obtention of point mutants (Y256C, Y257C, F258C, S259A, S259C, Y260C, V261C, G263C, D264C, A265C, D266C, L267C, F268C).
2. Purification of the mutants and reconstitution into model membranes.
3. Characterization of substrate binding using FTIR and fluorescence spectroscopies.
4. Protein crystallization

3 MATERIALS AND METHODS

3.1 Materials

3.1.1 Reagents

Table 3.1 Reagents

| No. | Name | CAS | Company |
|------|---|-------------|---------------|
| R 1 | Ammonium Chloride | 12125-02-9 | Merck |
| R 2 | Melibiose | 585-99-9 | Sigma aldrich |
| R 3 | Imidazole | 288-32-4 | Sigma aldrich |
| R 4 | Potassium Phosphate | 16788-57-1 | Merck |
| R 5 | Ampicillin Sodium Salt | 69-52-3 | Melford |
| R 6 | n-Dodecyl- β -D-maltoside | 69227-93-6 | Melford |
| R 7 | 2-Mercaptoethanol | 60-24-2 | Sigma aldrich |
| R 8 | DNase I | | Roche |
| R 9 | RNase | | Roche |
| R 10 | HIS-Select [®] Nickel Affinity Gel | | Sigma aldrich |
| R 11 | Bio-Beads SM-2 Adsorbents | | Bio-Rad |
| R 12 | EDTA Disodium Salt | 6381-92-6 | Melford |
| R 13 | Potassium chloride | 7447-40-7 | Melford |
| R 14 | MES monohydrate | 145224-94-8 | Melford |
| R 15 | Glycine | 56-40-6 | Melford |
| R 16 | Sucrose | 57-50-1 | Melford |
| R 17 | Sodium Chloride | 7647-14-5 | Melford |
| R 18 | Potassium Phosphate, Monobasic | 7778-77-0 | Melford |
| R 19 | TRIS, [Tris(hydroxymethyl) aminomethane] | 77-86-1 | Melford |
| R 20 | Glycerol | 56-81-5 | Melford |
| R 21 | Thiamine hydrochloride | 67-03-8 | Sigma aldrich |
| R 22 | Calcium chloride | 10035-04-8 | Sigma aldrich |

| | | | |
|------|---|--------------|------------------------------|
| R 23 | Magnesium sulfate heptahydrate | 10034-99-8 | Merck |
| R 24 | Lysozyme from chicken egg white | 12650-88-3 | Sigma aldrich |
| R 25 | Polyoxyethylenesorbitan, monolaurate [Tween 20] | 9005-64-5 | Melford |
| R 26 | Tetracycline hydrochloride $\geq 95\%$ | 64-75-5 | Sigma aldrich |
| R 27 | E. coli Total Lipid Extract | 1240502-50-4 | Avanti Polar Lipids, Inc. |
| R 28 | KOD Hot Start DNA Polymerase | | Merck |
| R 29 | DpnI R0176S | | New England Biolabs (UK) Ltd |

All other materials were obtained from commercial sources.

3.1.2 Kits

Table 3.2 Kits

| | Kits | Company |
|-----|---------------------------------|----------------|
| K 1 | QIAprep Spin Miniprep Kit (250) | QIAGEN |
| K 2 | DC™ Protein Assay | BIO-RAD |

3.1.3 Instruments

Table 3.3 Instruments

| | Name | Company |
|-----|--|--|
| M1 | MaxQ™ 4000 Benchtop Orbital Shakers | Thermo Fisher Scientific Inc. |
| M2 | Heraeus™ Multifuge™ X3 Centrifuge Series | Thermo Fisher Scientific Inc. |
| M3 | Incubador con agitaci3n orbital WY-111, COMECTA® | INSTRUMENTACION CIENTIFICA TECNICA |
| M4 | IKA Magnetic stirrers | IKA® -WERKE GMBH & CO.KG |
| M5 | BACTERIOLOGICAL INCUBATORS | JP SELECTA S.A. |
| M6 | Multi-Purpose Floor-Standing Centrifuge 1236R | LABOGENE, Inc. |
| M7 | Microultracentr fuga Sorvall Discovery M150 SE | Thermo Fisher Scientific Inc. |
| M8 | Ultracentrifuge Sorvall Combi Plus | Thermo Fisher Scientific Inc. |
| M9 | Revco Ultra-low Temperature Freezer | Thermo Fisher Scientific Inc. |
| M10 | Test tube shakers Reax top | Heidolph Instruments GmbH & Co.KG |
| M11 | Denver Instrument MXX-123 | Denver Instrument |
| M12 | Precisa Series Balances model 1834-43 | Precisa Gravimetrics AG |
| M13 | Elix® Essential 10 Water Purification Systems | Merck Millipore (is a division of Merck KGaA) |

| | | |
|-----|--|--------------------------|
| M14 | Scotsman AF80 Ice Flaker | Hubbard systems |
| M15 | Microfluidizer Model 1108 | Microfluidics |
| M16 | Tectron Bio-100 | JP SELECTA S.A. |
| M17 | Sartorius Basic plus BP3100P | Sartorius Spain S.A. |
| M18 | Medidor PH BASIC 20 | CRISON INSTRUMENTS, S.A. |
| M19 | Varian Cary 50 Bio UV/ Visible Spectrophotometer | Varian, Inc |
| M20 | Varian FTIR 700e | Varian, Inc |
| M21 | GRELCO G-1312 | Grelco |
| M22 | PCR Thermal Cyclers | VWR International, LLC |

3.1.4 Buffers

Table 3.4 buffers

| Name | Composition |
|---|--|
| Luria Bertani (LB) broth | 12 M Tryptone 3 M Yest extract 3 M NaCl |
| LB Agar | 12 M Tryptone 3 M Yest extract 3 M NaCl 9 M agar |
| MacConkey Agars | 40 M MacConkey Agar Base power 30 mM melibiose 0.1 M Ampicillin 10 mM Tetracycline |
| Buffer for prepare competent cells | |
| <i>Buffer I</i> | 12 M RbCl 9.9 M MnCl ₂ 4H ₂ O 3 % (v/v) 1 M K-Acetate pH 7.5 1.5 M CaCl ₂ 2H ₂ O 0.15 M Glycerol |
| <i>Buffer II</i> | 12 M RbCl 2 % (v/v) 0.5 M MOPS pH 6.8 1100 M CaCl ₂ 2H ₂ O 150 M Glycerol |
| M9 Medium | 7.5 M Na ₂ HPO ₄ 2H ₂ O |

| | |
|-----------------------------|------------------------------|
| | 3 M KH_2PO_4 |
| | 1 M NH_4Cl |
| | 0.5 M NaCl |
| | pH 7.5 |
| | 54 mM Glycerol |
| | 1 mM MgSO_4 |
| | 0.1 mM CaCl_2 |
| | 0.34 M Thiamine - HCl |
| | 2 M Casamino acid |
| | 0.1 M Ampicilin |
| Resuspension Buffer | 50 mM Tris - HCl |
| | 50 mM NaCl |
| | 5 mM 2 - Mercaptoethanol |
| | pH 8 |
| Purification buffer | |
| <i>Buffer I (2X)</i> | 20% (v/v) Glycerol |
| | 1.2 M NaCl |
| | 40 mM Tris - HCl pH 8 |
| | 10 mM 2-mercaptoethanol |
| <i>Buffer 9/10</i> | 10% (v/v) Glycerol |
| | 0.6 M NaCl |
| | 20 mM Tris - HCl pH 8 |
| | 5 mM 2-mercaptoethanol |
| | 10 mM Imidazol pH 8 |
| | 10 mM Melibiose |
| <i>Buffer A</i> | 10% (v/v) Glycerol |
| | 0.6 M NaCl |
| | 20 mM Tris - HCl pH 8 |
| | 5 mM 2-mercaptoethanol |
| | 10 mM Imidazol pH 8 |
| | 10 mM Melibiose |
| | 2 mM LAPAO |
| <i>Buffer B</i> | 10% (v/v) Glycerol |
| | 0.6 M NaCl |
| | 20 mM Tris - HCl pH 8 |
| | 5 mM 2-mercaptoethanol |
| | 10 mM Imidazol pH 8 |
| | 10 mM Melibiose |
| | 1 mM β -DDM |
| <i>Buffer C</i> | 10% (v/v) Glycerol |
| | 0.1 M NaCl |
| | 20 mM Tris - HCl pH 8 |
| | 5 mM 2-mercaptoethanol |
| | 10 mM Imidazol pH 8 |

| | |
|--|------------------------|
| | 10 mM Melibiose |
| | 1 mM β -DDM |
| Buffer D | 10% (v/v) Glycerol |
| | 0.1 M NaCl |
| | 20 mM Tris - HCl pH 8 |
| | 5 mM 2-mercaptoethanol |
| | 10 mM Imidazol pH 8 |
| | 10 mM Melibiose |
| | 1 mM β -DDM |
| Buffer of infrared spectroscopy experiments | |
| Wash-buffer | 20 mM MES |
| | 100 mM KCl |
| | pH 6.6 |
| Wash-buffer I | 20 mM MES |
| | 110 mM KCl |
| | pH 6.6 |
| Wash-buffer II | 20 mM MES |
| | 150 mM KCl |
| | pH 6.6 |
| 10 mM Na⁺ buffer | 20 mM MES |
| | 100 mM KCl |
| | 10 mM NaCl |
| | pH 6.6 |
| 50 mM Na⁺ buffer | 20 mM MES |
| | 100 mM KCl |
| | 50 mM NaCl |
| | pH 6.6 |
| 50 mM Mel buffer | 20 mM MES |
| | 100 mM KCl |
| | 50 mM Melibiose |
| | pH 6.6 |
| 10 mM Mel, 10 mM Na⁺ buffer | 20 mM MES |
| | 100 mM KCl |
| | 10 mM NaCl |
| | 10 mM Melibiose |
| | pH 6.6 |
| 50 mM Mel, 10 mM Na⁺ buffer | 20 mM MES |
| | 100 mM KCl |
| | 10 mM NaCl |
| | 50 mM Melibiose |
| | pH 6.6 |
| ISO buffer | |
| Wash buffer | 50 mM Tris-HCl |
| | pH 8.0 |

| | |
|-------------------------------------|---|
| <i>Storage buffer</i> | 100 mM Kpi 10 mM EDTA pH 7 |
| Crystallization buffer | |
| <i>Wash buffer/ Dialysis buffer</i> | 0.17 mM β -DDM 20 mM Tris pH 7.5 50 mM Glycerol 2 mM DTT 100 mM NaCl 10 mM Melibiose |
| <i>Elute buffer</i> | 0.17 mM β -DDM 20 mM Tris pH 7.5 50 mM Glycerol 2 mM DTT 100 mM NaCl 10 mM Melibiose 300 mM Imidazole |

3.2 Methods

3.2.1 Obtaining the mutant proteins and the Cless protein

3.2.1.1 Bacterial strains and plasmids

The *E. coli* strain DW2-R (*melA*⁺ Δ *melB*, Δ *lacZY*) was used in most of the study ¹. The strain was the *recA*-depleted version of the maternal DW2 strain, in which the genes of the melibiose permease (*MelB*) and lactose permease (*lacYZ*) have been depleted, and it has a tetracycline resistance gene. The recombinase A is encoded by the *recA* gene, which can cause homologous recombination. Thus, its depletion keeps plasmid integrity after insertion.

The plasmid pK95 Δ AHB used in this study was derived from the pKK 223-3 plasmid. The vector pK95 Δ AHB contains the *melB* gene with a genetically engineered six successive His residues at the C-terminal, an ampicillin resistant gene, and a part of the *melA* gene. The *melB* gene encodes for the melibiose permease and the *melA* gene for the α -galactosidase from *E. coli*. The presence of part of the *melA*

gene resulted in an increased expression of the melibiose permease. The expression of the *melB* gene and *melA* gene are controlled by a tac-promoter. The extra His-tag had no effect upon the transport activity of the melibiose permease ².

Another *E. coli* strain DH5 α was also used in our study, but only to amplify the pK95 Δ AHB plasmid after the PCR reaction, because of its high transformation efficiency.

3.2.1.2 Site-directed mutagenesis

The template *melB* gene used throughout our study was a Cless gene and the expressed protein showed the same activity as the wild type. The Cless means absence of cysteine in the *melB* gene, and the natural cysteine genes were replaced by valine (Cys-235) or serines (Cys-110, Cys-310 and Cys-364) ³.

The primers were designed from the website (<http://bioinformatics.org/primerx>). Table 5 shows the list of primers used in this study.

The parameters were set as: 1) melting temperature from 60 to 85 °C; 2) GC content 40-60%; 3) length: 25 to 45 bp; 4) the mutation site in the center; 5) termination in G or C is required for most cases; 6) the primer pair should be complementary to each other.

Table 3.5 The primers used in the PCR

| No. | Primer | Sequence ¹ | Amino acid change |
|-----|---------|--|-------------------|
| 1 | Y256C-F | 5' CCGGCTTTGCTATCTGTTATTCTCATATG 3' | Tyr → Cys |
| | Y256C-R | 5' CATATGAGAAATAACAGATAGCAAAGCCGG 3' | Tyr → Cys |
| 2 | Y257C-F | 5' CCGGCTTTGCTATCTATTGTTTCTCATATGTTATCGG 3' | Tyr → Cys |
| | Y257C-R | 5' CCGATAACATATGAGAAACAATAGATAGCAAAGCCGG 3' | Tyr → Cys |
| 3 | F258C-F | 5' CCGGCTTTGCTATCTATTATTGCTCATATGTTAYCGGTGATG 3' | Phe → Cys |
| | F258C-R | 5' CATCACCGATAACATATGAGCAATAATAGATAGCAAAGCCGG 3' | Phe → Cys |
| 4 | S259A-F | 5' GCTTTGCTATCTATTATTCGCATATGTTATCGGTGATGCGG 3' | Ser → Ala |

| | | | |
|----|---------|--|-----------|
| | S259A-R | 5' CCGCATCACCGATAACATATG C GAAATAATAGATAGCAAAGC 3' | Ser → Ala |
| 5 | S259C-F | 5' GGCTTTGCTATCTATTATTTCT GCT ATGTTATCGGTGATGCGGAT 3' | Ser → Cys |
| | S259C-R | 5' ATCCGCATCACCGATAACATA GC AGAAATAATAGATAGCAAAGCC 3' | Ser → Cys |
| 6 | Y260C-F | 5' CTATTATTTCTCAT GCG TTCGTTATCGGTGATGCG 3' | Tyr → Cys |
| | Y260C-R | 5' CGCATCACCGATAAC GC ATGAGAAATAATAG 3' | Tyr → Cys |
| 7 | V261C-F | 5' TTATTTCTCATAT TGC ATCGGTGATGCGG 3' | Val → Cys |
| | V261C-R | 5' CCGCATCACCGAT GCA ATATGAGAAATAA 3' | Val → Cys |
| 8 | G263C-F | 5' TTCTCATATGTTATCT TGCG ATGCGGATTTGTTCCC 3' | Gly → Cys |
| | G263C-R | 5' GGGAAACAAATCCGCAT CGCA GATAACATATGAGAAA 3' | Gly → Cys |
| 9 | A265C-F | 5' GTTATCGGTGAT TGCG GATTTGTTCCC 3' | Ala → Cys |
| | A265C-R | 5' GGGAAACAAAT GCA ATCACCGATAAC 3' | Ala → Cys |
| 10 | D266C-F | 5' CATATGTTATCGGTGATGCG TG TTTGTTCCTATTATCTG 3' | Asp → Cys |
| | D266C-R | 5' CAGATAATAGGGGAACAAA CA CGCATCACCGATAACATATG 3' | Asp → Cys |
| 11 | L267C-F | 5' CCGTGATGCGGATT GCT TCCCCTATTATCTG 3' | Leu → Cys |
| | L267C-R | 5' CAGATAATAGGGGAA GCA ATCCGCATCACCG 3' | Leu → Cys |
| 12 | F268C-F | 5' GTGATGCGGATTTGT G CCCCTATTATCTGTC 3' | Phe → Cys |
| | F268C-R | 5' GACAGATAATAGGGG C ACAAATCCGCATCAC 3' | Phe → Cys |

¹mutated nucleotides are written in red bold characters

The site-directed mutation PCR is a simple process, where a double-primer PCR mutagenesis protocol ⁴ was used, as shown in Figure 3.1.

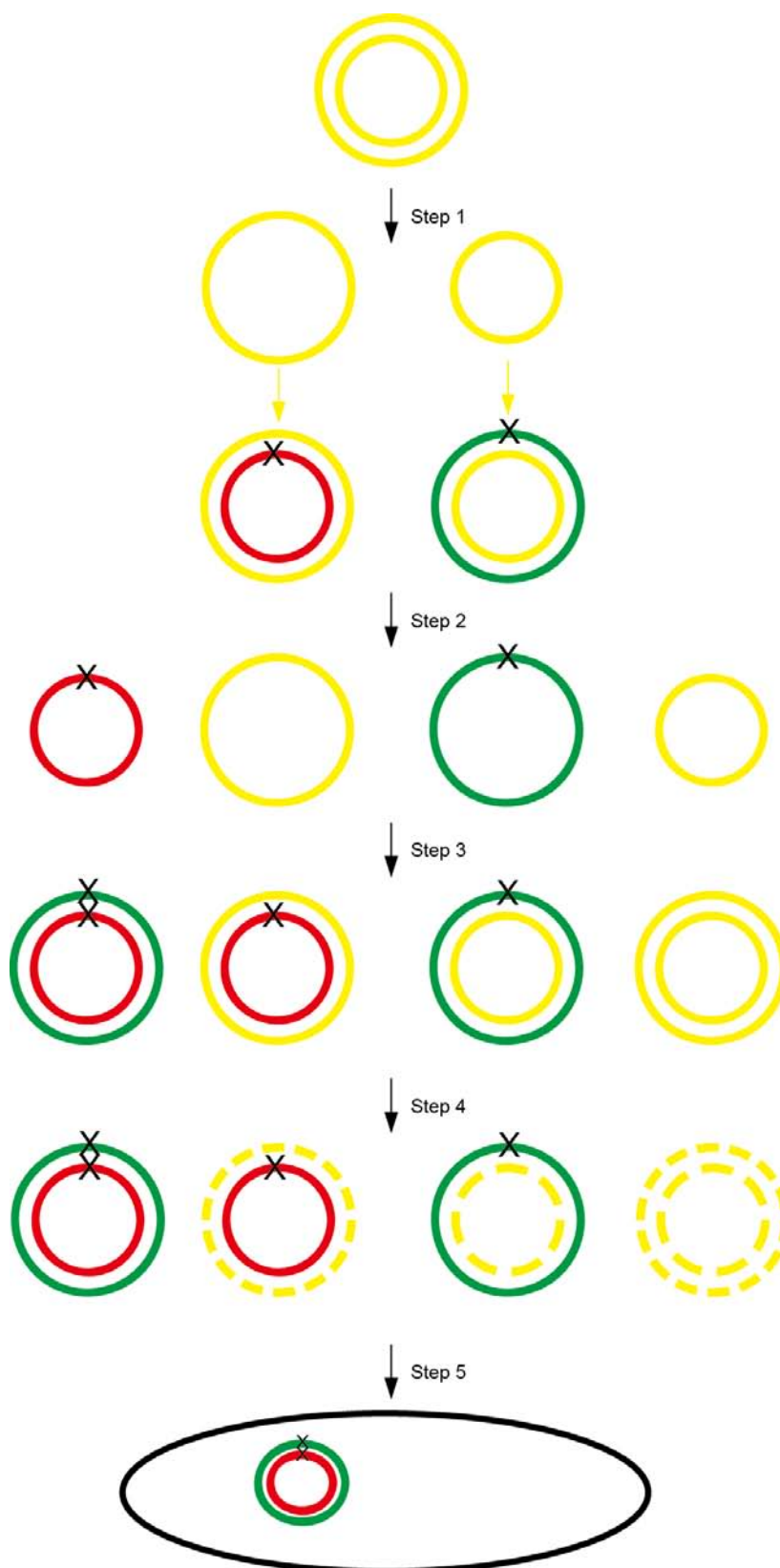


Figure 3.1 Schematic summary of the double-primer PCR mutagenesis protocol (see the text for explanation)

The site-directed mutagenesis procedure was as follows:

1. Forward or reverse primers were amplified in two separate PCR reactions containing the Cless template.

2. Forward and reverse primer PCR products were mixed in one test tube and denatured in order to separate the newly synthesized products from the plasmid template.

3. Complementary strands were allowed to anneal at the given temperature (55 °C).

4. Since the template DNA was methylated, but the mutated or the newly synthesized were not, the mixture was digested with DpnI.

5. The reannealed new plasmids were transformed into competent *E. coli* DH5 α cells.

The primers were synthesized by Invitrogen of Thermo Fisher Scientific Corporation. The initial quantity of template DNA required in the reaction as well as other components is listed in Table 3.6.

Table 3.6 The components of PCR

| Element | Tube 1 | Tube 2 |
|---|--------------|--------------|
| Template plasmid DNA | 500 ng | 500 ng |
| Forward primer | 40 pmol | - |
| Reverse primer | - | 40 pmol |
| MgCl ₂ | 0.2 mM | 0.2 mM |
| dNTPs | 0.2 mM | 0.2 mM |
| 10x PCR buffer for KOD hot start DNA polymerase | 2.5 μ L | 2.5 μ L |
| Sterile water | | |
| KOD hot start DNA polymerase | 4 U/ μ L | 4 U/ μ L |
| Final volume | 25 μ L | 25 μ L |

The programmed cycles were:

a) The initial denaturation was performed at 95 °C for five minutes.

b) The following process was repeated for 30 times: denaturing DNA at 95 °C for

50 Seconds; annealing the primer at 55 °C for 50 Seconds; elongating the DNA at 68 °C for seven minutes.

After the 30 cycles, the two products from the two tubes were mixed and then transferred into the PCR machine (VWR PCR Thermal Cyclers) again, with the following procedure: 95 °C for five minutes, 90 °C for 1 minute, 80 °C for one minute, 80 °C for 30 seconds, 70 °C for 30 seconds, 60 °C for 30 seconds, 40 °C for 30 seconds, 37 °C for one minute.

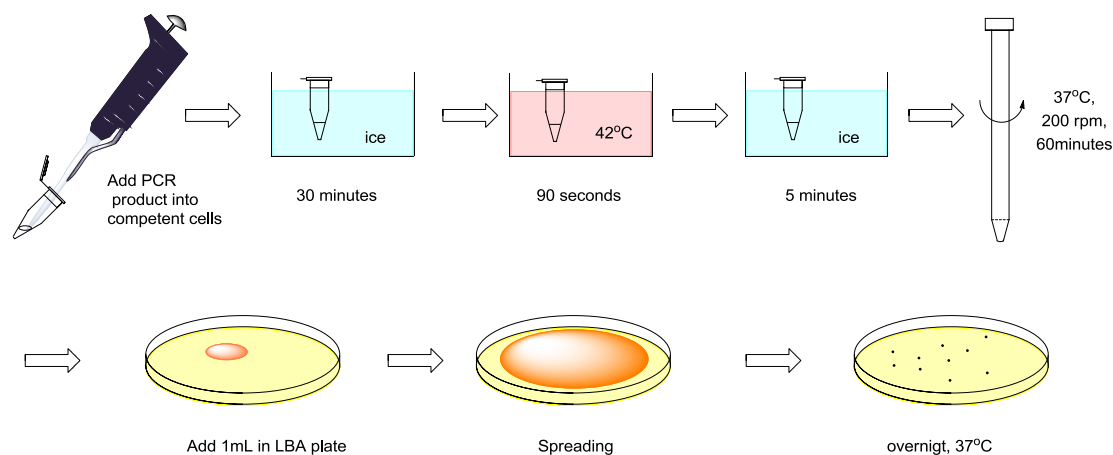


Figure 3.2 Obtaining the colonies

After mixing the products, a digestion with 600 U/mL DpnI at 37 °C was carried out overnight. The mixture was transformed into *E. coli* DH5 α competent cells by incubating 30 minutes on ice, followed by heat-shocking at 42 °C for 90 seconds and then transferred on ice for 5 minutes. After adding one mL LB medium, the cells were incubated using moderate shaking at 37 °C for 60 minutes. Then the cells were precipitated by centrifugation at 3000 g for five minutes (Multi-Purpose Floor-Standing Centrifuge 1236R). Pellets were resuspended in 100 μ L LB, and 100 μ L of the cell suspension was spread in a Petri dish containing 100 μ g/mL ampicillin (Figure 3.2). After incubating the plates overnight at 37 °C, 3 colonies were selected at random and grown overnight in 12 mL LB medium plus 100 μ g/mL ampicillin at 37 °C. The plasmids were isolated using a QIAprep Spin Miniprep Kit. The plasmids were checked by DNA sequencing at the Center for Research in Agricultural Genomics of the Universitat Autònoma de Barcelona. (See the results in the appendix

1).

The correct plasmids were amplified by using *E. coli* DH5 α cells and finally transformed into *E. coli* DW2-R cells for future use in protein purification.

In this thesis, the notation used for the MelB mutants has been the one-letter code followed by the position of the residue in the Cless (which we used as wild-type) protein and a final character indicating the amino acid substitution.

Table 3.7 Mutations

| Residue number | Amino acid change | Rename |
|----------------|-------------------|--------|
| 256 | Y→C | Y256C |
| 257 | Y→C | Y257C |
| 258 | F→C | F258C |
| 259 | S→A | S259A |
| 259 | S→C | S259C |
| 260 | Y→C | Y260C |
| 261 | V→C | V261C |
| 263 | G→C | G263C |
| 264 | D→C | D264C |
| 265 | A→C | A265C |
| 266 | D→C | D266C |
| 267 | L→C | L267C |
| 268 | F→C | F268C |

3.2.1.3 Bacterial cell culture

The *E. coli* DW2-R cells with a plasmid containing wild-type or mutated *melB* genes were stored in 30% glycerol solution at -80 °C. Before the large-scale expression of the MelB protein, the DW2-R cells were streaked on MacConkey plates and incubated at 30 °C overnight. A desired single colony from plates was inoculated into a mini culture of 12 mL LB containing 100 µg/mL ampicillin and 10 µg/mL

tetracycline and incubated at 30 °C at 200 rpm overnight. Subsequently, the 12 mL mini culture was poured into 400 mL M9 medium which was supplemented with 10 µg/mL tetracycline (midi culture) and incubated at 30 °C at 200 rpm for around 8 h. For the big cultures, 50 mL of the midi culture was poured into 1 L of M9 medium and incubated at 30 °C at 200 rpm overnight (Figure 3.3). Bacterial cells were harvested by centrifuging at 3134 g (Multi-Purpose Floor-Standing Centrifuge 1236R) for 30 minutes. Pellets were resuspended in resuspension buffer with supplemented 10-15% glycerol, and frozen at -80 °C until further use.

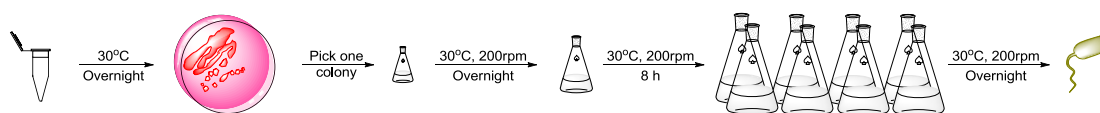


Figure 3.3 Cell growth

3.2.1.4 Protein purification

The protein purification protocol was based on the one described by Pourcher *et al.*². A summary of the protocol is given in Figure 3.5. The frozen cells were thawed at 30 °C in a water bath and washed with resuspension buffer. Then the cells were resuspended in the same buffer and incubated with 1 mM lysozyme and 15 mM EDTA (dissolved with 3 M NaOH) at 4°C for 30 minutes with slight shaking to destabilize the external bacterial membranes. Before the cells were lysed or disrupted using the microfluidizer three times at 20,000 psi, 20 µg/mL DNAase, 20 µg/mL RNAase, and 15 mM MgSO₄ were added as final concentrations. The pellets, containing the resulting inside out vesicles were collected at a centrifugal force of 100,000 g for 1 hour. The pellets were washed with purification buffer I and centrifuged again in the same conditions for one hour. The pellets were resuspended in buffer 9/10 and solubilized by adding 1% (w/v) LAPAO for 30 minutes at 4 °C or 1% (w/v) DDM and 0.1 mM AEBSF (protease inhibitor) for 2 hours at 4 °C. Following another ultracentrifugation at 100,000 g for 50 minutes, the supernatants were collected. To separate the MelB protein from other solubilized proteins,

Ni²⁺-NTA affinity resin was added into the detergent-protein mixture at 4 °C for 1 hour in an orbital shaker. Ni²⁺-NTA affinity resin was washed previously with water, buffer I (1X) for three times and finally stored in buffer A. The MelB protein binds to the Ni²⁺-NTA affinity resin by the genetically engineered histidine tag. The resin with the bound protein was collected by centrifuging at 4000g for 5 minutes, and the pellet was washed with the buffer A. This resin was loaded into the column (Bio-Rad), and washed with one column volume of buffer A. Thereafter, the detergent was exchanged by washing with three column volumes of buffer B (if LAPAO was used to solubilize the membrane, then it was exchanged to DDM. Otherwise this step is not needed). The next step is to reduce the concentration of salt by washing with three column volumes of the buffer C. The protein was eluted with buffer D, and the eluent was collected in 1.5 mL aliquots. The concentration of purified protein in each aliquot was estimated by measuring the UV absorbance at 280 nm using a quartz cuvette. The protein yield was calculated by the equation shown in Figure 3.4. In practice, following this method, the maximum amount of purified MelB Cless or mutants obtained from 4 L cells were between 1 and 8 mg. The pure protein was pooled and frozen at -80 °C until used.

$$\text{Yield (mg)} = \frac{\text{Absorbance at 280 nm} \times \text{Volume (mL)}}{\text{Extinction coefficient of MelB}}$$

Figure 3.4 Equation for the calculation of the yield of the purified MelB

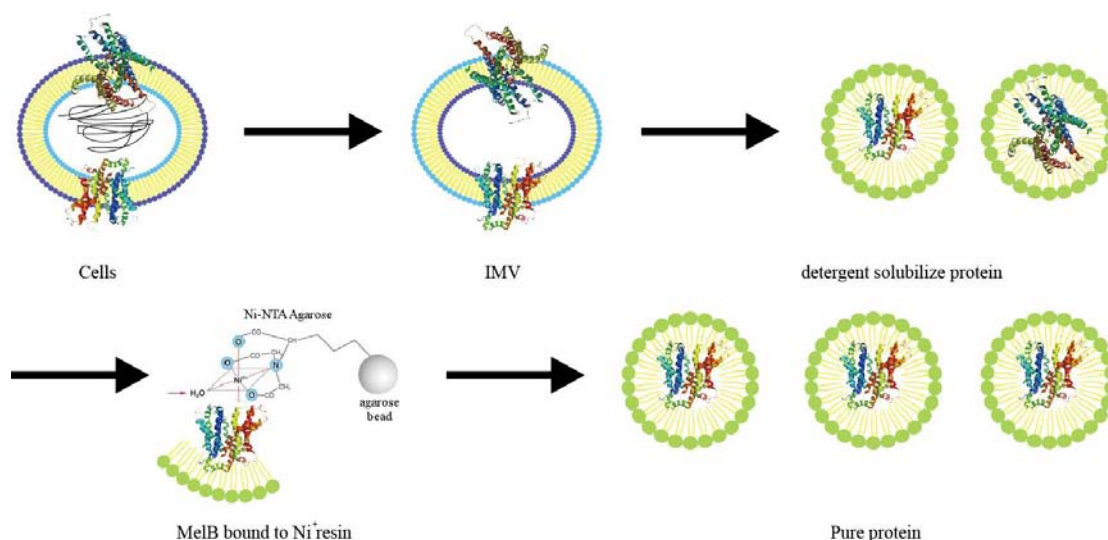


Figure 3.5 the purification process: the cells were broken to IMV, then detergent solubilized protein from IMV, the proteins contained His-tag were bound to nickel resin, after washed, the pure MelB proteins were eluted

3.2.1.5 Protein reconstitution

Protein reconstitution in model membranes (liposomes) was carried out following a procedure based on the adsorption of detergent with Bio-Beads. *E. coli* lipids were dissolved rapidly in chloroform, and the chloroform was evaporated using a rotary evaporator. In this way, a very thin lipid film was obtained. Usually, the *E. coli* total lipids were prepared from a stock solution at a concentration of 10 mg/mL buffer (20 mM MES, 100 mM KCl, pH 6.6). The lipid-buffer mix was vortexed for at least 5 min at room temperature to form large liposomes, and then it was aliquoted and stored at -80°C until further use. Those liposomes were disrupted by extrusion using $0.1\ \mu\text{m}$ pore-size filter in order to downsize the diameter and yield a homogeneous unilamellar liposome population prior to use. The liposomes were added at a ratio of 2:1 of lipid:protein (w/w) into the protein solution. Before use, Bio-Beads SM-2 (Bio-Rad) were washed more than 6 times with distilled water, and one time with buffer (20 mM MES, 100 mM KCl, pH 6.6). After drying, they were distributed into three aliquots based on 120 ~ 150 mg of Bio-Beads every one milliliter protein solution. The liposomes were directly added to the protein solution at 4°C and the Bio-Beads aliquots were added by 10 min interval, then for efficient

detergent adsorption and protein insertion into the liposomes, the mixture was incubated at 4 °C overnight with slight shaking. The proteoliposomes were formed as shown in Figure 3.6. The Bio-Beads were separated from the mixture by using a column (Bio-Rad). Proteoliposomes were collected by centrifuging at approximately 310,000 g at 4 °C for 35 min. The pellets were washed twice with buffer (20 mM MES, 100 mM KCl, pH 6.6). Proteoliposomes were finally resuspended in the same buffer at approximately 20 mg/mL, then aliquoted and frozen at -80 °C for subsequent use.

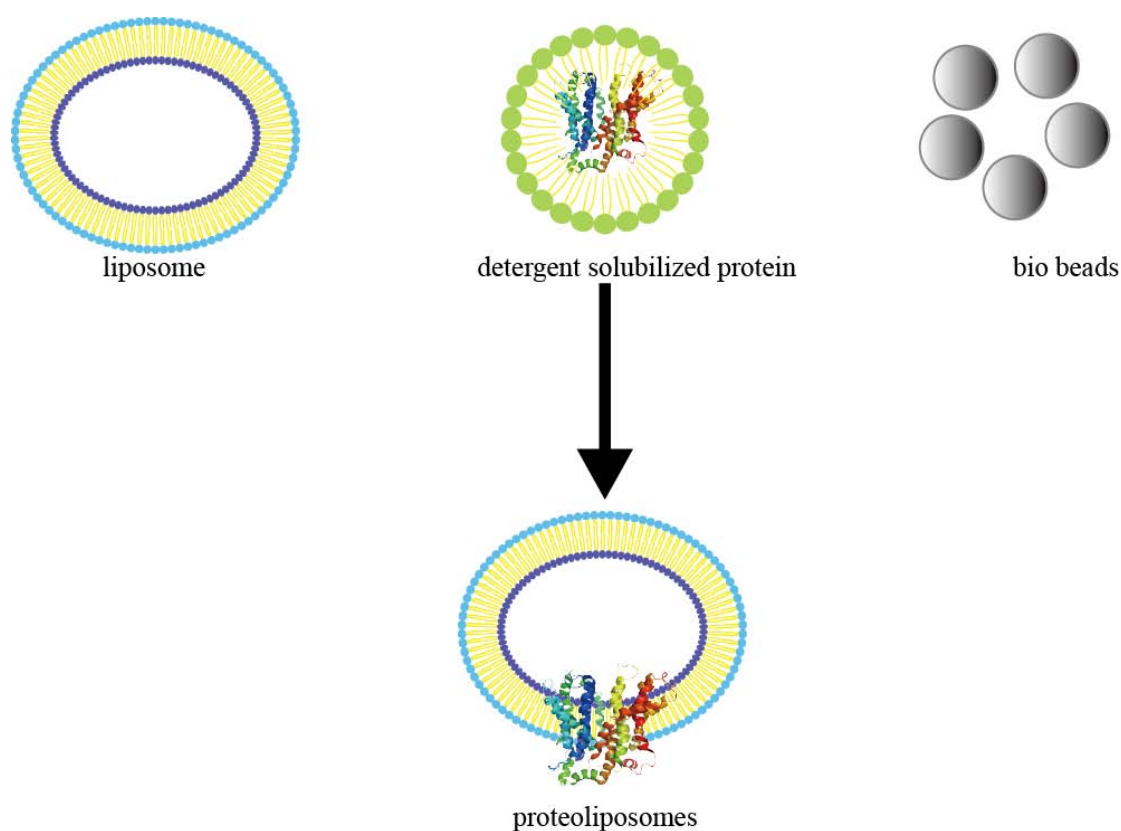


Figure 3.6 Protein reconstitution: detergent was adsorbed by bio-beads, and at the same time protein inserted into the liposomes

3.2.2 Preparation of vesicles

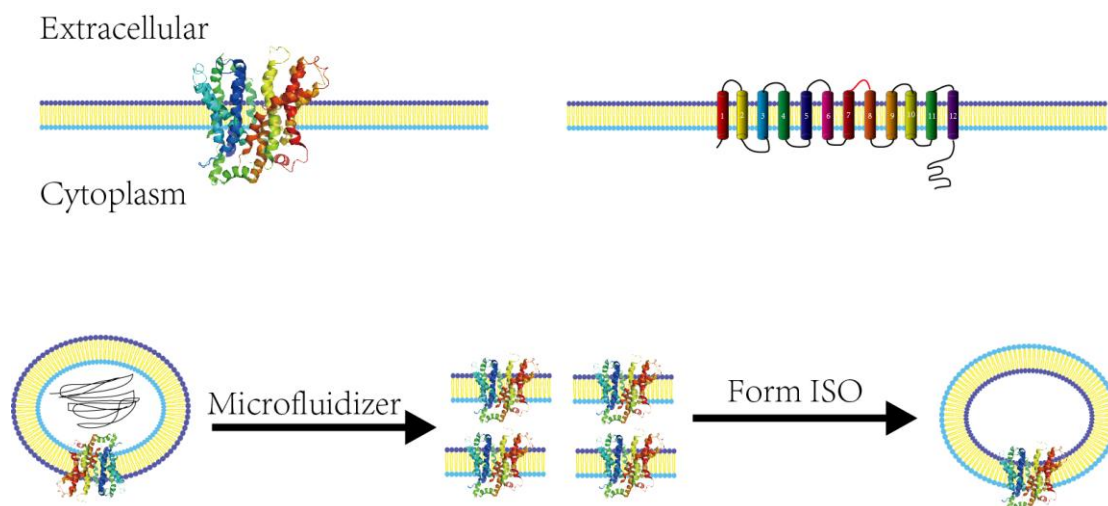


Figure 3.7 the formation of ISO vesicles.

3.2.2.1 Inside-out vesicles

The ISO membrane vesicles were prepared using a microfluidizer (Figure 3.7) which is similar as a French press^{2, 5}. In short, approximately 3 g (wet weight) of cells was rapidly thawed at 30 °C and washed twice with buffer (10 mM Tris-HCl, pH 8.0). Cells were resuspended in 100 ml of the same buffer supplemented with 558 mg EDTA (dissolved in KOH) and 100 mg lysozyme, then incubated at 4 °C for 30 min with slight shaking. Before applying a pressure of 20000 psi, 20 µg/mL of DNase and RNase were added and activated by 15 mM MgSO₄. This solution was passed through the microfluidizer 3 times. The unbroken cells and large debris were eliminated by centrifugation at 8000 g for 5 min. The supernatant was collected and centrifuged at 146,000 g for 35 minutes. The ISO membrane vesicles were washed 3 times with buffer (100 mM Kpi, 10 mM EDTA pH 7), and resuspended in the same buffer, frozen in liquid nitrogen and stored at -80 °C until use.

3.2.2.2 Protein quantification of Inside-out vesicles

The Lowry's method⁶ was used to check the total amount of protein in the ISO membrane vesicles. The MelB protein was determined by western blot (Figure 3.8) using the Histidine-Tag-specific reagent His-ProbeTM-HRP.

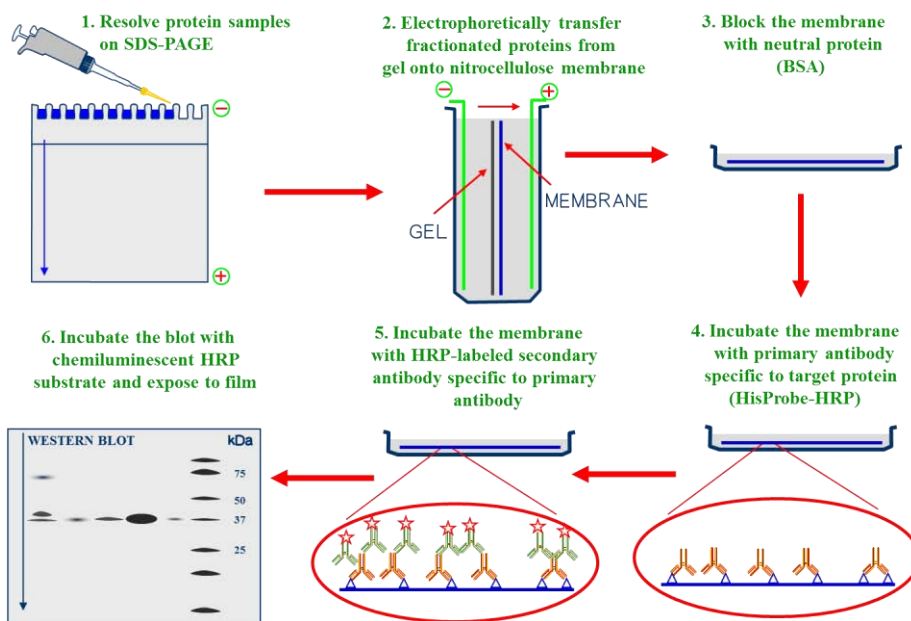


Figure 3.8 The western blot.

3.2.3 Fourier transform infrared spectroscopy (FTIR)

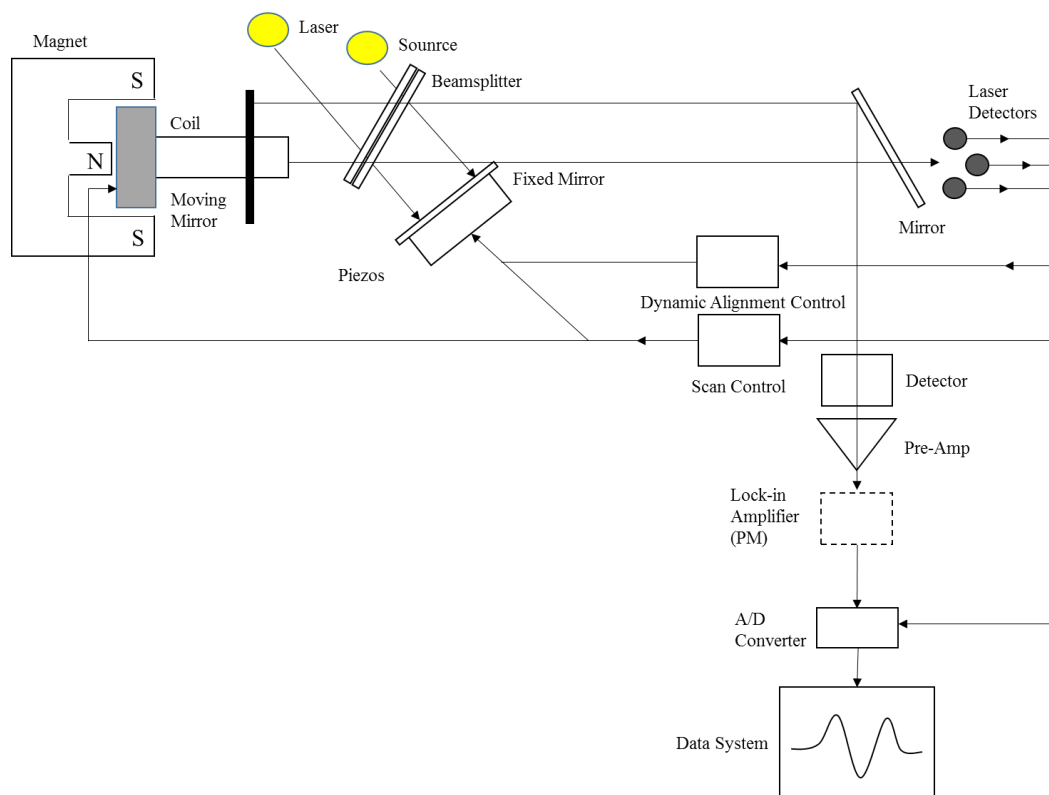


Figure 3.9 Schematic depiction of the Michelson interferometer

Infrared spectroscopy is one of the methods for protein structure determination.

A protein infrared spectrum provides a lot of information on the structure and the environment of the protein backbone and the amino acid side chains⁷. One of the advantages of this method is that in order to get the spectrum, there is no need to add any external probes. For the sample, one can reconstitute the membrane protein in liposomes⁸⁻¹⁰, resuspend it in solutions (organic, detergent or other buffers)^{8, 9, 11}, as well as in dry films¹².

The heart of an FTIR spectrometer is the Michelson interferometer shown in Figure 3.9. The interferometer contains a fixed mirror, a moving mirror, and a beamsplitter. The beamsplitter transmits half of the incident radiation to the moving mirror and reflects the other half to the fixed mirror. The two beams are reflected by these mirrors back to the beamsplitter, where they recombine. When the fixed mirror and the moving mirror are equidistant from the beamsplitter, the amplitudes of all frequencies are in phase and recombine constructively. This position of zero path difference (ZPD), or zero retardation, is where the interferogram center-burst occurs. As the moving mirror is moved away from the beamsplitter (retarded) an optical path difference is generated. As the position of the moving mirror changes, the two beams travel different distances within the interferometer before recombining. A pattern of constructive and destructive interferences is generated based on the position of the moving mirror and the frequency of the retardation. The intensity of the radiation varies in a complicated pattern as a function of the moving mirror position, and the output beam is the result of the modulation by the interferometer. This modulated output beam is then directed through the sample compartment to the detector. At the detector it generates a continuous electrical signal called an interferogram. Then the spectra is obtained from Fourier transformed interferograms (Figure 3.10).

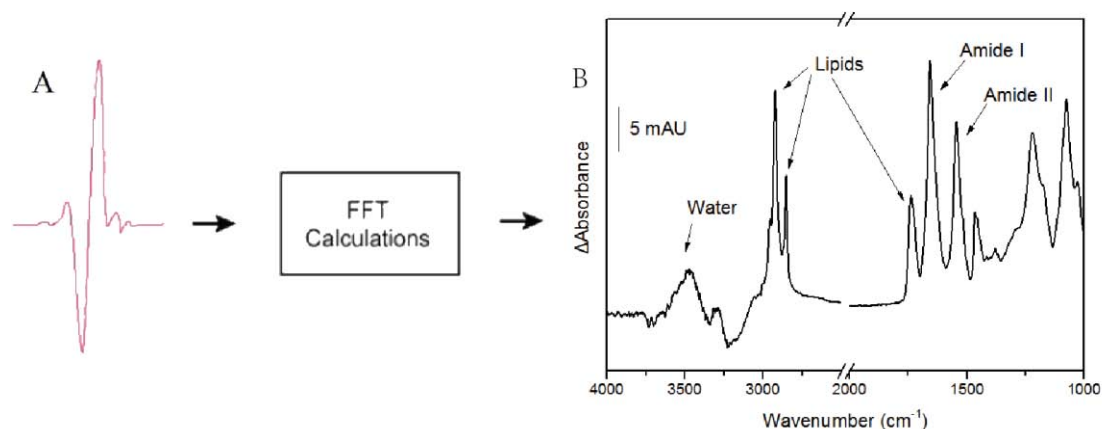


Figure 3.10 Translation of the interferogram into a spectrum by Fourier Transformation. (A) Interferogram. (B) An infrared spectrum, which plots absorption (or transmittance) versus wavenumber.

In the spectra there are many bands; an overview of amino acid side chain infrared bands is listed in Table 3.8.

Table 3.8 Overview of amino acid side chain infrared bands*

| Assignments | Band position/cm ⁻¹ , (ε/M ⁻¹ cm ⁻¹) in ¹ H ₂ O | Band position/cm ⁻¹ , (ε/M ⁻¹ cm ⁻¹) in ² H ₂ O |
|---|--|--|
| Cys, ν(SH) | 2551 | 1849 |
| Asp, ν(C=O) | 1716 (280) | 1713 (290) |
| Glu, ν(C=O) | 1712 (220) | 1706 (280) |
| Asn, ν(C=O) | 1677–1678 (310–330) | 1648 (570) |
| Arg, ν _{as} (CN ₃ H ₅ ⁺) | 1652–1695 (420–490) | 1605–1608 (460) |
| Gln, ν(C=O) | 1668–1687 (360–380) | 1635–1654 (550) |
| Arg, ν _s (CN ₃ H ₅ ⁺) | 1614–1663 (300–340) | 1581–1586 (500) |
| HisH ₂ ⁺ , ν(C=C) | 1631 (250) | 1600 (35), 1623 (16) |
| Lys, δ _{as} (NH ₃ ⁺) | 1626–1629 (60–130) | 1201 |
| Tyr-OH, ν(CC) δ(CH) | 1614–1621 (85–150) | 1612–1618 (160) |
| Asn, δ(NH ₂) | 1612–1622 (140–160) | |
| Trp, ν(CC), ν(C=C) | 1622 | 1618 |
| Tyr-O ⁻ , ν(CC) | 1599–1602 (160) | 1603 (350) |
| Tyr-OH, ν(CC) | 1594–1602 (70–100) | 1590–1591 (<50) |
| Gln, δ(NH ₂) | 1586–1610 (220–240) | 1163 |
| HisH, ν(C=C) | 1575, 1594 (70) | 1569, 1575 |
| Asp, ν _{as} (COO ⁻) | 1574–1579 (290–380) | 1584 (820) |
| Glu, ν _{as} (COO ⁻) | 1556–1560 (450–470) | 1567 (830) |
| Lys, δ _s (NH ₃ ⁺) | 1526–1527 (70–100) | 1170 |
| Tyr-OH, ν(CC), δ(CH) | 1516–1518 (340–430) | 1513–1517 (500) |

| | | |
|---|------------------------|------------------------|
| Trp, $\nu(\text{CN})$, $\delta(\text{CH})$, $\delta(\text{NH})$ | 1509 | |
| Tyr-O ⁻ , $\nu(\text{CC})$, $\delta(\text{CH})$ | 1498–1500 (700) | 1498–1500 (650) |
| Trp, $\nu(\text{CC})$, $\delta(\text{CH})$ | 1496 | |
| Phe, $\nu(\text{CCring})$ | 1494 (80) | |
| $\delta_{\text{as}}(\text{CH}_3)$ | 1445–1480 | |
| $\delta(\text{CH}_2)$ | 1425–1475 | |
| Pro, $\nu(\text{CN})$ | 1400–1465 | |
| Trp, $\delta(\text{CH})$, $\nu(\text{CC})$, $\nu(\text{CN})$ | 1462 | 1455 (200) |
| His ⁻ , $\delta(\text{CH}_3)$, $\nu(\text{CN})$ | 1439 | 1439 |
| Trp, $\delta(\text{NH})$, $\nu(\text{CC})$, $\delta(\text{CH})$ | 1412–1435 | 1382 |
| Gln, $\nu(\text{CN})$ | 1410 | 1409 |
| Glu, $\nu_s(\text{COO}^-)$ | 1404 (316) | 1407 |
| Asp, $\nu_s(\text{COO}^-)$ | 1402 (256) | 1404 |
| $\delta_s(\text{CH}_3)$ | 1375 or (1368, 1385) | |
| Trp | 1352–1361 | |
| Trp | 1334–1342 | 1334 (100) |
| $\delta(\text{CH})$ | 1315–1350 | |
| Trp, $\delta(\text{NH})$, $\nu(\text{CN})$, $\delta(\text{CH})$ | 1276 | |
| Tyr-O ⁻ , $\nu(\text{C-O})$, $\nu(\text{CC})$ | 1269–1273 (580) | |
| Asp, Glu, $\delta(\text{COH})$ | 1264–1450 | 955–1058 |
| Trp, $\delta(\text{CH})$, $\nu(\text{CC})$ | 1245 | |
| Tyr-OH $\nu(\text{C-O})$, $\nu(\text{CC})$ | 1235–1270 (200) | 1248–1265 (150) |
| His, $\delta(\text{CH})$, $\nu(\text{CN})$, $\delta(\text{NH})$ | 1217, 1229, 1199 | 1217, 1223, 1239 |
| Trp, $\nu(\text{CC})$ | 1203 | |
| Ser, $\delta(\text{COH})$ or $\delta(\text{CO}^2\text{H})$, $\nu(\text{CO})$ | 1181–1420 | 875–985 |
| $\gamma_w(\text{CH}_2)$ | 1170–1382 | |
| Tyr-OH, $\delta(\text{COH})$ | 1169–1260 (200) | 913 |
| Asp, Glu, $\nu(\text{C}\backslash\text{O})$ | 1160–1253 | 1250–1300 |
| His, $\nu(\text{CN})$, $\delta(\text{CH})$ | 1104, 1090, 1106, 1094 | 1104, 1096, 1107, 1110 |
| Trp, $\delta(\text{CH})$, $\nu(\text{NC})$ | 1092 | |
| Trp, $\nu(\text{NC})$, $\delta(\text{CH})$, $\nu(\text{CC})$ | 1064 | |
| $\gamma_t(\text{CH}_2)$ | 1063–1295 | |
| Thr, $\nu(\text{C-O})$ | 1075–1150 | |
| Ser, $\nu(\text{C-O})$ | 1030 | 1023 |
| Trp, $\nu(\text{CC})$, $\delta(\text{CH})$ | 1012–1016 | 1012 |
| Ser, $\nu(\text{CO})$ or $\nu(\text{CC})$ | 983 | |
| Ser, $\nu(\text{CO})$, $\delta(\text{CO}^2\text{H})$ | | 940 |
| Thr, $\delta(\text{CO}^2\text{H})$ | | 865–942 |
| $\gamma_r(\text{CH}_2)$ | 724–1174 | |

*detail information see reference¹³

In the protein backbone, the NH stretching vibrations-amide A and B is around ~ 3300 and ~ 3070 cm^{-1} ; Amide I is ~ 1650 cm^{-1} ; Amide II is ~ 1550 cm^{-1} ; Amide III is 1400 - 1200 cm^{-1} . The position of the peaks depends on the type of secondary structure and is sensitive to environment changes.

The ATR-FTIR spectroscopy is a powerful technique in avoiding the handling problems caused by the required short pathlength in transmission experiments¹³. It is useful to study the protein and lipid in the same spectrum and yielding a strong signal with only few micrograms of sample¹⁴.

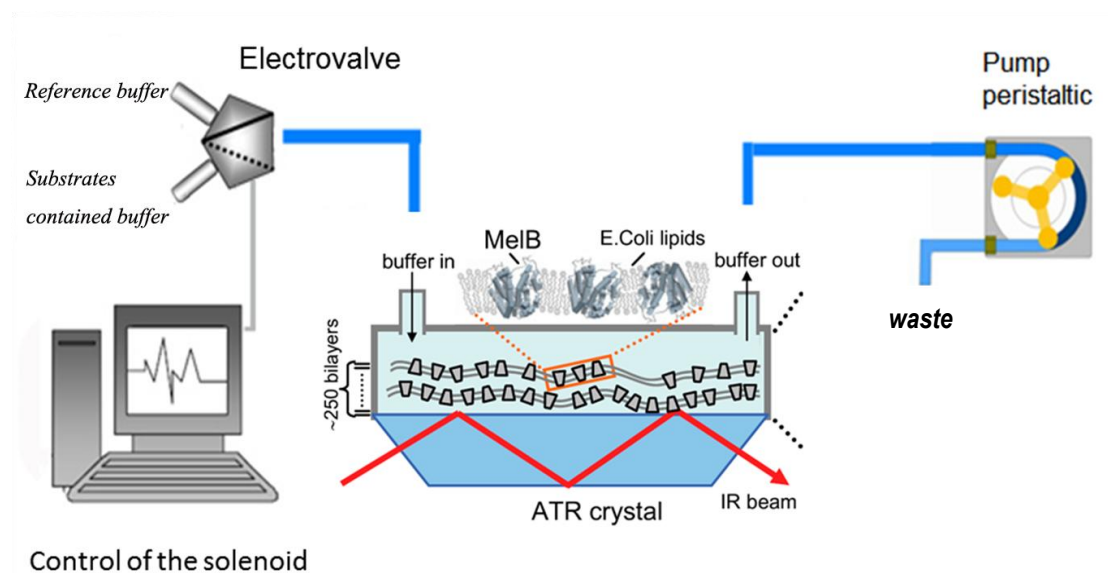


Figure 3.11 A typical ATR setup

In an ATR experiment MelB proteoliposomes are placed on a germanium ATR crystal (Harrick, Ossining, NY; $50 \times 10 \times 2$ mm, yielding 12 internal reflections at the sample side) with an index of refraction that is larger than that of the sample and typically larger than two. Infrared light goes into the crystal and is directed towards the sample interface at 45° (angle of incidence) so that it is totally reflected at the interface between the sample film and crystal. After several reflections the measuring light leaves the crystal and is focused on the detector. Upon reflection at the interface between proteoliposomes and crystal, light penetrates into the sample. This so-called evanescent wave has the same frequency as the incoming light but the amplitude of the electric field decays exponentially with the distance from the interface. The

evanescent wave is absorbed by the sample and thus the light reaching the detector carries the information about the infrared spectrum of the sample^{10, 14}. A typical ATR setup is shown in Figure 3.11. The whole experimental set up was illustrated by Lorenz *et al*¹⁵. In brief, the general setting up steps are listed here:

1) Before setting up ATR-IR difference spectra experiments, the germanium crystal was cleaned with a mild detergent, washed with distilled H₂O and dried before acquiring a background spectrum.

2) A proteoliposome sample was deposited on the crystal and air dried. And an absorbance spectrum was acquired.

3) The sample was rehydrated and then difference spectra were obtained. The conditions for obtaining the difference spectra are shown in Table 3.9.

Table 3.9 the conditions of IR difference spectrum for MelB

| Difference spectrum | Substrates buffer | | Reference buffer | |
|---|--------------------------|---------------------------------------|-------------------------|-----------------------------|
| <i>10 mM Na⁺ vs H⁺</i> | 2 min | <i>10 mM Na⁺</i> | 10 min | <i>Wash-buffer I</i> |
| <i>50 mM Na⁺ vs H⁺</i> | 4 min | <i>50 mM Na⁺</i> | 30 min | <i>Wash-buffer II</i> |
| <i>50 mM Mel vs H⁺</i> | 4 min | <i>50 mM Mel</i> | 30 min | <i>Wash-buffer</i> |
| <i>10 mM Mel 10 mM Na⁺ vs Na⁺</i> | 4 min | <i>10 mM Mel 10 mM Na⁺</i> | 10 min | <i>10 mM Na⁺</i> |
| <i>50 mM Mel 10 mM Na⁺ vs Na⁺</i> | 4 min | <i>50 mM Mel 10 mM Na⁺</i> | 30 min | <i>10 mM Na⁺</i> |

After obtaining the spectrum, the next step was to correct it for several contributions. These are the steps taken to obtain the final corrected difference spectrum:

a) Correction for the difference spectrum of the buffer

The difference spectra of the buffer were obtained in the same way as the sample, the only difference is that there was no sample on the crystal surface. The averaged buffer difference spectrum is shown in Figure 3.12.

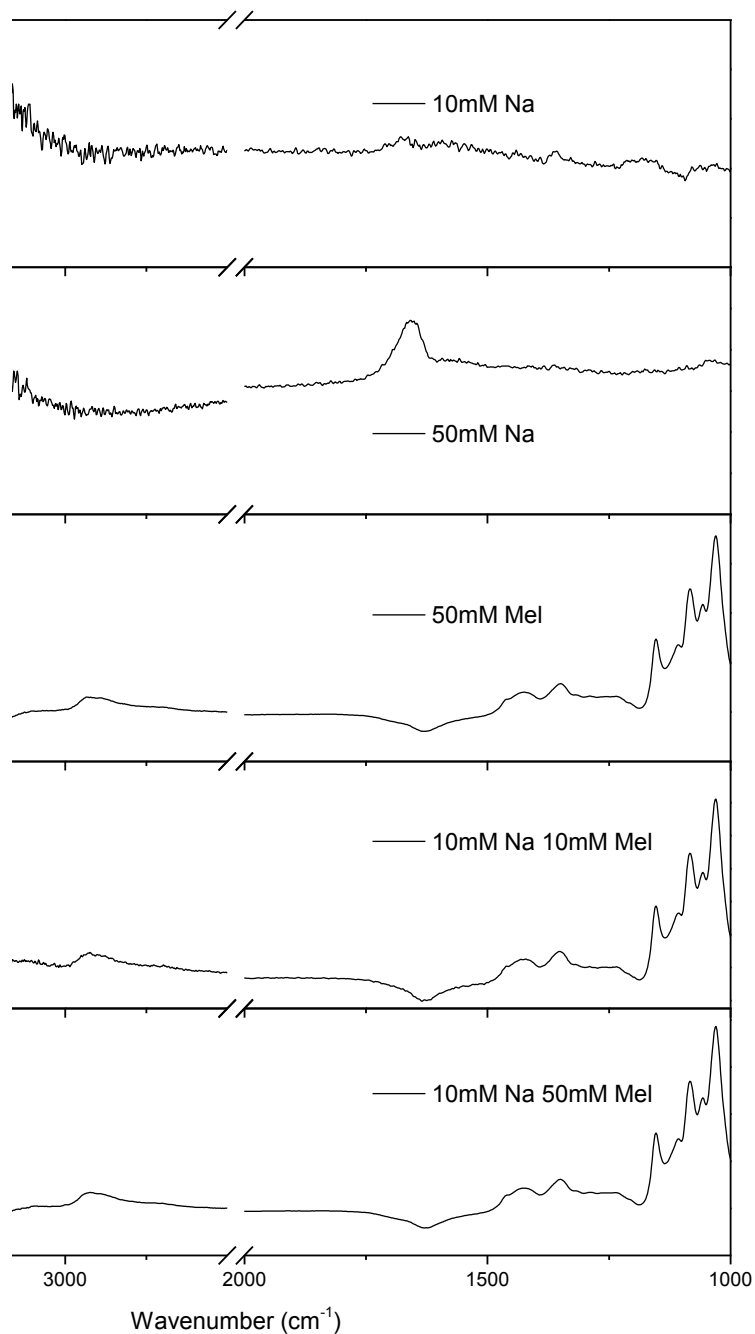


Figure 3.12 Averaged buffer difference spectra. First panel: difference spectrum for 10 mM Na⁺; Second panel: difference spectrum for 50 mM Na⁺; Third panel: difference spectrum for 50 mM melibiose; Fourth panel: difference spectrum for 10 mM melibiose in the presence of 10 mM Na⁺; Fifth panel: difference spectrum for 50 mM melibiose in the presence of 10 mM Na⁺.

b) Correction for the absorbance spectrum of MelB

The absorbance spectrum of MelB was corrected by using the absorbance spectrum of the sample immersed in the buffer minus the absorbance spectrum of the buffer alone.

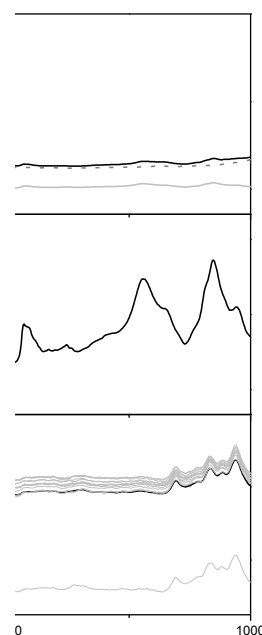


Figure 3.13 Absorbance spectrum correction of the reconstituted MelB variant applied to the Ge crystal. First panel: absorbance of the hydrated protein film (black line); also illustrated, absorbance spectrum of the plain buffer (dotted grey line); the corrected absorbance spectrum of the proteoliposomes of the MelB sample (in grey) using a subtraction factor of 0.95. Second panel: scaled absorbance spectrum of the protein film after subtraction of water bands. Third panel: Averaged difference spectrum for 10 mM melibiose in the presence of 10 mM Na⁺, in grey: single difference spectra acquired, in black: mean of the difference spectrum after averaging single difference spectra (before subtraction).

c) Averaged difference spectrum

To reduce the random error, we take the average of multiple measurements, as can be seen in the third panel of Figure 3.13.

d) Correction for the melibiose contribution

The IR difference spectrum induced by melibiose clearly indicates sugar absorption in the range from 1200 to 1000 cm⁻¹ (Figure 3.14 first panel). The effect of melibiose (1200 - 1000 cm⁻¹) was corrected by using the reference IR difference

spectrum of the buffer containing melibiose (Figure 3.14 first panel). Then the swelling of the protein film was eliminated (Figure 3.14 second panel). The absorbance spectrum might change over time because of the swelling of the protein film. Swelling means that the distance from the surface of protein film to the reflecting surface is increased, hence the absorbance spectrum intensity decreases. Finally, the difference spectrum was corrected for the effect of the atmospheric water resulting in the final melibiose-induced IR difference spectrum between wavenumbers 1950 and 1350 cm^{-1} . (Figure 3.15 third panel)

Figure 3.14 Corrected melibiose-induced IR difference spectrum in the presence of 10 mM Na^+ for the D266C melibiose permease; First panel: in black averaged IR difference spectrum of single difference spectra and in grey averaged IR difference spectra of the buffer; Second panel: melibiose induced-IR difference spectra in the presence of 10 mM Na^+ in black and in grey: absorbance spectrum of the sample used to eliminate the effect of the lipid; Third panel: final melibiose-induced IR difference spectra.

e) Correction for Na^+ contribution

The protocol for the correction of the IR difference spectrum induced by Na^+ was similar to the previously described melibiose-induced difference spectrum. The Na^+ is

non-IR active and therefore has no contribution to the spectrum. First, the negative peak of lipids were correct, then the buffer contribution was eliminated (Figure 3.15).

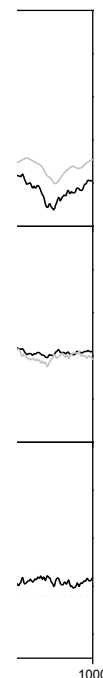


Figure 3.15 Corrected 10 mM Na⁺-induced IR difference spectrum for the D266C melibiose permease; First panel: in black averaged IR difference spectrum of single difference spectra and in grey swelling of the protein film; Second panel: Na⁺ induced-IR difference spectra in black and in grey: averaged IR difference spectra of the buffer; Third panel: final Na⁺-induced IR difference spectra.

f) Final IR difference spectrum

The difference spectra data were treated with Varian Resolution Pro 4.0. Subsequent analysis has been performed by the OriginPro 8.5.1 software.

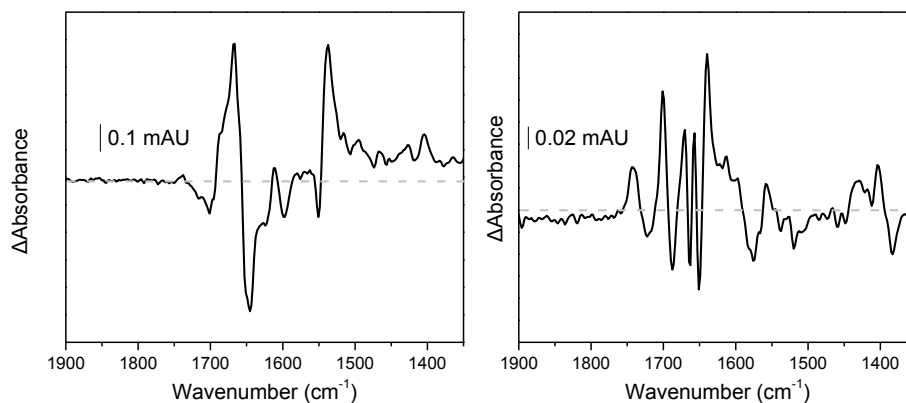


Figure 3.16 Final IR difference spectra for D266C MelB; Left side, melibiose-induced IR difference spectrum in the presence of 10 mM Na⁺ (10 mM melibiose); Right side, 10 mM Na⁺-induced IR difference spectrum in the presence of H⁺.

In order to compare the IR spectra of the mutant proteins, the spectra were normalized by the intensity of amide I and II regions in the absorbance spectra according to Granell *et al*¹⁶.

To make the quantitative comparison between any mutant and Cless, a linear regression analysis in the 1,710–1,500 cm⁻¹ interval of two normalized difference spectra was carried out using the first derivative of the spectra in order to eliminate base line contributions (Figure 3.17) was used. This global analysis provides two outputs. First, the linear correlation parameter, R², quantifies the spectral similarity (shape) between a mutant spectrum and the Cless spectrum. Second, the slope of the linear correlation gives the relative intensity of the spectral features with respect to the Cless spectrum.¹⁶

Figure 3.17 Linear regression analysis of the IR δ relative intensity and similarity compared to the Cless reference spectrum. In the left panel difference spectra Na⁺ 10 mM vs H⁺ of Cless (black), F258C (red) between wavenumbers 1500 and 1710 cm⁻¹. In the right panel: linear regression using the slope (m) as the relative intensity and the R² value as relative similarity.

3.2.4 Förster resonance energy transfer spectroscopy (FRET)

Förster resonance energy transfer describes an energy transfer mechanism (Figure 3.18) between two fluorescent molecules (in our case transfer from Trp to D²G) that occurs when there exists overlapping between the emission band of donor and the absorbing band of acceptor. The fluorescent donor Trp was excited at 290 nm. By a long-range dipole-dipole coupling mechanism, the excitation energy is then nonradiatively transferred to D²G, the acceptor, while the donor returns to the electronic ground state. Although the term “fluorescence resonance energy transfer” is often used, it should be noted that the energy is actually not transferred by fluorescence.¹⁷

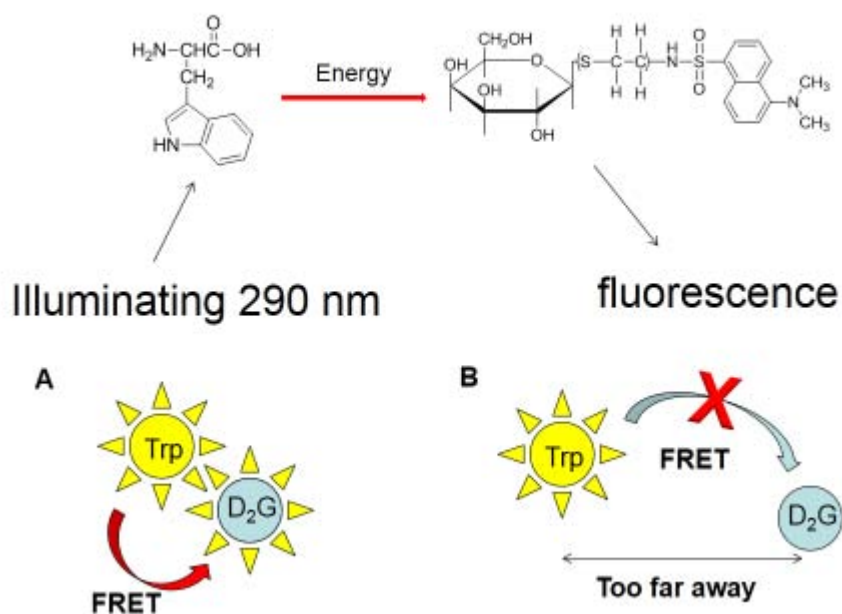


Figure 3.18 The chromophore of Trp absorbs light at 290 nm and emits light at 325 nm. The D²G that absorbs light at around 325 nm and emits light at around 460 nm. If these two molecules are closer, the light emitted from Trp is partly absorbed by D²G due to FRET.

The measurements were performed at 20 °C in a 1 cm quartz cuvette (Hellma

GmbH & Co. KG, Germany) with a UV-visible QuantaMaster™ spectrofluorimeter and processed with the Felix 32 software (Photon Technology International). FRET spectra from Trp to D²G was obtained by setting the excitation wavelength at 290 nm and collecting the emission spectrum in the interval 310 - 570 nm, in 0.1 M KPi, 0.1 M KCl, pH 7.0 buffer with the addition of substrates as described below.

Figure 3.19 Emission spectrum of D²G in the buffer containing 0.1 M KPi, 0.1 M KCl, pH 7.0 by illuminating at 290 nm.

Before starting the measures, the proteoliposomes and ISO membrane vesicles were subjected to 30 seconds of sonication in an ultrasonic bath (Ultrasonic cleaner, Fungilab US, Keyland Court, NY, USA). After acquiring the protein emission spectrum, 10 μ M of D²G was added to the MelB protein suspension, the spectrum was acquired and 10 mM NaCl was added to the sample. Finally, to displace the fluorescent sugar from the MelB binding site, 10 mM melibiose was added to the quartz cuvette. Each MelB fluorescence spectrum is the average of at least two independent scans. When illuminated at 290 nm, D²G dissolved in the buffer emits fluorescence with a maximum intensity at 558 nm (Figure 3.19). Contributions due to the emission of free D²G were corrected by subtracting the emission spectrum obtained in the buffer in the absence of protein from the protein-containing buffer.

The subtraction factor was adjusted to removing completely the D²G band at 558 nm.

3.2.5 X-ray crystallography

The MelB purification and crystallization procedure is summarized in Figure 3.20.

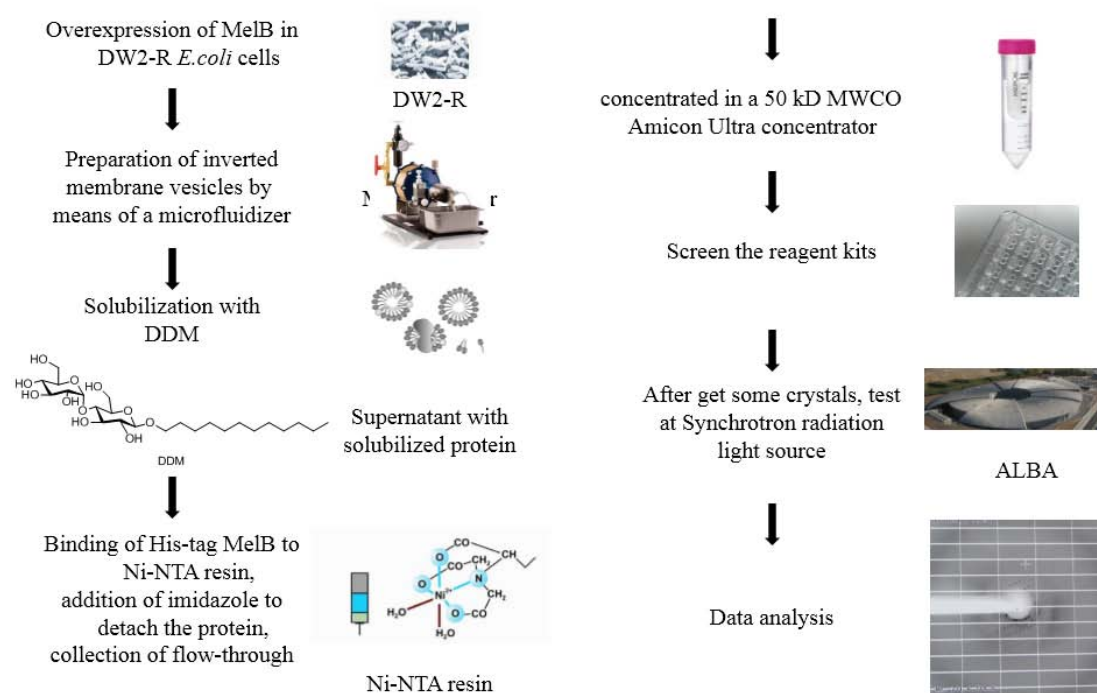


Figure 3.20 Flow chart of the protein purification and crystallization procedure

3.2.5.1 Protein preparation

MelB was expressed and purified similarly as described before. The protein eluted from the Ni-NTA affinity resin column was concentrated using a 50 kDa Amicon Ultra-4 (Millipore) filter and washed against the crystallization buffer composed of 20 mM Tris pH 7.5, 5% glycerol, 2 mM DTT, 100 mM NaCl (3 times). The following steps were followed to reduce the concentration of DDM: The purified protein with Ni-NTA resin (1 ml resin can bind 15 mg protein) was mixed in a 1.5 ml eppendorf tube, and washed with crystallization buffer (20 mM Tris pH 7.5, 5%

glycerol, 2 mM DTT, 100 mM NaCl) 6 times; The protein was eluted with a buffer containing 20 mM pH 7.5 Tris, 5% glycerol, 2 mM DTT, 100 mM NaCl and 300 mM imidazole; Then the protein was dialyzed against the buffer (20 mM Tris pH 7.5, 5% glycerol, 2 mM DTT, 100 mM NaCl) for 3 h. This protein sample was aliquoted and could be used in the crystallization experiments.

3.2.5.2 Crystallization and X-ray diffraction

MelB purified protein in different detergents were subjected to extensive crystallization screens consisting of PEG400 and PEG200 at pH 4.2 and intervals of 1% PEG concentration, as well as six major commercial crystal screening kits: MemGold, MemGold-2, PEG/ION, STRUCTURE SCREEN, INDEX and PACT (Molecular Dimension). Additives such as α -NPG, detergents, MPD, NEM and glycerol were screened to improve crystal order and packing. Crystallization drops were assembled in a hanging drop fashion in 24-well plate or sitting drop fashion (Figure 3.21) in 96-well plate.

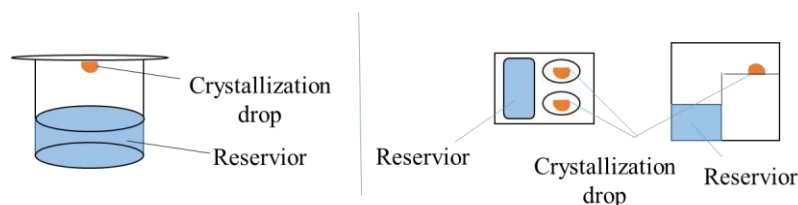


Figure 3.21 Hanging drop fashion (left) and sitting drop fashion

MelB crystals were fished and frozen in liquid nitrogen. Crystals were examined by a synchrotron source at ALBA beamlines 13 - XALOC in Spain. Diffraction data were processed by using iMosflm.

3.2.6 Molecular dynamics simulation

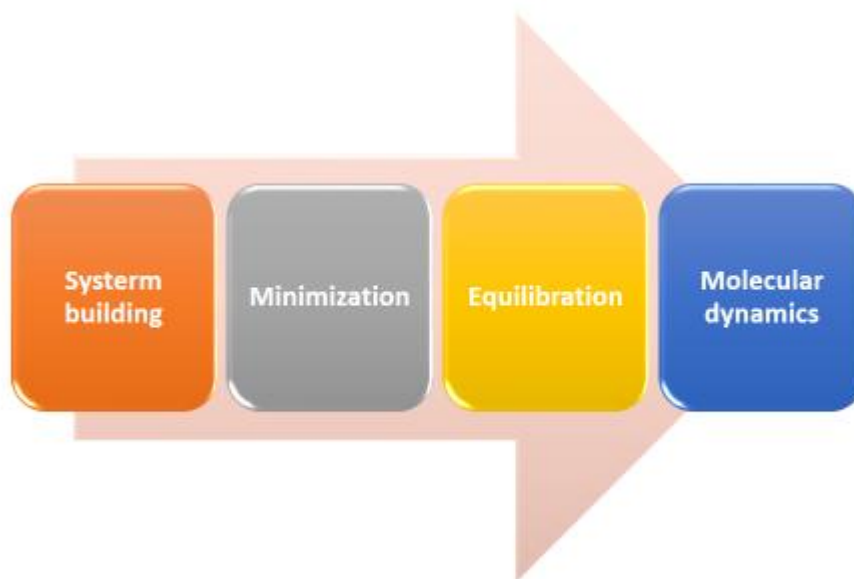


Figure 3.22 Flow chart of the molecular dynamics simulation

3.2.6.1 System Setup

The model of MelB_{EC} was built using the structure A of the 3.35 Å resolution crystal structure of MelB_{ST} (PDB accession code 4M64)¹⁸ with the CHARMM-GUI server^{19, 20}. First, the side chains of MelB_{ST} different from those of MelB_{EC} were mutated to those of MelB_{EC} (See details in the appendix 3). The final monomeric structure contained 448 residues. The protein was oriented by selecting the option “Align the first principal axis along Z”. And then, after determining the system size, a bilayer of 1-Palmitoyl-2-oleoyl-sn-glycero- 3-phosphoethanolamine (POPE) lipid molecules of 90 x 90 Å² was produced by the replacement method. The replacement method distributes lipid-like pseudo atoms around the protein, and substitutes each atom with a lipid molecule that is randomly selected from a lipid molecular library²¹. The output of the CHARMM-GUI server was the MelB_{EC} inserted into the bilayer. Then, the system was loaded into the Visual Molecular Dynamics program (VMD 1.9.2) which allowed adding water molecules and 0.15 M NaCl ions. These additions were generated using the solvate and autoionize modules of VMD²². The overview of

this step was shown in Figure 3.23.

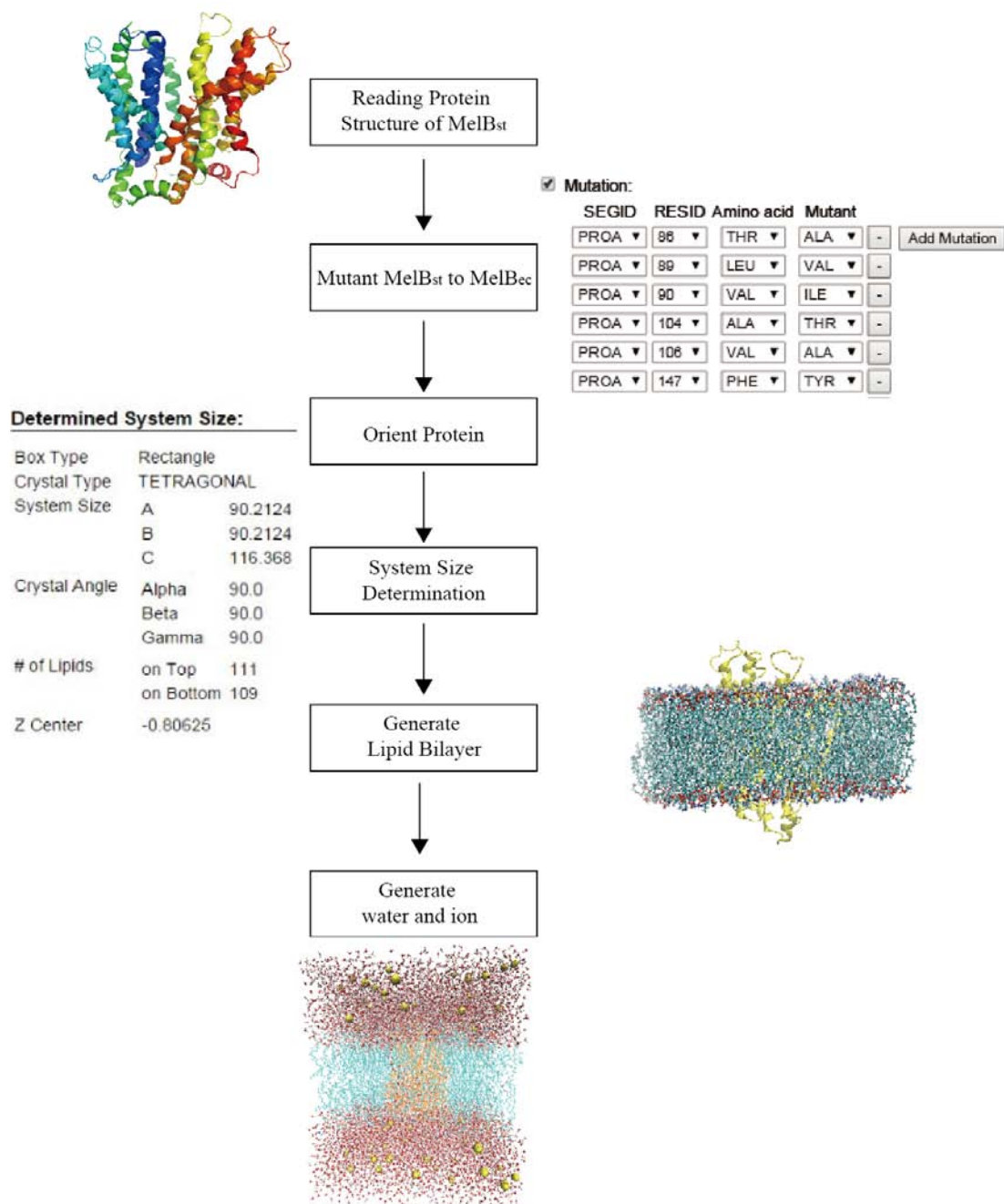


Figure 3.23 Overview of generalized process of building protein/membrane complex system in CHARMM-GUI and VMD.

3.2.6.2 Minimization and Equilibration

The energy minimization was performed in vacuo using the NAMD2.1 program²³ (<http://www.ks.uiuc.edu/Research/namd/>) to remove any possible steric conflicts,

for 100000 steps. Equilibration was done by using rigid bonds, a time step of 1 fs, cutoff of 10 Å, switch distance of 8 Å, and slowly heating the system from 0 to 298 K in steps of 2 K for 200 ps using an NVT conditions. The system settled down to the desired condition and was ready for the production period to begin. For protein and lipid atoms, the CHARMM36 force field parameters²⁴⁻²⁷ were used; for water, the TIP3P model²⁸ was used. The configuration files were shown in the appendix 2.

3.2.6.3 Production runs

Molecular Dynamics was produced using the ACEMD²⁹ program. ACEMD is a new generation molecular dynamics software which runs only on graphics processing units (GPUs) at the equivalent speed of hundreds of standard processors³⁰. A combined parameter file which was generated from “par_all36_lipid.prm”^{27, 31}, “par_all36_prot.prm”²⁴⁻²⁶ and “par_all36_water_ions.prm”²⁸ was used. And a timestep of 4.0 fs (owing to the use of the hydrogen mass repartition scheme implemented in ACEMD³²) was used. Different replicas were produced using the particle mesh Ewald method full-system periodic electrostatics^{30, 33} at a minimum of 250 ns in constant pressure and temperature for the mutants and at a minimum of 100 ns for several replicas of WT. Root-mean-square-deviation (RMSD) was calculated using the VMD extension “RMSD Visualizer Tool” module after alignment of the backbone C_α atoms. The Contact maps and the heatmap of helices curvature per residue were calculated using the VMD extension “Contact map” and “Bendix”³⁴ module.

REFERENCES

1. Botfield, M. C., and Wilson, T. H. (1988) Mutations that simultaneously alter both sugar and cation specificity in the melibiose carrier of *Escherichia coli*, *The Journal of biological chemistry* 263, 12909-12915.
2. Pourcher, T., Leclercq, S., Brandolin, G., and Leblanc, G. (1995) Melibiose permease of *Escherichia coli*: large scale purification and evidence that H⁺, Na⁺, and Li⁺ sugar symport is catalyzed by a single polypeptide, *Biochemistry* 34, 4412-4420.
3. Weissborn, A. C., Botfield, M. C., Kuroda, M., Tsuchiya, T., and Wilson, T. H. (1997) The construction of a cysteine-less melibiose carrier from *E. coli*, *Biochimica et biophysica acta* 1329, 237-244.
4. Edelheit, O., Hanukoglu, A., and Hanukoglu, I. (2009) Simple and efficient site-directed mutagenesis using two single-primer reactions in parallel to generate mutants for protein structure-function studies, *BMC biotechnology* 9, 61.
5. Reenstra, W. W., Patel, L., Rottenberg, H., and Kaback, H. R. (1980) Electrochemical proton gradient in inverted membrane vesicles from *Escherichia coli*, *Biochemistry* 19, 1-9.
6. Lowry, O. H., Rosebrough, N. J., Farr, A. L., and Randall, R. J. (1951) Protein measurement with the Folin phenol reagent, *The Journal of biological chemistry* 193, 265-275.
7. Barth, A. (2000) The infrared absorption of amino acid side chains, *Progress in biophysics and molecular biology* 74, 141-173.
8. Dave, N., Troullier, A., Mus-Veteau, I., Dunach, M., Leblanc, G., and Padros, E. (2000) Secondary structure components and properties of the melibiose permease from *Escherichia coli*: a fourier transform infrared spectroscopy analysis, *Biophysical journal* 79, 747-755.
9. Lorenz, V. A., Villaverde, J., Trezeguet, V., Lauquin, G. J., Brandolin, G., and Padros, E. (2001) The secondary structure of the inhibited mitochondrial ADP/ATP transporter from yeast analyzed by FTIR spectroscopy, *Biochemistry* 40, 8821-8833.
10. Lin, Y., Fuerst, O., Granell, M., Leblanc, G., Lorenz-Fonfria, V., and Padros, E. (2013) The substitution of Arg149 with Cys fixes the melibiose transporter in an inward-open conformation, *Biochimica et biophysica acta* 1828, 1690-1699.
11. Torres, J., and Padros, E. (1995) Spectroscopic studies of bacteriorhodopsin fragments dissolved in organic solution, *Biophysical journal* 68, 2049-2055.
12. Lorenz-Fonfria, V. A., Villaverde, J., Trezeguet, V., Lauquin, G. J., Brandolin, G., and Padros, E. (2003) Structural and functional implications of the instability of the ADP/ATP transporter purified from mitochondria as revealed by FTIR spectroscopy, *Biophysical journal* 85, 255-266.
13. Barth, A. (2007) Infrared spectroscopy of proteins, *Bba-Bioenergetics* 1767, 1073-1101.
14. Goormaghtigh, E., Raussens, V., and Ruyschaert, J. M. (1999) Attenuated total reflection infrared spectroscopy of proteins and lipids in biological membranes, *Bba-Rev Biomembranes* 1422, 105-185.
15. Lorenz-Fonfria, V. A., Leon, X., and Padros, E. (2012) Studying substrate binding to reconstituted secondary transporters by attenuated total reflection infrared difference spectroscopy, *Methods in molecular biology* 914, 107-126.
16. Granell, M., Leon, X., Leblanc, G., Padros, E., and Lorenz-Fonfria Victor, A. (2010) Structural

- insights into the activation mechanism of melibiose permease by sodium binding, *Proceedings of the National Academy of Sciences of the United States of America* 107, 22078-22083.
17. Helms, V. (2008) *Principles of Computational Cell Biology*, Wiley.
 18. Ethayathulla, A. S., Yousef, M. S., Amin, A., Leblanc, G., Kaback, H. R., and Guan, L. (2014) Structure-based mechanism for Na(+)/melibiose symport by MelB, *Nature communications* 5, 3009.
 19. Jo, S., Kim, T., Iyer, V. G., and Im, W. (2008) CHARMM-GUI: a web-based graphical user interface for CHARMM, *Journal of computational chemistry* 29, 1859-1865.
 20. Wu, E. L., Cheng, X., Jo, S., Rui, H., Song, K. C., Davila-Contreras, E. M., Qi, Y., Lee, J., Monje-Galvan, V., Venable, R. M., Klauda, J. B., and Im, W. (2014) CHARMM-GUI Membrane Builder toward realistic biological membrane simulations, *Journal of computational chemistry* 35, 1997-2004.
 21. Jo, S., Kim, T., and Im, W. (2007) Automated builder and database of protein/membrane complexes for molecular dynamics simulations, *PLoS one* 2, e880.
 22. Humphrey, W., Dalke, A., and Schulten, K. (1996) VMD: visual molecular dynamics, *Journal of molecular graphics* 14, 33-38, 27-38.
 23. Phillips, J. C., Braun, R., Wang, W., Gumbart, J., Tajkhorshid, E., Villa, E., Chipot, C., Skeel, R. D., Kale, L., and Schulten, K. (2005) Scalable molecular dynamics with NAMD, *Journal of computational chemistry* 26, 1781-1802.
 24. Best, R. B., Zhu, X., Shim, J., Lopes, P. E. M., Mittal, J., Feig, M., and MacKerell, A. D. (2012) Optimization of the Additive CHARMM All-Atom Protein Force Field Targeting Improved Sampling of the Backbone phi, psi and Side-Chain chi(1) and chi(2) Dihedral Angles, *J Chem Theory Comput* 8, 3257-3273.
 25. MacKerell, A. D., Feig, M., and Brooks, C. L. (2004) Improved treatment of the protein backbone in empirical force fields, *J Am Chem Soc* 126, 698-699.
 26. MacKerell, A. D., Bashford, D., Bellott, M., Dunbrack, R. L., Evanseck, J. D., Field, M. J., Fischer, S., Gao, J., Guo, H., Ha, S., Joseph-McCarthy, D., Kuchnir, L., Kuczera, K., Lau, F. T. K., Mattos, C., Michnick, S., Ngo, T., Nguyen, D. T., Prodhom, B., Reiher, W. E., Roux, B., Schlenkrich, M., Smith, J. C., Stote, R., Straub, J., Watanabe, M., Wiorkiewicz-Kuczera, J., Yin, D., and Karplus, M. (1998) All-atom empirical potential for molecular modeling and dynamics studies of proteins, *J Phys Chem B* 102, 3586-3616.
 27. Klauda, J. B., Venable, R. M., Freites, J. A., O'Connor, J. W., Tobias, D. J., Mondragon-Ramirez, C., Vorobyov, I., MacKerell, A. D., and Pastor, R. W. (2010) Update of the CHARMM All-Atom Additive Force Field for Lipids: Validation on Six Lipid Types, *J Phys Chem B* 114, 7830-7843.
 28. Jorgensen, W. L., Chandrasekhar, J., Madura, J. D., Impey, R. W., and Klein, M. L. (1983) Comparison of Simple Potential Functions for Simulating Liquid Water, *J Chem Phys* 79, 926-935.
 29. Harvey, M. J., Giupponi, G., and De Fabritiis, G. (2009) ACEMD: Accelerating Biomolecular Dynamics in the Microsecond Time Scale, *J Chem Theory Comput* 5, 1632-1639.
 30. Harvey, M. J., and De Fabritiis, G. (2009) An Implementation of the Smooth Particle Mesh Ewald Method on GPU Hardware, *J Chem Theory Comput* 5, 2371-2377.
 31. Klauda, J. B., Monje, V., Kim, T., and Im, W. (2012) Improving the CHARMM Force Field for Polyunsaturated Fatty Acid Chains, *J Phys Chem B* 116, 9424-9431.

32. Feenstra, K. A., Hess, B., and Berendsen, H. J. C. (1999) Improving efficiency of large time-scale molecular dynamics simulations of hydrogen-rich systems, *Journal of computational chemistry* 20, 786-798.
33. Essmann, U., Perera, L., Berkowitz, M. L., Darden, T., Lee, H., and Pedersen, L. G. (1995) A Smooth Particle Mesh Ewald Method, *J Chem Phys* 103, 8577-8593.
34. Dahl, A. C., Chavent, M., and Sansom, M. S. (2012) Bendix: intuitive helix geometry analysis and abstraction, *Bioinformatics* 28, 2193-2194.

4 RESULTS AND DISCUSSION

4.1 Analysis of the conserved residues in loop 7-8/end of helix VII

There are 11 loops in the melibiose structure, as shown in Figure 4.1. A homologous sequence alignment indicates that in loop 7-8/end of helix VII Tyr-256, Tyr-257, Phe-258 and Tyr-260 have a high level of conservation. At the same time, there are two negatively charged amino acids (Asp-264 and Asp-266) in this loop. Apart from the four conserved amino acids, there is one more aromatic amino acid inside this loop. Given the high content of aromatic side chains and their high conservation the loop 7-8/end of helix VII may play an important role in the transport mechanism of the melibiose transporter. In order to elucidate the function of the loop, we carried out a cysteine-scanning mutagenesis of it and studied some properties of the mutants.

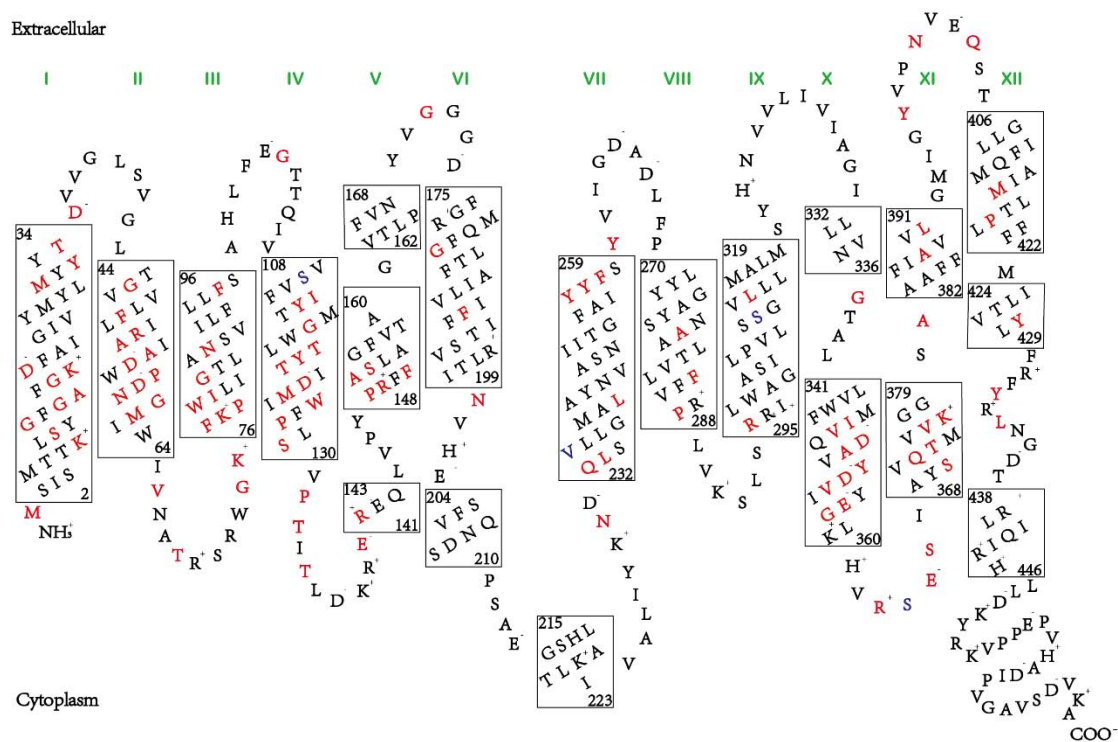


Figure 4.1 Secondary structure of MelB (It was obtained by homologous sequence alignment with MelB_{st}¹) from *E. coli* with conserved amino acids indicated in red color, with a conservation score of 9 calculated with ConSurf² (see the results in the appendix 4). The blue-colored letters represent

the replaced cysteines by Ser or Val.

4.2 Cysteine-scanning mutagenesis of loop 7-8/end of helix VII

Tyr-256, Tyr-257, Phe-258, Ser-259, Tyr-260, Val-261, Gly-263, Asp-264, Ala-265, Asp-266, Leu-267 and Phe-268 were replaced one at a time by cysteine (except for Ser-259 also replaced by alanine) to study the importance of loop 7-8/end of helix VII (Ile-262 was studied by Lin³, so there are no related results present in this thesis). The mutants were successfully obtained by using a double-primer PCR mutagenesis protocol as described in Materials and Methods. A common feature observed in all the mutants was the reduction of expression levels with respect to Cless except for S259A and Y260C (Figure 4.2). The calculations of the protein expression level for each mutant based on protein yields after the purification were approximate since the preparations vary from one to another. However, compared to the Cless control, larger culture volumes were required for the mutants of loop 7-8/end of helix VII to purify sufficient amount of functional protein.

Figure 4.2 Maximum yield of purified MelB protein from 4 L cells.

The melibiose transport properties of the conserved amino acid mutant strains

were tested by growing on MacConkey agar plates. The Cless MelB protein expressed in the DW2R strain exhibits red colonies on the MacConkey agar plate which contained melibiose as the main carbon source (Figure 4.3). The colored colonies indicated a pH change of the media because of the metabolization of the melibiose. After the melibiose enters into the cell, it is cleaved intracellularly by the α -galactosidase into the monosaccharides glucose and galactose. Then the monosaccharides are decomposed into some acidic substances (like pyruvate, lactic acid and so on). This reaction causes the acidification of the plate, indicated by the neutral red, which is a pH indicator, staining the medium to a red color. However, a red bacterial colony does not necessarily be interpreted as proof of active transport of the melibiose. It might be passive sugar transport by MelB due to a higher concentration of melibiose in the surrounding medium than in the cytoplasm. However, it was interesting to find out that most of the conserved amino acid mutants do not show red colonies. The color of the colonies can indicate the absence of melibiose transport since the sugar does not enter the bacterial cells, no metabolizing activity exists, and the pH of the medium will not drop.

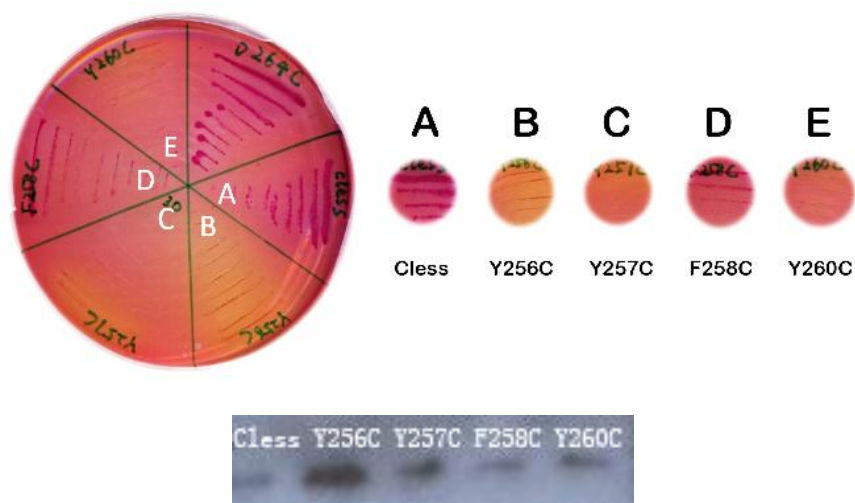


Figure 4.3 Top: Melibiose fermentation. *E. coli* DW2R strain containing MelB mutants on MacConkey agar plates supplemented with 10 mM melibiose, 10 μ g/mL tetracycline and 100 μ g/mL ampicillin are shown. Bottom: Western blotting (37 kDa). The mutant cells were loaded on each well and the MelB protein detected by anti-His-tag reagent.

The molecular weight of the MelB protein is around 52 kDa. But in the western blot the corresponding band usually shows at around 37 kDa. In Figure 4.4 the UV absorption spectra of the solubilized and purified MelB proteins for all the mutants are shown. They have a common peak at around 280 nm which is the characteristic peak of the protein.

Figure 4.4 UV absorption spectra of the solubilized MelB proteins

4.3 Fluorescence results

4.3.1 FRET in proteoliposomes

A β -galactoside-derivative, the fluorescent sugar (2'-N-5-dimethylamino-naphthalene-1-sulfonyl)-aminoethyl-1-thio- β -D-galactopyranoside (D²G) is able to bind to MelB to the same binding site as melibiose (Figure 4.5). Compared to the

physiological melibiose, D²G has shown to have higher affinity for MelB.⁴

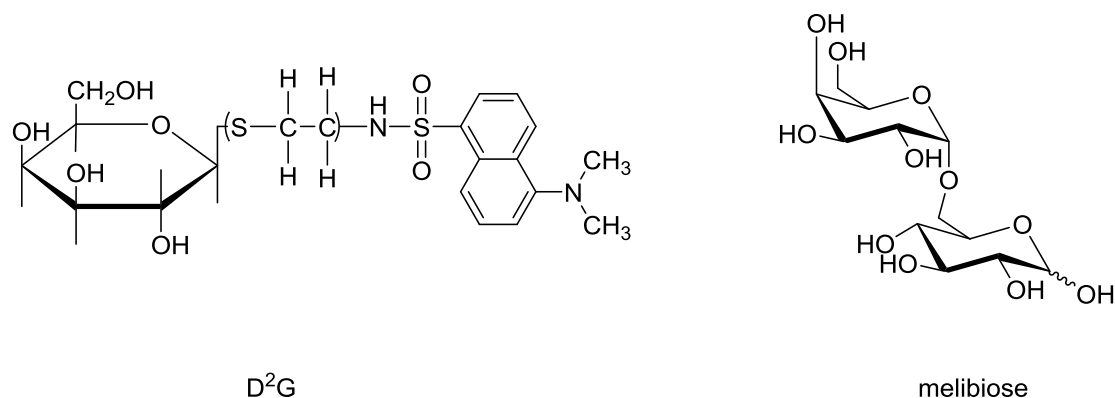


Figure 4.5 the structures of D²G and melibiose

The fluorescence spectra for the MelB proteoliposomes were collected in an interval from 310 nm to 570 nm. The experiments were done by exciting the sample with light of 290 nm. The light of this wavelength is absorbed by the intrinsic Trp. The FRET phenomenon occurs because there is overlapping between the D²G excitation spectrum and the Trp emission spectrum.

The spectrum of the Cless proteoliposomes (Figure 4.6) displays the typical Trp peak with the maximum around 325 nm (black line). After the addition of 10 μ M D²G (red line), the signal of the Trp residues decreases due to energy transfer to D²G as well as because an inner filter effect and non-specific fluorescence quenching by the fluorescent sugar in the medium.⁴ Concomitantly a small peak appears around 460 nm due to D²G emission. The addition of sodium (blue line) results in a further decrease of the Trp fluorescence around 325 nm and simultaneously, the peak around 460 nm increases in intensity because of increasing amount of bound D²G. An addition of 10 mM melibiose (magenta line) reverses the effects by displacing D²G from the binding site, decreasing the D²G FRET signal around 460 nm and increasing the Trp fluorescence. This method is used to determine the capability of substrate's binding for specific mutants^{1, 5-9}.

As shown in Figure 4.6, none of the mutants of the conserved amino acids showed any energy transfer upon D²G addition. Except these four mutants, the other

mutants respond to the consecutive additions of D²G, Na⁺, and melibiose to different levels, indicating that all of them preserve the capability of sugar/Na⁺ binding with some changes in the intensity of signal. This suggests that the mutations may affect the affinity of the substrates. Especially, MelB D266C mutant shows a little increase in the intensity of the signal when compared with Cless while the other mutants all decrease.

The increase in the fluorescence intensity at 460 nm upon D²G addition reflects the fact that melibiose permease can bind the sugar in the absence of Na⁺ (i.e., it can use H⁺ as coupling ions in the transport process). Figure 4.7 shows the fluorescence increase upon D²G addition of the mutants in the loop 7-8/end of helix VII in the absence of Na⁺ (i.e., in the presence of H⁺). The conserved aromatic amino acids show nearly zero intensity compared with Cless, indicating lack of binding of D²G. The mutants G263C and L267C show a small signal, whereas Ser-259 shows variable intensity depending on the substituting side chain. This points to a substantial role of these side chains in substrate binding in the presence of H⁺. The rest of mutants have between half and the same intensity of Cless.

Upon Na⁺ addition the mutants Y256C, Y257C and Y260C, showed no increase in the fluorescence intensity (Figure 4.8), thus no D²G binding in the presence of Na⁺ can be detected for these mutants. And the mutants F258C and S259A showed very low affinity for D²G in the presence of 10 mM sodium. Surprisingly, the addition of sodium in the solution appeared to bring a strong signal in mutant D266C, nearly two fold that of Cless.

When melibiose was added to displace the bound D²G, the signal did not change for mutants Y256C, Y257C, F258C and Y260C, as expected since there is no D²G bound in these mutants. However, for the other mutants, the melibiose successfully replaced the D²G (Figure 4.9)

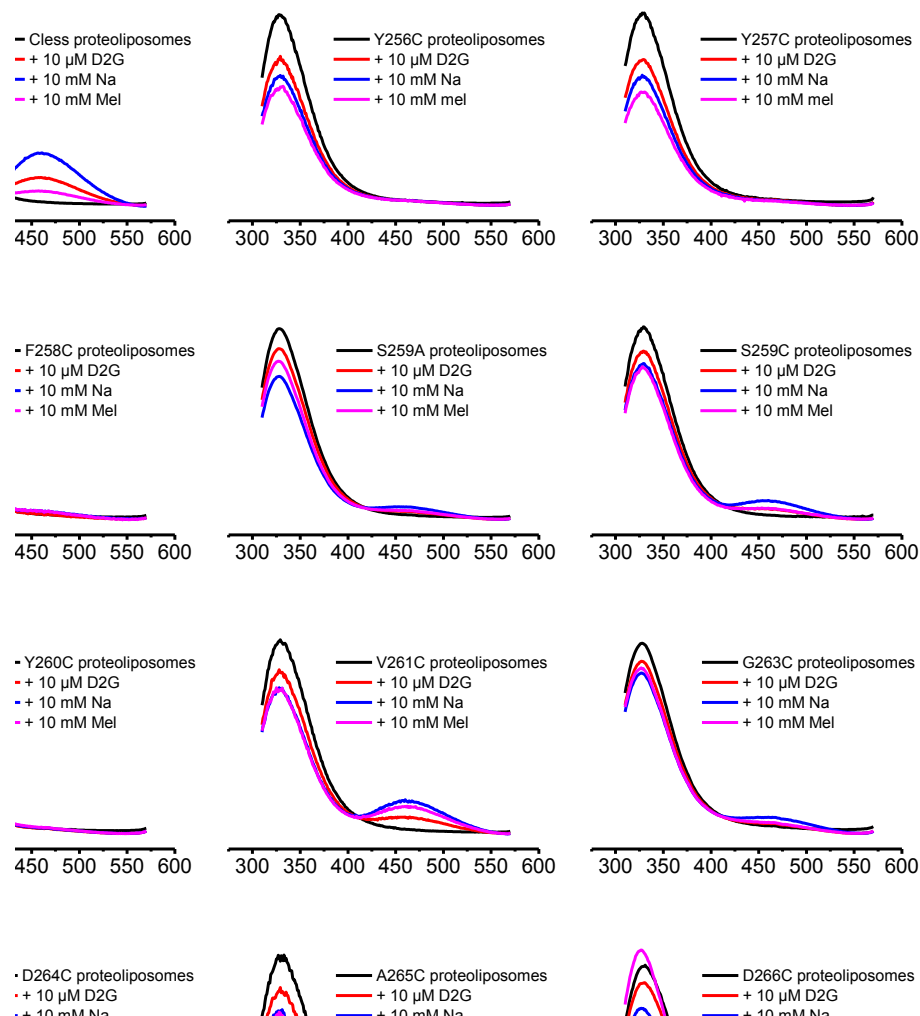


Figure 4.6 Substrates-induced Trp→D²G FRET signal changes of MelB mutants in proteoliposomes. Representative plot of fluorescence changes of different MelB mutants induced by the sequential addition of proteoliposomes (black), D²G (red), NaCl (blue) and melibiose (magenta). The samples were illuminated at 290 nm, and the emission spectra were collected at 310-570 nm. The spectra were normalized to the same amount of protein. Abscissa, wavelength (nm); ordinate, fluorescence intensity. Each data is the average of at least two scans.

Figure 4.7 FRET between Trp and D²G. The protein samples reconstituted in liposomes in 100 mM KPi and 100 mM KCl pH7.0, were illuminated at 290 nm, and the emission spectra were collected at 310-570 nm. The graph here represents the percentage of increase between after and before the addition of 10 μ M D²G at 460 nm with respect to Cless. Each data is the average of at least two scans.

Figure 4.8 Effect of Na⁺ addition on the FRET signal. The protein samples reconstituted in liposomes in 100 mM KPi and 100 mM KCl pH7.0 with 10 μ M D²G, were illuminated at 290 nm, and the emission spectra were collected at 310-570 nm. The graph here represents the percentage of increase between after and before the addition of 10 mM NaCl at 460 nm with respect to Cless. Each data is the average of at least two scans.

Figure 4.9 Effect of melibiose addition on the FRET signal. The protein samples reconstituted in liposomes in 100 mM KPi and 100 mM KCl pH7.0 with 10 μ M D²G, 10 mM Na⁺, were illuminated at 290 nm, and the emission spectra were collected at 310-570 nm. The graph here represents the percentage of increase between after and before the addition of 10 mM Melibiose at 460 nm with respect to Cless. Each data is the average of at least two scans

4.3.2 FRET of Inside Out (ISO) vesicles

The activity of membrane proteins can be modulated by the phospholipid composition of the membrane. The reconstitution of membrane proteins into a model membrane allows investigation of individual features and activities of a given cell membrane component. However, the activity of membrane proteins is often difficult to sustain following purification and reconstitution, since the composition of the detergents and the liposomes differs from that of the native cell membrane. In the vesicles, the protein is localized in its natural lipid bilayer conserving the original three-dimensional structure after the expression and insertion into the cell membrane.

We therefore obtained ISO vesicles with the same total protein and nearly equal MelB protein content (Figure 4.10). The FRET results of the ISO vesicles after adding D²G (Figure 4.11) are mainly consistent with our earlier research of proteoliposomes. The Cless and DW2R vesicles are the control vesicles. The Cless vesicles demonstrate a significant fluorescence increase after the addition of 10 mM NaCl to

the sample in the presence of 10 μM D²G. The DW2R *E. coli* strain containing the same mixture of membrane proteins except MelB is the negative control. In this control the D²G does not cause any increase of the fluorescence signal in the ISO vesicles.

The results from the measurements with ISO vesicles of Y256C, Y257C, F258C and Y260C results are in agreement with the proteoliposomes data where the D²G does not produce an increase of the fluorescence signal. And for other mutants, the results are similar to Cless except a little change of the intensity.

Therefore, fluorescence results are in line with the fact that Tyr-256, Tyr-257, Phe-258 and Tyr-260 are conserved amino acids. If we change those amino acids, the protein will lose the function since no longer can bind the sugar.

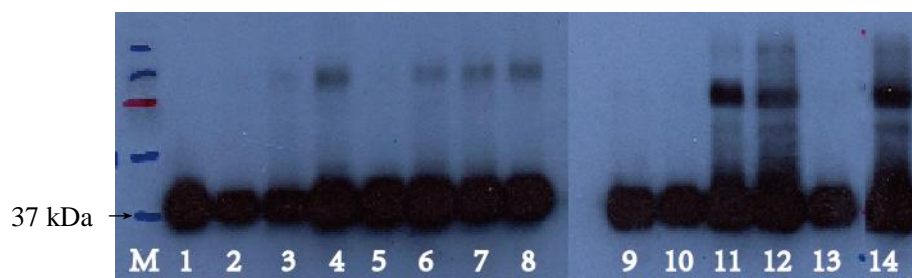


Figure 4.10 Western blotting. The ISO vesicles of the mutants were loaded on each well and the MelB protein detected by anti-His-tag reagent. M: Marker; 1: Cless; 2: Y256C; 3: Y257C; 4: F258C; 5: S259A; 6: S259C; 7: Y260C; 8: V261C; 9: G263C; 10: D264C; 11: A265C; 12: D266C; 13: L267C; 14: F268C.

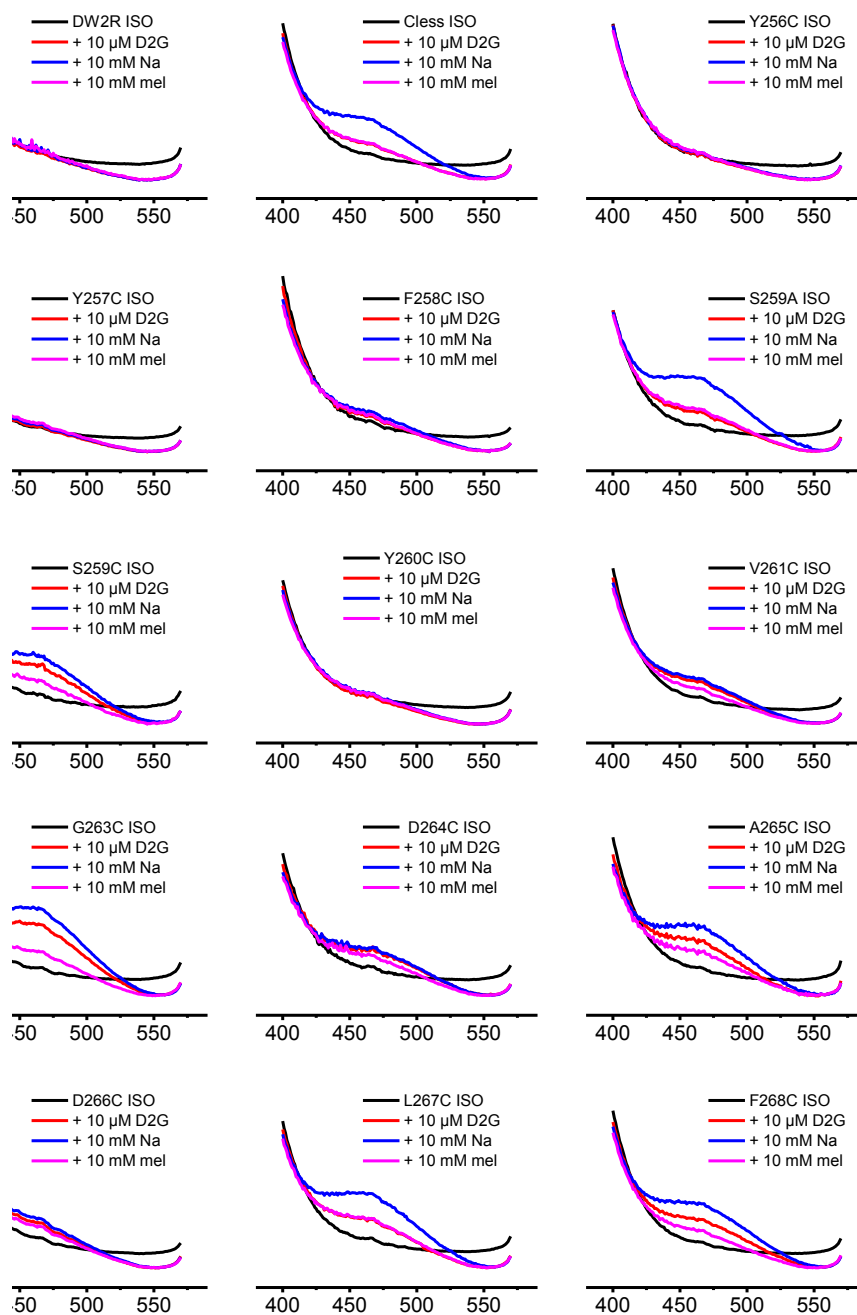


Figure 4.11 Substrates-induced Trp→D2G FRET signal changes of MelB mutants in ISO membrane vesicles. The graph shows representative plots of fluorescence changes of different MelB mutants induced by the sequential addition of ISO vesicles (black), 10 μ M D²G (red), 10 mM NaCl (blue) and 10 mM melibiose (magenta). The ISO membrane vesicles in 100 mM KPi and 100 mM KCl pH7.0 with different substrates where indicated, were illuminated at 290 nm, and the emission spectra were collected at 400-570 nm. Abscissa, wavelength (nm); ordinate, fluorescence intensity. Each data is the average of at least two scans.

4.3.3 Conclusions from the fluorescence results

Y256C, Y257C, F258C and Y260C in ISO vesicles and reconstituted in proteoliposomes do not bind the fluorescent sugar D²G, as demonstrated in the FRET experiments.

4.4 The infrared difference spectra

The MelB transporter was expressed, purified, solubilized and reconstituted into liposomes (*E. coli* lipids). In proteoliposomes the binding of substrates to the MelB transporter was assessed by infrared difference spectroscopy using buffers supplemented with the substrates of MelB at different concentrations.

4.4.1 General features of the infrared difference spectra

We take as an example the spectra in Figure 4.11 where they were acquired in the presence or absence of 10 mM sodium. The Cless infrared difference spectrum in the first row on the left displays different positive and negative peaks. The difference spectrum is the subtraction between the absorbance spectrum in the absence of the sodium and the absorbance spectrum in the presence of the sodium. A peak-less spectrum visible as a nearly straight line would imply an absence of interaction of the sodium with MelB. The positive and negative peaks indicate vibrational differences between the states in the absence of sodium (or the states in the presence of proton) and the states in the presence of sodium. This can be interpreted as structural changes of the MelB transporter when replacing the proton with sodium in the ion binding site. The Cless carrier possesses almost identical properties as the wild-type transporter.¹⁰ Throughout the study we used Cless as a control for infrared difference spectra.

Although we acquired the difference spectrum from 4000 to 1000 cm^{-1} , the most interesting part of a difference spectrum is the amide region (1700-1500 cm^{-1}) containing the protein major bands amide I and II. Therefore, we focus on the vibrational changes appearing in the amide I (1700-1600 cm^{-1}) and amide II (~1550 cm^{-1}) region to explain the conformational changes. The major peaks correspond to α helices (1668-1650 cm^{-1} region) or to β -sheets, 3_{10} helices or open loops¹¹ in the 1700 cm^{-1} or the 1645 cm^{-1} regions. On the other hand, the region between 1400 cm^{-1} and 1350 cm^{-1} may be important for fingerprint analysis of certain amino acid side chains,

like the carboxylic acids peaks at 1598-1600 cm^{-1} , 1576-1579 cm^{-1} , 1404 cm^{-1} and 1383 cm^{-1} .¹⁰

4.4.2 Conserved amino acids in loop 7-8

As mentioned above, the study of the homologous sequence alignment showed four conserved amino acids (Tyr-256, Tyr-257, Phe-258 and Tyr-260). Here, we will discuss three mutants (Y256C, F258C and Y260C) of the conserved amino acids.

4.4.2.1 Sodium-induced IR difference spectra of Y256C, F258C and Y260C mutants

Figure 4.11 10 mM Na^+ -induced IR difference spectra of Cless, Y256C, F258C and Y260C. The spectra correspond to the effect of 10 mM NaCl at 25 °C and pH 6.6 in a buffer containing 20 mM MES and 100 mM KCl.

By comparing the infrared difference spectra of the Y256C, F258C and Y260C mutants with Cless, one can conclude the lack of apparent response of these mutants to Na^+ addition. No significant 10 mM Na^+ -induced spectral intensity was obtained for any of the MelB mutants shown in Figure 4.11. The mutations have either blocked

the access to the cation binding site, or the replacement of the protons by sodium ions is inhibited due to a reduced affinity for the latter. In all three cysteine replaced mutants, the spectral intensity and similarity were lower than that of Cless, and thus considered insignificant. Therefore, it can be concluded that sodium does not interact with any of the three mutants (Y256C, F258C and Y260C).

50 mM sodium was used to detect whether the effect of the three mutants was due to a reduced affinity for sodium. It can clearly be seen that Y256C, F258C, and Y260C MelB mutations cause the absence of cation binding of MelB (Figure 4.12). Since even a high sodium concentration could not induce any clear signal in the IR difference spectra of these mutants, one can say that the three mutants are defective in cation binding.

Figure 4.12 50 mM Na⁺-induced IR difference spectra of Cless, Y256C, F258C and Y260C. The spectra correspond to the effect of 50 mM NaCl at 25 °C and pH 6.6 in a buffer containing 20 mM MES and 100 mM KCl.

4.4.2.2 Melibiose-induced IR difference spectra of Y256C, F258C and Y260C mutants

The same technique has been used to acquire difference spectra induced by melibiose interaction. The melibiose-induced difference spectrum for the Cless carrier differs in its characteristics from the sodium-mediated difference spectrum. The Cless transporter was used as the reference again. The 50 mM melibiose-induced difference spectrum in the absence of sodium displayed a variety of different positive and negative peaks. The difference spectra suggest an extremely decreased melibiose binding affinity for the three mutants (Figure 4.13).

To check if the melibiose could produce structural changes in the presence of the co-substrate sodium, the difference spectra were acquired by supplementing the buffer with 10 mM NaCl in the presence of 10 mM or 50 mM melibiose. The difference spectrum from Cless mutant works as a control again.

Figure 4.13 50 mM Melibiose-induced IR difference spectra of Cless, Y256C, F258C and Y260C. The spectra correspond to the effect of 50 mM melibiose at 25 °C and pH 6.6 in a buffer containing 20 mM MES and 100 mM KCl.

The melibiose-induced difference spectrum in the presence of 10 mM sodium displayed a variety of different positive and negative peaks (Figure 4.14), like the Na⁺-induced spectra. The main peaks occur in the region between 1668 and 1652 cm⁻¹

corresponding to α -helix structures.¹¹ Melibiose-induced IR difference spectra for the MelB mutants were first acquired in the absence of the sodium and then in the presence of 10 mM sodium. Sodium increases the affinity for the sugar^{12, 13}, which could be observed by higher spectral intensity compared to the spectrum in the absence of sodium.

None of the three mutants showed melibiose-induced conformational rearrangements similar to the Cless, as shown by the lack of clear peaks in the IR difference spectra. The quantitative comparison of the region between 1500 and 1710 cm^{-1} by the first derivative of IR difference spectra with respect to the Cless confirmed the lack of melibiose binding in the MelB mutants of Y256C and Y260C in the presence of 10 mM sodium (Figure 4.14). Nevertheless, the mutant F258C displays some features in the difference spectrum. The evaluation of the difference spectra was further assessed by using the spectral intensity and the spectral similarity with respect to the Cless spectrum. A detailed description of how the calculation was done is included in the Materials and Methods section. This offers the idea that this mutant might preserve the binding ability, but be affected by a decreased affinity constant, requiring an elevated concentration of melibiose to stimulate binding events. Therefore, as we did when testing for sodium binding, the three mutants were also exposed to higher sugar concentrations (50 mM melibiose), still in the presence of 10 mM sodium.

Figure 4.14 In the left panel: 10 mM Melibiose-induced IR difference spectra in the presence of 10 mM sodium of Cless, Y256C, F258C and Y260C. The spectra correspond to the effect of 10 mM melibiose at 25 °C and pH 6.6 in a buffer containing 20 mM MES, 100 mM KCl and 10 mM NaCl. In the right panel: Spectral similarity and intensity in the 1710-1500 cm^{-1} interval on the first derivative of the 10 mM Melibiose-induced IR difference spectra in the presence of 10 mM sodium of Cless and F258C.

A lower IR difference spectra intensity compared with Cless can be interpreted either as a reduced affinity or a reduced protein stability. At a concentration of 50 mM melibiose (Figure 4.15), the Y256C and Y260C mutants generated also a feature-less difference spectrum which indicated the lack of melibiose-induced structural changes of the transporter. Only the F258C mutant presents a difference spectrum with high similarity (80%), although the spectral intensity is reduced (30% compared to Cless). Therefore, the Y256C and Y260C mutants lost the binding of both substrates, whereas F258C shows decreased affinity.

Figure 4.15 In the left panel: 50 mM Melibiose-induced IR difference spectra in the presence of 10 mM sodium of Cless, Y256C, F258C and Y260C. The spectra correspond to the effect of 50 mM melibiose at 25 °C and pH 6.6 in a buffer containing 20 mM MES, 100 mM KCl and 10 mM NaCl. In the right panel: Spectral similarity and intensity in the 1710-1500 cm^{-1} interval on the first derivative of the 50 mM Melibiose-induced IR difference spectra in the presence of 10 mM sodium of Cless and F258C.

4.4.2.3 Evaluation of the absorbance spectra of the Y256C, F258C and Y260C mutants

Figure 4.16 Comparison of absorbance spectra of the three conserved mutants with Cless in the left panel; Second derivative of the absorbance spectra in the right panel. The dashed lines mark the maximum of lipid C=O (around 1740 cm^{-1}), the maximum of the amide I (1659 cm^{-1}) and the amide II (1546 cm^{-1}) band.

Since the cysteine replacement of single amino acid in position 256, 258 and 260 tremendously alter the binding characteristics for both substrates, either these residues are essential for the transferring of both substrates, or more likely the mutation might affect the protein structure. The IR absorption spectra in the protein backbone sensitive region $1700 - 1500 \text{ cm}^{-1}$ for each mutant compared with Cless was analyzed to check the latter hypothesis (Figure 4.16). In the broad amide I and II bands, the stretching vibrations of the C=O and C-N groups were the main structural information one can obtain in the IR absorption spectra. At first sight, the absorbance spectra of the three conserved mutants are similar in the amide I and amide II region to the reference spectra of the fully functional Cless transport protein (Figure 4.16). Because of the broad band in the protein structure sensitive amide I and II region, the hidden patterns can't be easily distinguished from the absorbance spectra. So the second derivative of the absorbance spectrum was computed to resolve small structural changes caused by the single cysteine replacement. The second derivative leads to narrow bands in the amide I and amide II regions of proteins as well as flattening of the baselines.

For the mutants Y256C and Y260C, the second derivative spectra demonstrate small spectral differences with Cless at around 1630 cm^{-1} , used for the comparison (Figure 4.16). But for the mutant F258C, that peak was not present around 1630 cm^{-1} . This wavenumber was attributed to β -sheets. The replacement of tyrosine by cysteine seems to cause some structural alterations in MelB which could block the substrates passway. Most noteworthy, in all three mutants the amide I peak at 1659 cm^{-1} is shifted to 1657 cm^{-1} . As observed for other MelB mutants.¹⁴ It can be concluded that the mutations at 256, 258 or 260 produce some minor structural alterations, but global conformational changes can be discarded.

4.4.3 Charged amino acids in loop 7-8:D264C and D266C

4.4.3.1 Sodium-induced IR difference spectra of D264C and D266C mutants

Figure 4.17 In the left panel: 10 mM Na⁺-induced IR difference spectra of Cless, D264C and D266C. The spectra correspond to the effect of 10 mM NaCl at 25 °C and pH 6.6 in a buffer containing 20 mM MES and 100 mM KCl. In the right panel: Spectral similarity and intensity in the 1710-1500 cm⁻¹ interval on the first derivative of the 10 mM Na⁺-induced IR difference spectra of Cless, D264C and D266C.

Few alterations are observed when one compares the difference spectra induced by Na⁺ binding with D266C and Cless (Figure 4.17). The structural changes resulting from the replacement of the coupling H⁺ by Na⁺ are therefore alike in both permeases. Some variations are visible in the difference spectrum between D264C and Cless, suggesting that D264C is involved in the transport mechanism of MelB or has some structural role.

In order to know if the effect on charged amino acids in loop 7-8 is due to a reduced affinity for sodium, sodium-induced difference spectra were acquired also at 50 mM. The 50 mM Na⁺-induced IR difference spectra (Figure 4.18) showed similar result as 10 mM sodium.

Figure 4.18 In the left panel: 50 mM Na⁺-induced IR difference spectra of Cless, D264C and D266C. The spectra correspond to the effect of 50 mM NaCl at 25 °C and pH 6.6 in a buffer containing 20 mM MES and 100 mM KCl. In the right panel: Spectral similarity and intensity in the 1710-1500 cm⁻¹ interval on the first derivative of the 50 mM Na⁺-induced IR difference spectra of Cless, D264C and D266C.

4.4.3.2 Melibiose-induced IR difference spectra of D264C and D266C mutants

Figure 4.19 In the left panel: 50 mM Melibiose-induced IR difference spectra of Cless, D264C and D266C. The spectra correspond to the effect of 50 mM melibiose at 25 °C and pH 6.6 in a buffer containing 20 mM MES and 100 mM KCl. In the right panel: Spectral similarity and intensity in the 1710-1500 cm⁻¹ interval on the first derivative of the 50 mM Melibiose-induced IR difference spectra of Cless and D266C.

The sugar-induced difference spectrum gives further insights of how MelB is eventually influenced by the replacement of the charged amino acids in the periplasmic loop 7-8. The spectrum of D266C corresponding to 50 mM melibiose in the presence of H⁺ showed almost the same degree of similarity and intensity as the 10 mM Na⁺-induced difference spectrum when compared with the spectrum of Cless (Figure 4.19). However, the 50 mM melibiose-induced difference spectrum of D264C suggested an extremely decreased melibiose binding affinity.

Figure 4.20 In the left panel: 10 mM Melibiose-induced IR difference spectra in the presence of 10 mM sodium of Cless, D264C and D266C. The spectra correspond to the effect of 10 mM melibiose at 25 °C and pH 6.6 in a buffer containing 20 mM MES, 100 mM KCl and 10 mM NaCl. In the right panel: Spectral similarity and intensity in the 1710-1500 cm⁻¹ interval on the first derivative of the 10 mM Melibiose-induced IR difference spectra in the presence of 10 mM sodium of Cless and D266C.

To check if the melibiose could produce structural changes in the presence of sodium, the difference spectra were acquired in the presence of both substrates.

The presence of sodium can increase the melibiose binding affinity of MelB. The spectra of D266C and D264C were the same either in the absence or presence of sodium (Figure 4.20 and 4.21). The D266C showed almost the same spectra as Cless while the D264C almost did not show any peak in the difference spectra. This

suggests that the Asp-264 may play a more important role than Asp-266.

Figure 4.21 In the left panel: 50 mM Melibiose-induced IR difference spectra in the presence of 10 mM sodium of Cless, D264C and D266C. The spectra correspond to the effect of 50 mM melibiose at 25 °C and pH 6.6 in a buffer containing 20 mM MES, 100 mM KCl and 10 mM NaCl. In the right panel: Spectral similarity and intensity in the 1710-1500 cm^{-1} interval on the first derivative of the 50 mM Melibiose-induced IR difference spectra in the presence of 10 mM sodium of Cless and D266C.

4.4.3.3 Evaluation of the absorbance spectra of the D264C and D266C mutants

Figure 4.22 Comparison of absorbance spectra of the two charged mutants with Cless in the left panel; Second derivative of the absorbance spectra in the right panel. The dashed lines marked the maximum of lipid C=O (around 1740 cm^{-1}), the maximum of the amide I (1659 cm^{-1}) and the amide II (1546 cm^{-1}) band.

The mutants D264C and D266C display similar small secondary structure alterations as already seen in the Y256C and Y260C mutants. They show a peak shift from 1659 to 1657 cm^{-1} as well as small alterations at lower wavenumbers. Therefore, no gross alterations in the protein secondary structure are induced by the mutation.

4.4.4 The unconserved aromatic amino acid in loop 7-8: F268C

4.4.4.1 Sodium-induced IR difference spectra of F268C mutant

Unlike F258C, the mutant F268C under normal conditions demonstrates a Cless like interaction with the substrates. As Figure 4.23 and 4.24 show, the sodium-induced IR difference spectra are similar to those of Cless, illustrating that the F268C mutant behaves similar to Cless with respect to sodium binding.

Figure 4.23 In the left panel: 10 mM Na^+ -induced IR difference spectra of Cless and F268C. The spectra correspond to the effect of 10 mM NaCl at 25 °C and pH 6.6 in a buffer containing 20 mM MES and 100 mM KCl. In the right panel: Spectral similarity and intensity in the 1710-1500 cm^{-1} interval on the first derivative of the 10 mM Na^+ -induced IR difference spectra of Cless and F268C.

Figure 4.24 In the left panel: 50 mM Na⁺-induced IR difference spectra of Cless and F268C. The spectra correspond to the effect of 50 mM NaCl at 25 °C and pH 6.6 in a buffer containing 20 mM MES and 100 mM KCl. In the right panel: Spectral similarity and intensity in the 1710-1500 cm⁻¹ interval on the first derivative of the 50 mM Na⁺-induced IR difference spectra of Cless and F268C.

4.4.4.2 Melibiose-induced IR difference spectra of F268C mutant in the presence of sodium

The melibiose-induced difference spectra of the F268C mutant in the presence of 10 mM sodium (Figures 4.26 and 4.27) exhibit similarities and intensities high enough indicating that the phenylalanine in position 268 is not essential for the sugar binding.

Figure 4.26 In the left panel: 10 mM Melibiose-induced IR difference spectra in the presence of 10 mM sodium of Cless and F268C. The spectra correspond to the effect of 10 mM melibiose at 25 °C and pH 6.6 in a buffer containing 20 mM MES, 100 mM KCl and 10 mM NaCl. In the right panel: Spectral similarity and intensity in the 1710-1500 cm^{-1} interval on the first derivative of the 10 mM Melibiose-induced IR difference spectra in the presence of 10 mM sodium of Cless and F268C.

Figure 4.27 In the left panel: 50 mM Melibiose-induced IR difference spectra in the presence of 10 mM sodium of Cless and F268C. The spectra correspond to the effect of 50 mM melibiose at 25 °C and pH 6.6 in a buffer containing 20 mM MES, 100 mM KCl and 10 mM NaCl. In the right panel: Spectral similarity and intensity in the 1710-1500 cm^{-1} interval on the first derivative of the 50 mM Melibiose-induced IR difference spectra in the presence of 10 mM sodium of Cless and F268C.

4.4.4.3 Evaluation of the absorbance spectra of the F268C mutant

In Figure 4.28 the qualitative approach of comparing the second derivative of the absorbance spectra of the mutant with the Cless reference demonstrate that the mutant F268C almost overlap with the Cless spectrum in the main peaks of amino I and II. Therefore, the F268C mutation produces no major alterations of the protein structure.

Figure 4.28 Comparison of absorbance spectra of F268C with Cless in the left panel; Second derivative of the absorbance spectra in the right panel. The dashed lines marked the maximum of lipid C=O (around 1740 cm^{-1}), the maximum of the amide I (1659 cm^{-1}) and the amide II (1546 cm^{-1}) band.

4.4.4.4 Summary and conclusions from the infrared difference spectra results

| A | 10mM Na | 50mM Na | 50mM mel | 10mM Na 10mM mel | 10mM Na 50mM mel |
|----------|---------|---------|----------|------------------|------------------|
| Y256C | | | | | |
| F258C | | | | | |
| Y260C | | | | | |
| D264C | | | | | |
| D266C | | | | | |
| F268C | | | | | |
| B | | | | | |

Figure 4.29 **A:** IR difference spectra of the indicated MelB mutants. **B:** Comparison of absorbance spectra of the MelB mutants with Cless

In the IR difference spectra of MelB mutants (Figure 4.29), the mutants Y256C

and Y260C showed no difference spectra; F258C showed difference spectra only in the presence of both substrates; D264C only exhibited a reduced intensity and similarity in the sodium-induced difference spectra; D266C and F268C indicated similar substrate binding as Cless.

All the mutants showed very similar absorbance spectra when compared with Cless except several small shifts on the main peak. The spectra suggested some conformational changes in the MelB protein.

4.5 Molecular dynamics

A protein atomistic model for the *E. coli* MelB was build using the tridimensional coordinates of *S. typhimurium*'s MelB structure and changing the required amino acids to those of *E. coli* MelB. This model was inserted into a POPE lipid bilayer, and then water and ions were added into the system. After checking the correctness of the system, the minimization and equilibration was carried out.

4.5.1 Minimization and Equilibration

Figure 4.30 In the left panel: RMSD of protein backbone during the minimization procedure; In the right panel: RMSD of protein backbone during the equilibration procedure.

The root-mean-square-deviation (RMSD) during the minimization procedure showed that the system was stable¹⁵ after 100,000 steps in all the mutants and wild type MelB_{EC} (Figure 4.30, left panel). The gaps between the boxes in the periodic systems were checked to make sure the atoms will not be lost in the simulation procedure. Then the system was heated slowly from 0 to 298 K in 2K increments. The RMSD of protein backbone of the equilibration procedure showed a stable movement of the atoms from 0 to 298 K (Figure 4.30, right panel). Now, the model was ready for the Molecular Dynamics simulations.

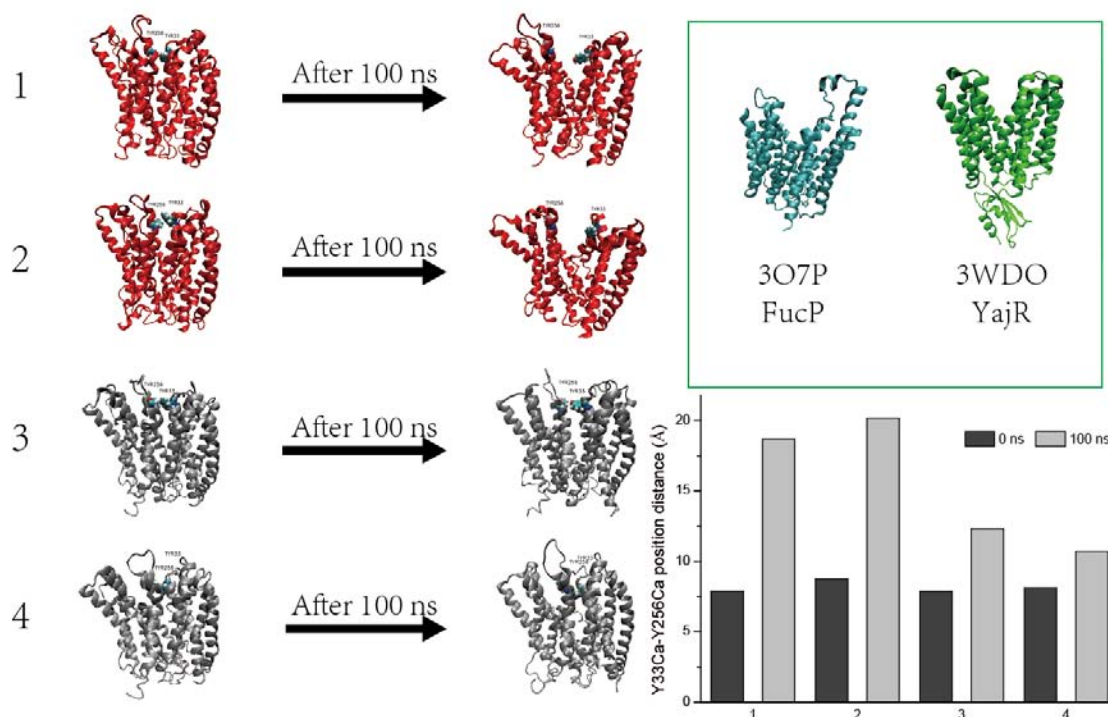
4.5.2 Molecular Dynamics of wild type MelB_{EC}

Figure 4.31 In the left panel: structural changes of wild type MelB_{EC} after 100 ns molecular dynamics (red: open conformation); In the right panel: The distance between the carbon alpha of Tyr-256 and that of Tyr-33 is plotted as a measure of extracellular opening. The crystal structures of outward open conformation of the fucose transporter FucP and the putative drug efflux protein YajR are shown for comparison.

Twelve replicas of the wild type simulation were produced for 100 ns each, starting from two different equilibrated systems. From these, two replicas of the wild type simulation yielded an outward open state (Figure 4.31: 1 and 2), one from each equilibrated system, whereas ten replicas yielded a partially occluded-like state or even a totally occluded state (Figure 4.31: 3 and 4, for two representative partially occluded states) as judged by the plot of distances between the alpha carbon of Tyr-33 and Tyr-256, compared to the initial state (0 ns). It is shown that the distance change between Tyr-33-C_α and Tyr-256-C_α in the open conformation was nearly two times more than the initial state. Opening to the periplasmic space was further confirmed by a surface representation of the water molecules (Figure 4.32). In models 1 and 2, the solvent accessible surfaces of the transport area in the periplasmic side were bigger

than in 3 and 4.

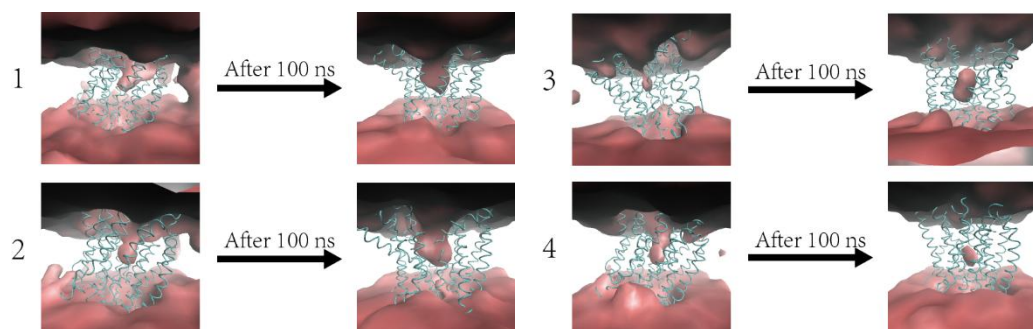


Figure 4.32 the surface representation of water molecules allows identifying the water occupancy in the 0 ns and 100 ns states. The numbers of the models are the same as in **Figure 4.31**.

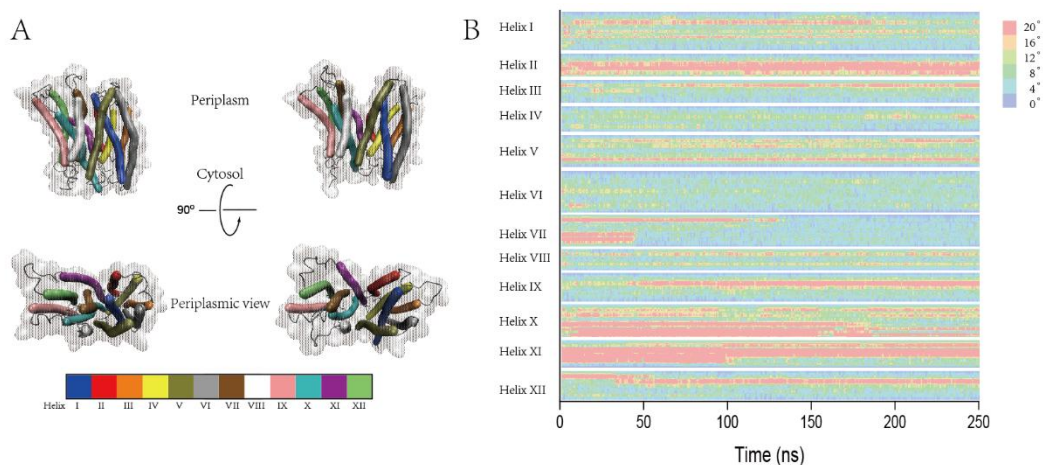


Figure 4.33 **A.** Bendix plot¹⁶ rendered in VMD representing the transition from 0 ns (outward partially occluded) to 250 ns (outward fully opened) for a WT simulation. **B.** Heatmap of helices curvature per residue as a function of time.

The MD for one of the two outward open models was extended up to 250 ns (Figure 4.33) to search for further conformational changes. Only small changes were observed beyond the first 100 ns (Figure 4.33A and Figure 4.34A, B). The dynamics reveals that the loop 7-8 suffers conformational changes (Figure 4.34D) involving also a curvature change in helix VII at around 50 ns (Figure 4.33B). This change was mainly at the Gly-252 position, and we can see from the figure that the helix curvature was decreased (Figure 4.34B). This change causes the separation of the helix VII and helix I resulting in the open conformation of MelB. The interaction between helix I

and VII was broken as we can see in Figure 4.35. The intra-helix conformational changes of Helix VII represent a deviation from the rigid body rocking-bundle model (Figure 4.34B). At around 100 ns, the protein shows a fully open shape that hardly changes until the end of the simulation (Figures 4.33B, 4.34C and D). As reported by Stelzl *et al* for other transporters,¹⁷ the periplasmic gate distance of the open conformation was estimated by C_α atoms of the residues in helix I and VII (FucP: Gln-51/Ile-282; YajR: Thr-37/Pro-236), which is around 20 Å (measured by VMD). This value fits well with the values found in our case of about 25 Å (Figure 4.31 and 4.34C).

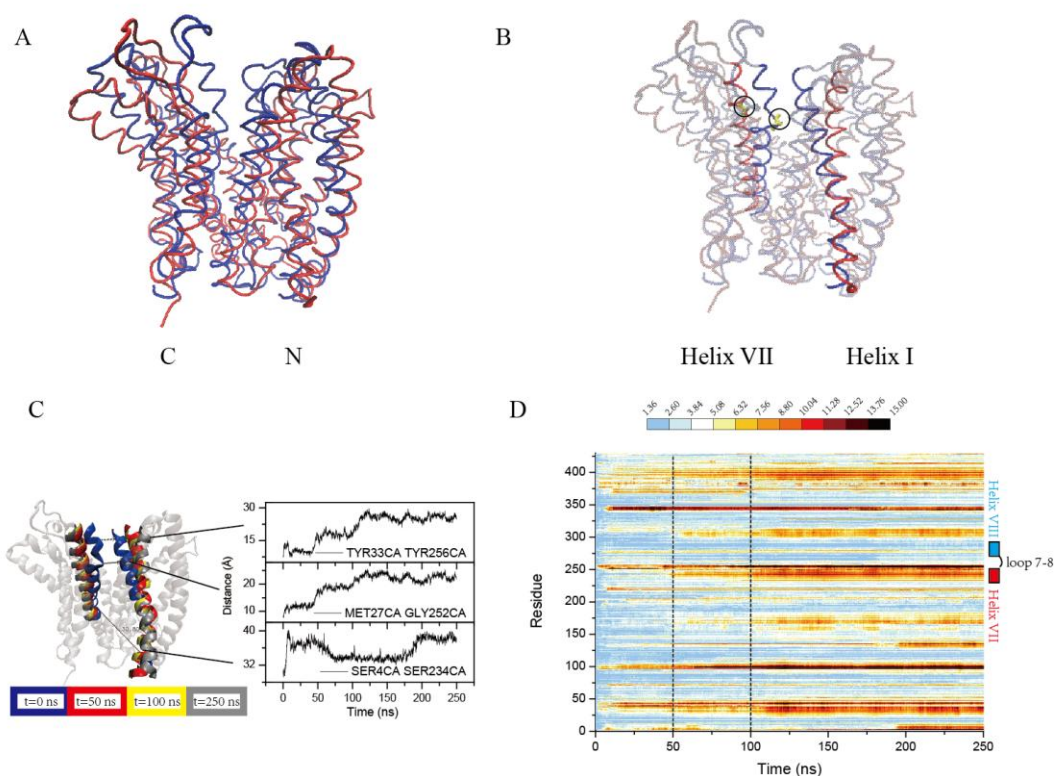


Figure 4.34 **A.** Initial (blue) and final (250 ns, red) states of MelB_{EC} after spatial alignment. **B.** Initial (blue) and final (red) states of helix VII and I in MelB_{EC} after spatial alignment; Gly 252 was colored in yellow and inside the circle. **C.** Helical motions in MelB_{EC} on reaching the open conformation. Four superimposed conformations of helix VII and helix I (left): initial (t = 0 ns; blue) and final (t = 250 ns; grey) along with two intermediate snapshots (t = 50 ns; red, t = 100 ns; yellow) are shown. Distances between the helix VII and helix I (right) measured by C_α atoms of representative residues are shown in the figure. **D.** RMSD per residue of the MelB_{EC} opening. The scale bar indicates RMSD in Å.

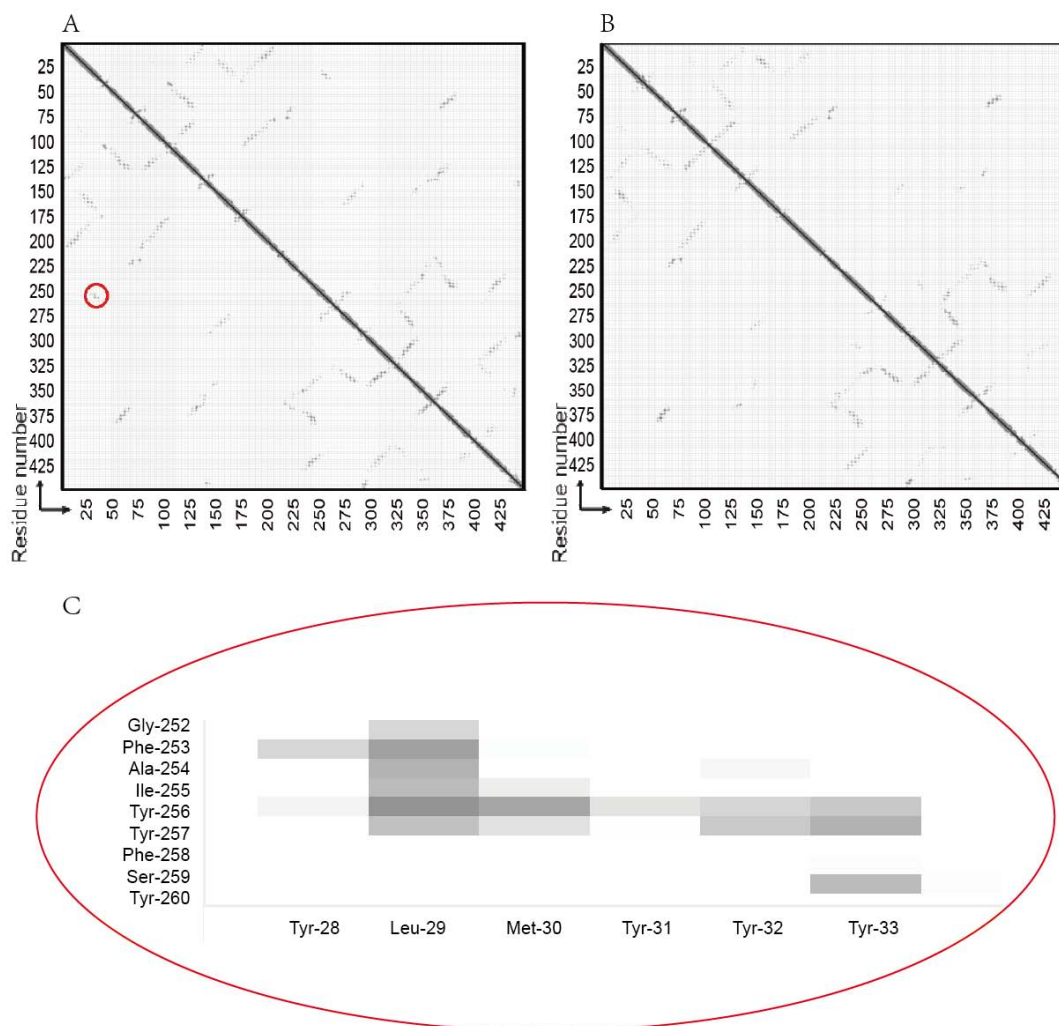


Figure 4.35 Residue-residue contact maps in VMD from the first MDS of wild type MelB_{EC} (1 of **Figure 4.31**): A. 0 ns; B. 250 ns. The red circle represent the changed interaction of helix VII between 0 ns and 250 ns. C. The amplified red circle showing residue-residue contacts that disappear after 250 ns simulation. The alpha-Carbon to alpha-Carbon distance for each pair is plotted. A graph square is colored black at 0.0 Å distance, to a linear gray scale between 0.0 and 10.0 Å, and white when equal to or greater than 10.0 Å.

The *S. typhimurium* outward partially occluded state of MelB contains a set of ionic locks and hydrophobic patches¹. We have mapped this set of interactions in our *E. coli* MelB system (figure not shown). One of the possible hydrophobic locks is shown in Figure 4.36. The conserved residues of loop 7-8/end of helix VII are colored in blue (Tyr-256, Tyr-257, Phe-258 and Tyr-260). On going from the partially occluded to the open form, the conformation of these residues changed significantly, breaking their interaction with the cluster located in the end of helix I (especially, Tyr-33 and Met-30).

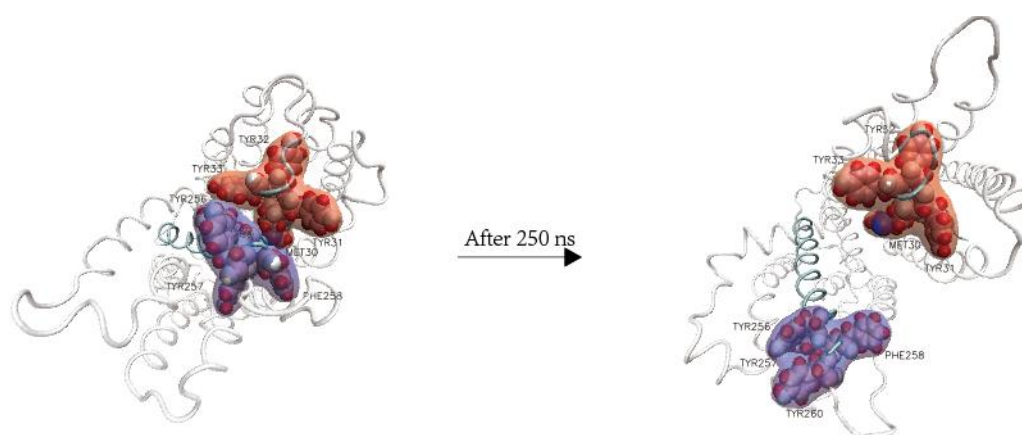


Figure 4.36 Details of the partially occluded state (0 ns) and the outward full open state (250 ns). Illustrative representation highlighting the hydrophobic lock between helix VII and I. The conserved residues of helix VII are shown in blue and the four residues of helix I are shown in red.

4.5.3 Molecular Dynamics of MelB mutated at conserved amino acids in loop 7-8/end of helix VII

Two replicas of each mutants (Y256C, Y257C, F258C and Y260C) yielded relatively small changes during the simulation. Y256C and F258C showed a moderate tendency to open, giving in each case a partially occluded-like state more open than the initial state. Y257C and Y260C showed almost no changes during simulations. To illustrate changes, Figure 4.37 shows the plot of distances between the carbon alpha of Tyr33 and residue 256, compared to the initial state (0 ns). The observed change of the periplasmic space was further confirmed by a surface representation of the water molecules (Figure 4.38). And the curvature analysis of helix VII (figure 4.39) showed only few changes after the first 50 ns of simulation. It is possible that more replicas or longer simulations could show differences compared to WT.

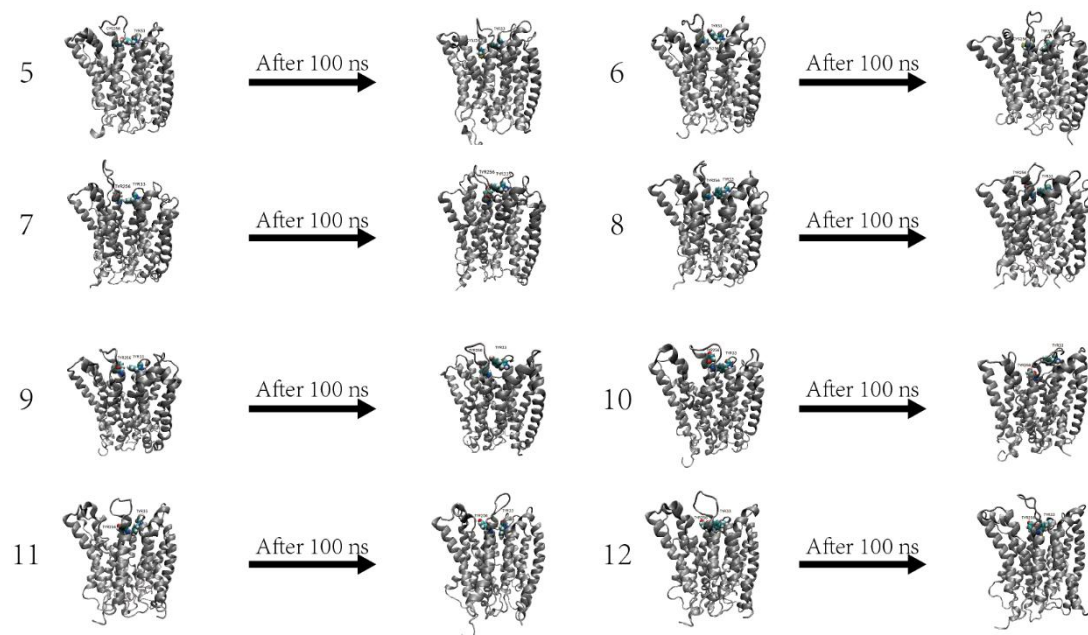


Figure 4.37 In the upper panel: the structure of MelB_{EC} mutants changes from 0 ns to 100 ns (5 and 6: Y256C; 7 and 8: Y257C; 9 and 10:F258C; 11 and 12: Y260C); In the lower panel: The distance between the carbon alpha of Tyr33 and the residue of 256 is plotted as a measure of extracellular opening.

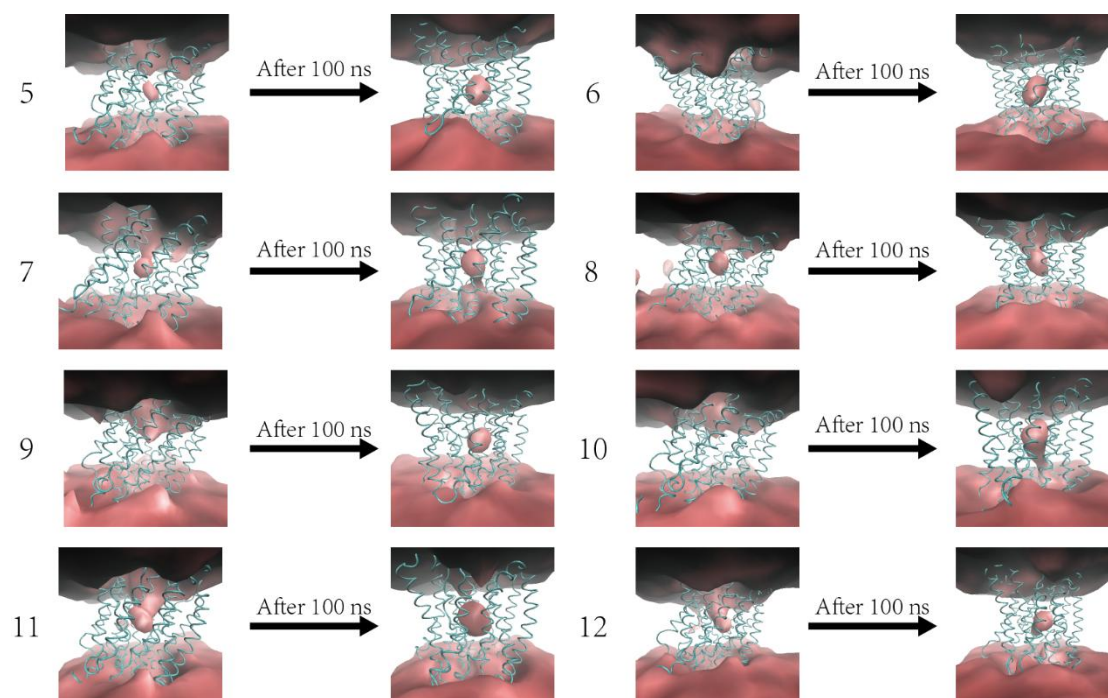


Figure 4.38 the surface representation of water molecules allows identifying the water occupancy in the 0 ns and 100 ns. The numbers for the replicas were the same as in **Figure 4.37**.

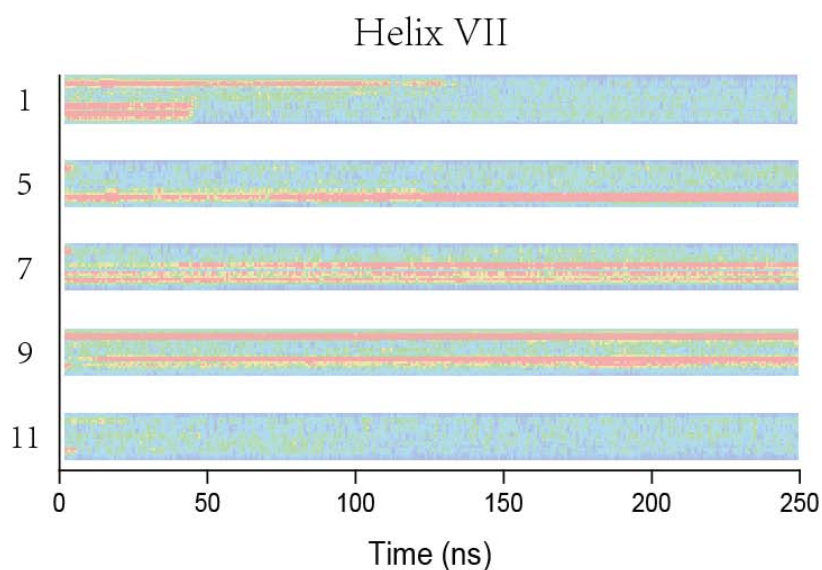


Figure 4.39 Heatmap of helix VII curvature per residue as a function of time of WT (1), Y256C (5), Y257C (7), F258C (9), and Y260C (11) MelB_{EC} mutants.

4.5.4 Conclusions from the molecular dynamics results

The open conformation of MelB protein proceeds through a considerable

movement on the helices, especially on helix VII.

The conserved amino acids in loop 7-8/end of helix VII may be important to help controlling the open movement of the protein, since they interact with residues on helix I in the occluded state.

4.6 Crystallization studies of MelB R149C mutant

The conformational dynamics of secondary transporters make it difficult to get a good resolution crystal. So, a mutant with decreased conformational flexibility may help the crystallization of transporters. Our group found that the R149C mutant⁹ can bind substrates and also traps the protein in an inward-facing conformation. Therefore, it seems that this R149C mutant is suitable for crystallization trials.

As described in the Materials and Methods, we purified the R149C protein and prepared this protein at enough high concentration, then commercial crystal screening kits were assayed to try to improve the previous conditions obtained by Lin³.

We successfully got crystals in a condition containing 0.1 M MES, pH 7, 0.1 M NaCl and 34% PEG 300 (Figure 4.40). But the diffraction patterns of these crystals yielded resolutions around 7 Å, a little better than previously described, but not good enough to be processed. Although we tried to optimize the conditions (pH, different PEG concentration and so on), no better crystals were obtained.

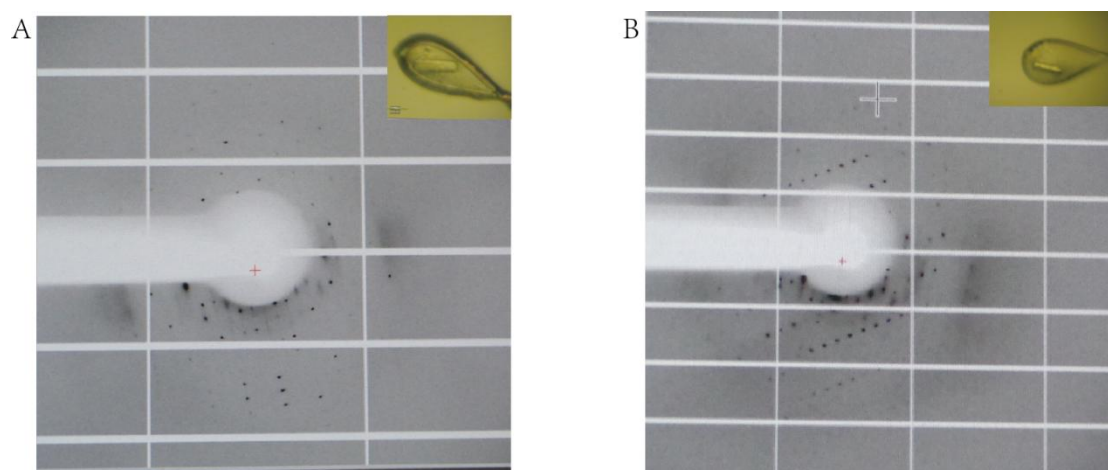


Figure 4.40 X-ray diffraction patterns of R149C crystals obtained at synchrotron ALBA XALOC-13 beamline.

REFERENCES

1. Ethayathulla, A. S., Yousef, M. S., Amin, A., Leblanc, G., Kaback, H. R., and Guan, L. (2014) Structure-based mechanism for Na⁽⁺⁾/melibiose symport by MelB, *Nature communications* 5, 3009.
2. Goldenberg, O., Erez, E., Nimrod, G., and Ben-Tal, N. (2009) The ConSurf-DB: pre-calculated evolutionary conservation profiles of protein structures, *Nucleic acids research* 37, D323-327.
3. Lin, Y. (2012) Structural and functional studies of melibiose permease of *Escherichia coli*, In *Department of Biochemistry and Molecular Biology*, Universitat Autònoma de Barcelona.
4. Maehrel, C., Cordat, E., Mus-Veteau, I., and Leblanc, G. (1998) Structural studies of the melibiose permease of *Escherichia coli* by fluorescence resonance energy transfer. I. Evidence for ion-induced conformational change, *The Journal of biological chemistry* 273, 33192-33197.
5. Cordat, E., Mus-Veteau, I., and Leblanc, G. (1998) Structural studies of the melibiose permease of *Escherichia coli* by fluorescence resonance energy transfer. II. Identification of the tryptophan residues acting as energy donors, *The Journal of biological chemistry* 273, 33198-33202.
6. Abdel-Dayem, M., Basquin, C., Pourcher, T., Cordat, E., and Leblanc, G. (2003) Cytoplasmic loop connecting helices IV and V of the melibiose permease from *Escherichia coli* is involved in the process of Na⁺-coupled sugar translocation, *J Biol Chem* 278, 1518-1524.
7. Guan, L., Nurva, S., and Ankeshwarapu, S. P. (2011) Mechanism of melibiose/cation symport of the melibiose permease of *Salmonella typhimurium*, *The Journal of biological chemistry* 286, 6367-6374.
8. Guan, L., Jakkula, S. V., Hodkoff, A. A., and Su, Y. (2012) Role of Gly117 in the cation/melibiose symport of MelB of *Salmonella typhimurium*, *Biochemistry* 51, 2950-2957.
9. Lin, Y., Fuerst, O., Granell, M., Leblanc, G., Lorenz-Fonfria, V., and Padros, E. (2013) The substitution of Arg149 with Cys fixes the melibiose transporter in an inward-open conformation, *Biochimica et biophysica acta* 1828, 1690-1699.
10. Leon, X., Leblanc, G., and Padros, E. (2009) Alteration of sugar-induced conformational changes of the melibiose permease by mutating Arg141 in loop 4-5, *Biophys. J.* 96, 4877-4886.
11. Leon, X., Lemonnier, R., Leblanc, G., and Padros, E. (2006) Changes in secondary structures and acidic side chains of melibiose permease upon cosubstrates binding, *Biophysical journal* 91, 4440-4449.
12. Ganea, C., Pourcher, T., Leblanc, G., and Fendler, K. (2001) Evidence for intraprotein charge transfer during the transport activity of the melibiose permease from *Escherichia coli*, *Biochemistry* 40, 13744-13752.
13. Ganea, C., and Fendler, K. (2009) Bacterial transporters: charge translocation and mechanism, *Biochimica et biophysica acta* 1787, 706-713.
14. Fuerst, O., Lin, Y., Granell, M., Leblanc, G., Padros, E., Lorenz-Fonfria, V. A., and Cladera, J. (2015) The Melibiose Transporter of *Escherichia coli*: CRITICAL CONTRIBUTION OF LYS-377 TO THE STRUCTURAL ORGANIZATION OF THE INTERACTING SUBSTRATE BINDING SITES, *The Journal of biological chemistry* 290, 16261-16271.
15. Law, R. J., Capener, C., Baaden, M., Bond, P. J., Campbell, J., Patargias, G., Arinaminpathy, Y.,

- and Sansom, M. S. (2005) Membrane protein structure quality in molecular dynamics simulation, *Journal of molecular graphics & modelling* 24, 157-165.
16. Dahl, A. C., Chavent, M., and Sansom, M. S. (2012) Bendix: intuitive helix geometry analysis and abstraction, *Bioinformatics* 28, 2193-2194.
 17. Stelzl, L. S., Fowler, P. W., Sansom, M. S., and Beckstein, O. (2014) Flexible gates generate occluded intermediates in the transport cycle of LacY, *Journal of molecular biology* 426, 735-751.

5 GENERAL DISCUSSION

Some studies show that the loops are important for the structure and function of membrane proteins. For example, research on Lac permease shows that a minimum length of the central cytoplasmic loop is necessary for activity, stability, and insertion into the membrane.¹ A loop of the calcium pump was found to be important for the transport process: the loop is mediating contact between the intramembranous Ca^{2+} -binding sites and the cytosolic phosphorylation site²; the loop 6-7 participates in the formation of an entrance port, before subsequent high affinity binding of Ca^{2+} inside the membrane³. A study about the cytoplasmic loop 4-5 of MelB suggests that it is involved in the process of Na^{+} -coupled sugar translocation⁴.

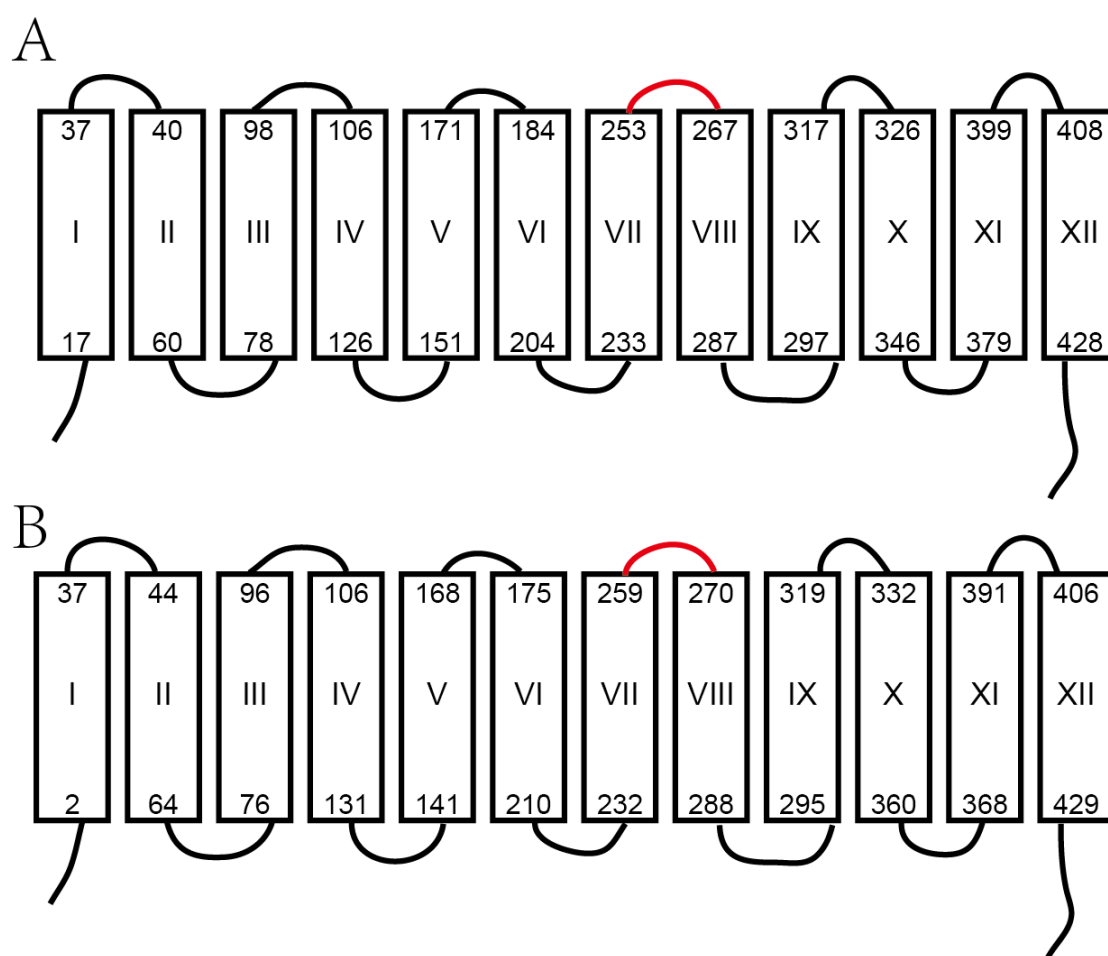


Figure 5.1 The distribution of helices and loops. A. Before the 3D structure was solved.⁵ B. After the 3D structure was solved.⁶

The fact that four aromatic amino acids (Tyr-256, Tyr-257, Phe-258 and Tyr-260) that have a high level of conservation are located in the loop 7-8 and the end of helix VII suggested that this loop/end of helix may also have some role in the transport mechanism of MelB. In addition, there are two negatively charged residues (Asp-264 and Asp-266) and one more aromatic amino acid (Phe-268) in this loop, out of the residues mentioned before.

At the beginning of this project, the MelB 3D structure was not known, and the distribution of helices and loops was that established by prediction methods⁵ as shown in Figure 5.1A. Shortly afterward, the transporter 3D structure was published⁶, establishing some differences in the distribution of helices and loops (Figure 5.1B). It therefore resulted that three of the conserved residues are in fact located at the end of helix VII.

For all the mutants described in this thesis, the FRET (Trp \rightarrow D²G) of MelB-containing proteoliposomes and ISO vesicles was measured. The results show that the mutants of the four conserved amino acids are almost unable to bind D²G and no subsequent effect of Na⁺ or melibiose were observed. On the other hand, the IR difference spectra of Y256C and Y260C do not show the same peaks as in Cless, after Na⁺ or melibiose addition. These set of experiments demonstrate the absence of interaction of the MelB substrates with these mutants. However, F258C showed some peaks in the difference spectra, suggesting a low binding affinity of substrates for this mutant. The positions of the four conserved residues are shown in Figure 5.2. Except for Tyr-260 in the loop 7-8, the other three residues (Tyr-256, Tyr-257 and Phe-258) are located at the end of helix VII. When these amino acids are mutated to cysteine, the occupied volumes are decreased since the volume of cysteine is smaller than tyrosine or phenylalanine. The results of two repeats of 250 ns molecular dynamics simulation of each of the mutants Y256C, Y257C, F258C and Y260C showed only small changes in the protein conformation. However, the fact that these mutants are unable to bind the substrates indicates that these four residues are very important in the MelB transport mechanism, in keeping with the conservation analysis. As Guan *et*

al⁶ indicated, LacY and MelB have similar sugar specificity as well as similar location of the sugar-recognition site, and the aromatic residues may contribute to interact with the sugar by CH/ π -interactions with the pyranosyl ring. Therefore, these four residues could help the sugar to find the right way to go inside the MelB protein. However, the fact that the mutated MelB also lack interaction with the co-substrate Na⁺ calls for a more structural role. In the context of this hypothesis, it was shown by Molecular Dynamics that the interactions between the end of helices VII and I (the hydrophobic lock) in which these four aromatic side chains participate are broken upon opening of the extracellular side (Figure 5.5). Thus, this hydrophobic lock may have a role on the opening/closing mechanism necessary for permitting substrates binding/release and thus necessary for the transport mechanism.

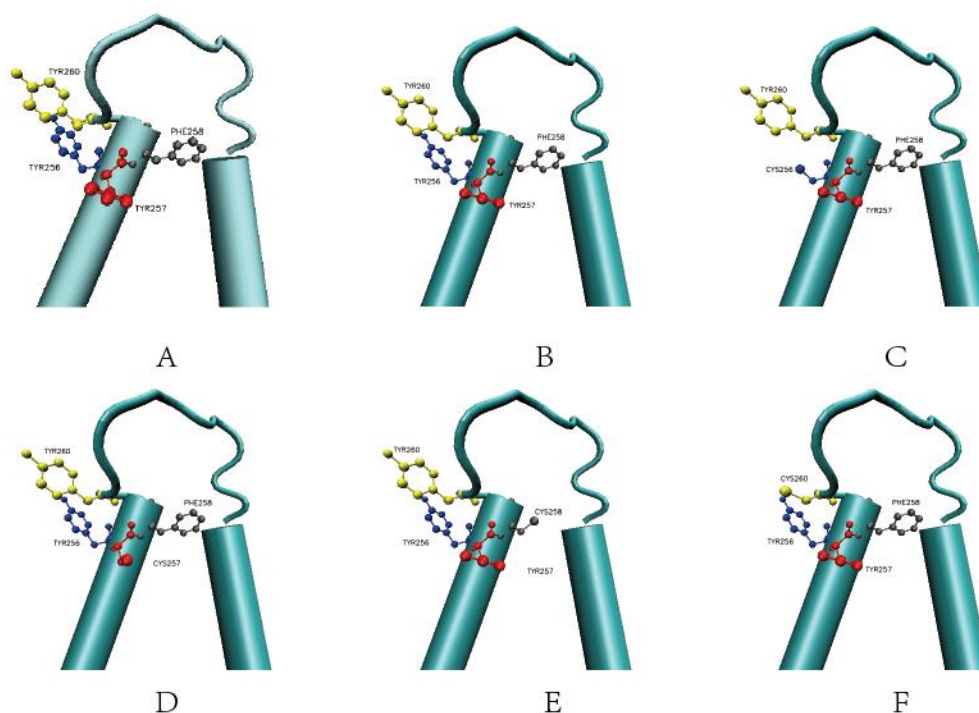


Figure 5.2 The positions of four conserved amino acids in loop 7-8/end of helix VII of the MelB. A, MelB_{ST-A}⁶; B, Wild type-MelB_{EC}; C, Y256C-MelB_{EC}; D, Y257C-MelB_{EC}; E, F258C-MelB_{EC}; F, Y260C-MelB_{EC}. (256-yellow; 257-red; 258-blue; 260-grey)

Apart from the four conserved residues, there are two negatively charged residues (Asp-264 and Asp-266) in loop 7-8 (Figure 5.3). The mutation of these two

charged residues shows similar results in FRET experiments as for Cless. But the IR difference spectra show somewhat altered results. The IR difference spectra of D266C have almost the same peaks as Cless, however, D264C only shows similar peaks as Cless in the presence of sodium but not in the presence of melibiose. It is possible that mutation of Asp-264 affects the melibiose binding site thus giving rise to altered IR difference spectra.

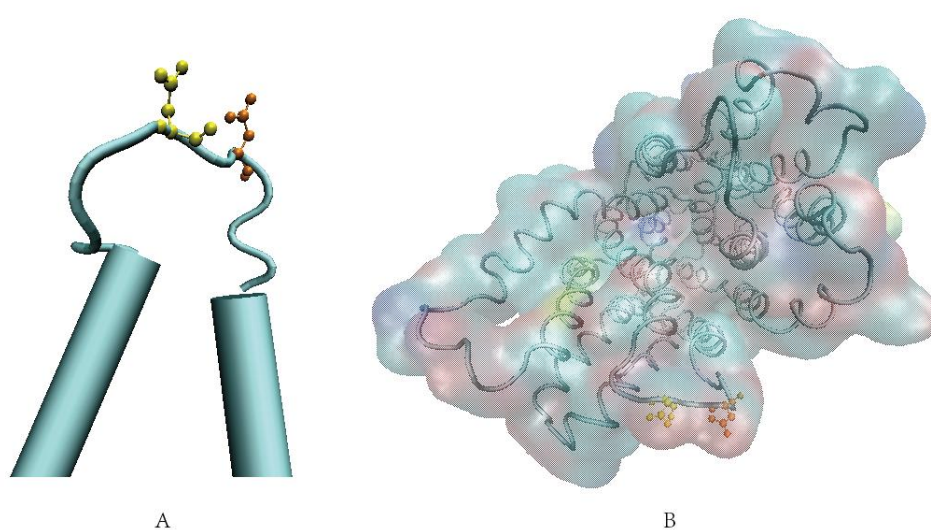


Figure 5.3 The two charged amino acids of loop 7-8 in the MelB_{ST}-A⁶. (Asp-264: yellow; Asp-266: orange)

There is another aromatic amino acid in loop 7-8, Phe-268. The FRET shows that F268C keeps the ability to bind sodium, D²G and melibiose. The IR difference spectra give an identical conclusion. Some other residues (S259A, S259C, V261C, G263C, A265C, L267C) of the loop 7-8/helix VII were also studied in FRET experiments; they show the capability of binding Na⁺, D²G and melibiose to different levels.

The loop 7-8 had not been studied before, whereas other loops such as 4-5 or 10-11 have merited interest in the past. The Arg-141 and Arg-149 in loop 4-5 were found to be involved in the reaction of co-substrate translocation or substrate release in the inner compartment.⁴ Later research suggested that Arg-149 was not in the loop but in the helix V⁷; the Arg-141 has a role in catalyzing the subsequent

conformational change necessary for substrate translocation.⁸ Another study suggested that the loop 4-5 contributes to the coordinated interactions between the ion and sugar binding sites; it also participates in an electrogenic conformational transition after melibiose binding.⁹ A cysteine scan on the loop 10-11 shows that in the melibiose transporter functionally charged residues are structurally conserved.¹⁰ The loop 10-11 was not totally exposed in the cytoplasmic side, as some parts have a re-entrant loop structure.¹¹

Since the loop 7-8 is located in the inner part of the periplasmic side of the protein, its movement can cause a considerable effect on the protein conformation. As shown in Figure 5.4, when the loop bends to the inner side of the cave, the open area will become smaller. Which looks like a part of the gates as hypothesis in a 6-state model of SGLTs 2 (see in the Introduction part: Figure 1.10).

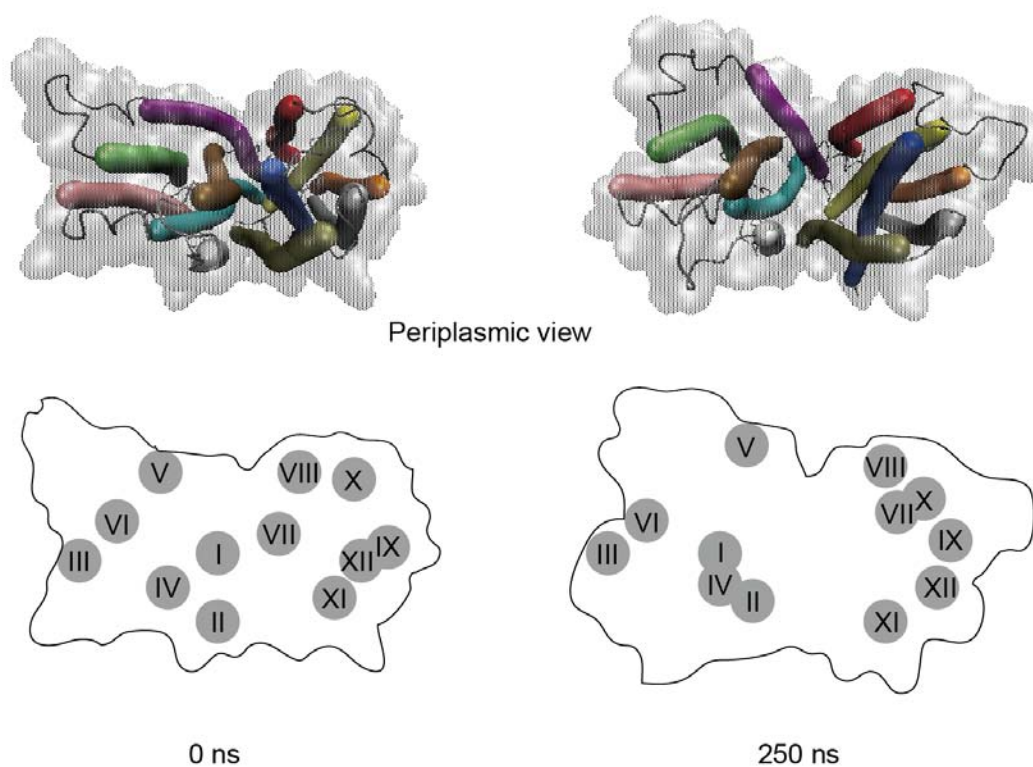


Figure 5.4 The scheme of the helices positions from the open conformation of MelB_{EC} of MDS.

Left: 0 ns; Right: 250 ns

Considering the existing hypothetical mechanisms of sugar transporters (LacY¹²,¹³, SGLTs¹⁴ and MelB_{ST}⁶), the following mechanism is proposed (Figure 5.6) : 1. occluded-empty state; 2. Outward-empty state; 3. Outward sodium bound state. Binding of a Na⁺ to the cation-binding site induces an increase in sugar affinity, maybe let the sugar binding site form; 4. Outward sodium and melibiose bound state. The sodium was binding in the middle of a trigonal bipyramid formed by the residues at positions Asp-55/Asp-59/Asp-124 and Tyr-120/Thr-121/Thr-373⁶. And the melibiose is near Asp-124^{6, 15} which is the area of sugar binding site; 5. Occluded sodium and melibiose bound state; 6. Inward sodium and melibiose bound state; 7. Inward melibiose released state; 8. Inward sodium released state. The transport process is continuous from 1 to 8.

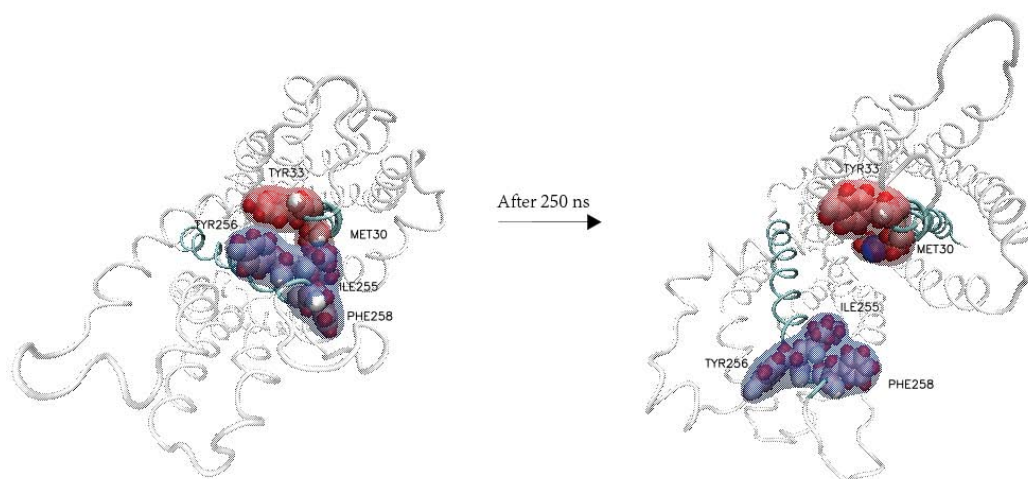


Figure 5.5 Details of the partially occluded state (0 ns) and the outward full open state (250 ns). Illustrative representation highlighting one of the hydrophobic lock (between helix VII and I), the residues of helix VII are showed in blue and the residues of helix I are showed in red.

Our results are relevant for several steps of the transport cycle (see Figure 5.6). In the empty transporter, interactions between the extremes of helices I and VII such those we describe (the hydrophobic lock) appear to be important for the equilibrium outwardly open \leftrightarrow occluded \leftrightarrow inwardly open (steps 2, 1, 8). To allow the equilibrium, the hydrophobic lock should remain sufficiently weak. After binding of substrates, an increase in the interaction force within the lock drives the transporter to a stabilized

form predominantly opened toward the cytoplasm to allow the release of substrates (steps 6, 7, 8). This strengthening of the lock could occur by substrate-induced conformational changes leading to a more favorable interaction. The protein returns to the initial equilibrium state requiring a weaker force of interaction involved in the hydrophobic lock, upon substrates release. Finally, it is interesting to remark that helix VII is not moving as a rigid body, but a kink initially present at the level of Gly-252 disappears, giving rise to a straight helix upon opening of the extracellular side, as can be seen in Figure 5.7.

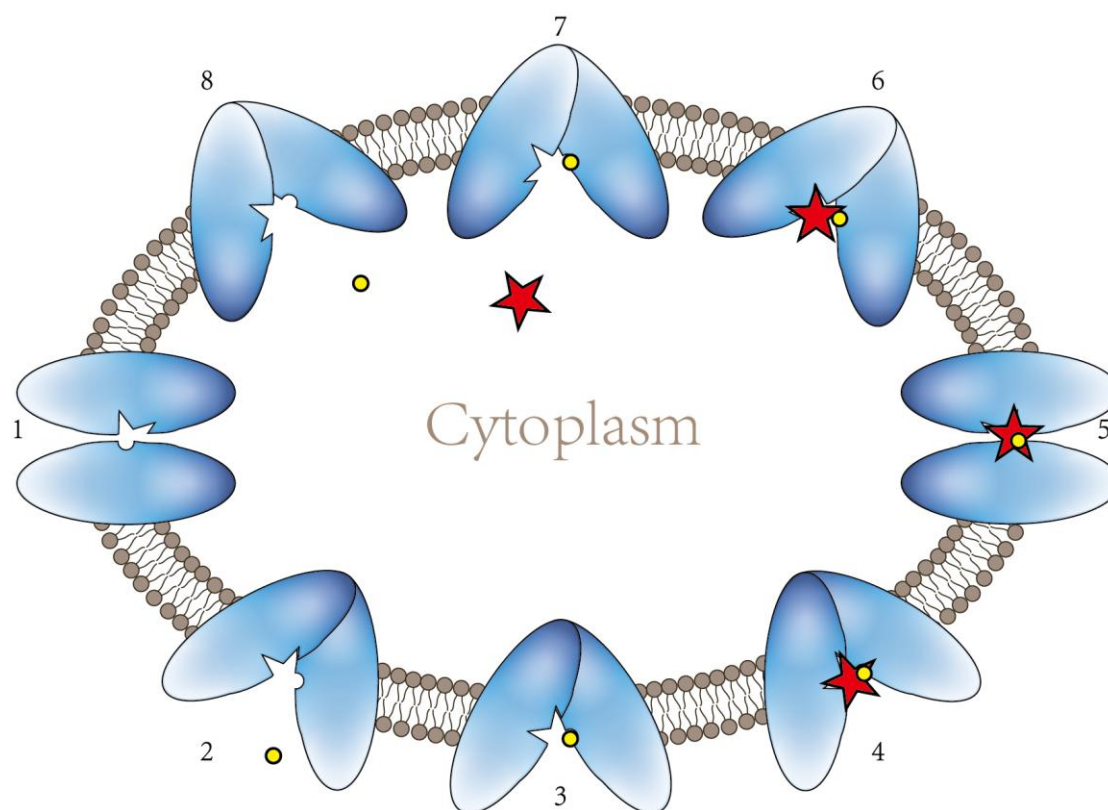
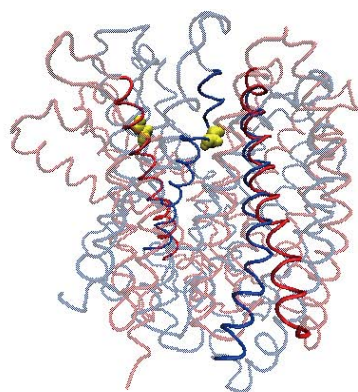


Figure 5.6 The scheme of kinetic steps for Na^+ /melibiose symport. 1. occluded-empty state; 2. Inward-empty state; 3. Inward sodium bound state; 4. Inward sodium and melibiose bound state; 5. Occluded sodium and melibiose bound state; 6. Outward sodium and melibiose bound state; 7. Outward melibiose released state; 8. Outward sodium released state. Sodium: yellow circle; melibiose: red star.

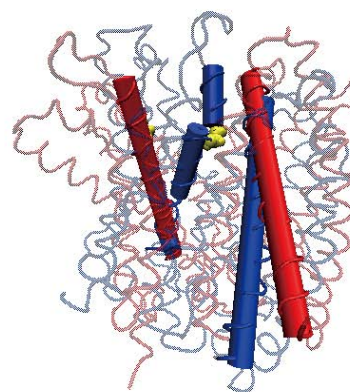
A



Helix VII

Helix I

B



Helix VII

Helix I

Figure 5.7 Initial (blue) and final (red) states of helix VII and I in MeIB_{EC} after spatial alignment, Gly 252 was colored by yellow. Drawing method of helix VII and I: A. Tube; B. Cartoon.

REFERENCES

1. Weinglass, A. B., and Kaback, H. R. (2000) The central cytoplasmic loop of the major facilitator superfamily of transport proteins governs efficient membrane insertion, *Proceedings of the National Academy of Sciences of the United States of America* 97, 8938-8943.
2. Zhang, Z., Lewis, D., Sumbilla, C., Inesi, G., and Toyoshima, C. (2001) The role of the M6-M7 loop (L67) in stabilization of the phosphorylation and Ca(2+) binding domains of the sarcoplasmic reticulum Ca(2+)-ATPase (SERCA), *The Journal of biological chemistry* 276, 15232-15239.
3. Menguy, T., Corre, F., Juul, B., Bouneau, L., Lafitte, D., Derrick, P. J., Sharma, P. S., Falson, P., Levine, B. A., Moller, J. V., and le Maire, M. (2002) Involvement of the cytoplasmic loop L6-7 in the entry mechanism for transport of Ca²⁺ through the sarcoplasmic reticulum Ca²⁺-ATPase, *The Journal of biological chemistry* 277, 13016-13028.
4. Dayem, M. A., Basquin, C., Pourcher, T., Cordat, E., and Leblanc, G. (2003) Cytoplasmic loop connecting helices IV and V of the melibiose permease from *Escherichia coli* is involved in the process of Na⁺-coupled sugar translocation, *Journal of Biological Chemistry* 278, 1518-1524.
5. Pourcher, T., Bibi, E., Kaback, H. R., and Leblanc, G. (1996) Membrane topology of the melibiose permease of *Escherichia coli* studied by melB-phoA fusion analysis, *Biochemistry* 35, 4161-4168.
6. Ethayathulla, A. S., Yousef, M. S., Amin, A., Leblanc, G., Kaback, H. R., and Guan, L. (2014) Structure-based mechanism for Na(+)/melibiose symport by MelB, *Nature communications* 5, 3009.
7. Lin, Y., Fuerst, O., Granell, M., Leblanc, G., Lorenz-Fonfria, V., and Padros, E. (2013) The substitution of Arg149 with Cys fixes the melibiose transporter in an inward-open conformation, *Biochimica et biophysica acta* 1828, 1690-1699.
8. Leon, X., Leblanc, G., and Padros, E. (2009) Alteration of sugar-induced conformational changes of the melibiose permease by mutating Arg141 in loop 4-5, *Biophys. J.* 96, 4877-4886.
9. Meyer-Lipp, K., Sery, N., Ganea, C., Basquin, C., Fendler, K., and Leblanc, G. (2006) The inner interhelix loop 4-5 of the melibiose permease from *Escherichia coli* takes part in conformational changes after sugar binding, *The Journal of biological chemistry* 281, 25882-25892.
10. Ding, P. Z. (2003) An investigation of cysteine mutants on the cytoplasmic loop X/XI in the melibiose transporter of *Escherichia coli* by using thiol reagents: implication of structural conservation of charged residues, *Biochemical and biophysical research communications* 307, 864-869.
11. Ding, P. Z. (2004) Loop X/XI, the largest cytoplasmic loop in the membrane-bound melibiose carrier of *Escherichia coli*, is a functional re-entrant loop, *Biochimica et biophysica acta* 1660, 106-117.
12. Madej, M. G., Sun, L., Yan, N., and Kaback, H. R. (2014) Functional architecture of MFS D-glucose transporters, *Proceedings of the National Academy of Sciences of the United States of America* 111, E719-727.
13. Stelzl, L. S., Fowler, P. W., Sansom, M. S., and Beckstein, O. (2014) Flexible gates generate

- occluded intermediates in the transport cycle of LacY, *Journal of molecular biology* 426, 735-751.
14. Wright, E. M., Loo, D. D., and Hirayama, B. A. (2011) Biology of human sodium glucose transporters, *Physiological reviews* 91, 733-794.
 15. Shaikh, S. A., Li, J., Enkavi, G., Wen, P. C., Huang, Z., and Tajkhorshid, E. (2013) Visualizing functional motions of membrane transporters with molecular dynamics simulations, *Biochemistry* 52, 569-587.
 16. Fuerst, O., Lin, Y., Granell, M., Leblanc, G., Padrós, E., Lorenz-Fonfria, V. A., and Cladera, J. (2015) The Melibiose Transporter of *Escherichia coli*: CRITICAL CONTRIBUTION OF LYS-377 TO THE STRUCTURAL ORGANIZATION OF THE INTERACTING SUBSTRATE BINDING SITES, *The Journal of biological chemistry* 290, 16261-16271.

CONCLUSIONS

1) There are four conserved amino acids (Tyr-256, Tyr-257, Phe-258 and Tyr-260) in the loop 7-8/end of helix VII.

2) The Förster Resonance Energy Transfer and infrared difference spectra results of Y256C and Y260C show that the mutants are not able to bind D²G, Na⁺ or melibiose.

3) The FRET spectra of Y257C and F258C suggest the mutants have lost the binding ability with D²G, Na⁺ or melibiose. But the IR difference spectra of F258C have some peaks in the presence of sodium and melibiose, indicative of low binding affinity.

4) D264C gave similar FRET spectra as Cless in ISO vesicles and proteoliposomes, although of reduced intensity. But the IR difference spectra showed peaks only in the presence of Na⁺ (i.e. there are no peaks in the presence of melibiose). These results suggest that Asp-264 has some structural role in the transport mechanism.

5) The mutants S259A, S259C, V261C, G263C, A265C, D266C, L267C and F268C are able to give a similar response as Cless in the fluorescence experiments when D²G, Na⁺ or melibiose was added. And the IR difference spectra of D266C and F268C also show similar peaks as Cless.

6) Molecular dynamics simulations of MelB_{EC} show conformational changes from an occluded state to an outward open state. The helix VII undergoes significant changes, during which the extracellular part separates from helix I. Combining these results with those from FRET and IR spectra, it is suggested that the conserved residues may form a hydrophobic lock which may be important in the transport process.

7) We got some crystals of R149C which can diffract to a resolution near 7 Å.

However, the data from the diffraction patterns are not good enough to be processed to get structural information.

APPENDIX

Appendix 1 Sequencing of mutants. Comparison with Cless.

Y256C

| | |
|--|--|
| <p>c-less MSISMTTKLSYGFAGKDFAIIVMYMLYYTDDVGLSVGLVSTLFLVARINDAINDP y256c MSISMTTKLSYGFAGKDFAIIVMYMLYYTDDVGLSVGLVSTLFLVARINDAINDP</p> <p>c-less IMGWIVNATRSRWGKFKPFWILIGTLANSVILFLFSAHLEFEGTQIVFVSVTYILWGNTY y256c IMGWIVNATRSRWGKFKPFWILIGTLANSVILFLFSAHLEFEGTQIVFVSVTYILWGNTY</p> <p>c-less TIMDIPFWSLVPTIILDKREREQLVYPRFFASLAGFVTAGVTLFPVNVYGGGDRGFGFQ y256c TIMDIPFWSLVPTIILDKREREQLVYPRFFASLAGFVTAGVTLFPVNVYGGGDRGFGFQ</p> <p>c-less MFTLVLIAFFIVSTIILNVEHFSSDQPSAEGSHLTKAIVALIYKNDQSVLLGMA y256c MFTLVLIAFFIVSTIILNVEHFSSDQPSAEGSHLTKAIVALIYKNDQSVLLGMA</p> <p>c-less LAYNVAENIITGFAIYFVSIVIGDADLFPYLSYAGAANLTVLFFPRLVKLSRRILWA y256c LAYNVAENIITGFAIYFVSIVIGDADLFPYLSYAGAANLTVLFFPRLVKLSRRILWA</p> | <p>c-less HLTLKAIVALIYKNDQSVLLGMAIYVNASNIITGFAIYFVSIVIGDADLFPYLSYAG y256c HLTLKAIVALIYKNDQSVLLGMAIYVNASNIITGFAIYFVSIVIGDADLFPYLSYAG</p> <p>c-less AANLTVLFFPRLVKLSRRILWAGASILPVLSSGVLLMALMSYHNVLIVIAGILLNV y256c AANLTVLFFPRLVKLSRRILWAGASILPVLSSGVLLMALMSYHNVLIVIAGILLNV</p> <p>c-less GTALFWLVQIMVADIVDYGKLVHRSSEIAYSQVTMVKGGSAFAAFFIAVVLGMIGY y256c GTALFWLVQIMVADIVDYGKLVHRSSEIAYSQVTMVKGGSAFAAFFIAVVLGMIGY</p> <p>c-less VFNVEQSTQALLGMQFIMIALPTLFFMVTLLIYFRFRYRNGDTRRIQIHLDRKRVPEP y256c VFNVEQSTQALLGMQFIMIALPTLFFMVTLLIYFRFRYRNGDTRRIQIHLDRKRVPEP</p> <p>c-less EPVHADIPVGVSDVKAHHHHHH y256c EPVHADIPVGVSDVKAHHHHHH</p> |
|--|--|

Y257C

| | |
|--|--|
| <p>c-less MSISMTTKLSYGFAGKDFAIIVMYMLYYTDDVGLSVGLVSTLFLVARINDAINDP y257c MSISMTTKLSYGFAGKDFAIIVMYMLYYTDDVGLSVGLVSTLFLVARINDAINDP</p> <p>c-less IMGWIVNATRSRWGKFKPFWILIGTLANSVILFLFSAHLEFEGTQIVFVSVTYILWGNTY y257c IMGWIVNATRSRWGKFKPFWILIGTLANSVILFLFSAHLEFEGTQIVFVSVTYILWGNTY</p> <p>c-less TIMDIPFWSLVPTIILDKREREQLVYPRFFASLAGFVTAGVTLFPVNVYGGGDRGFGFQ y257c TIMDIPFWSLVPTIILDKREREQLVYPRFFASLAGFVTAGVTLFPVNVYGGGDRGFGFQ</p> <p>c-less MFTLVLIAFFIVSTIILNVEHFSSDQPSAEGSHLTKAIVALIYKNDQSVLLGMA y257c MFTLVLIAFFIVSTIILNVEHFSSDQPSAEGSHLTKAIVALIYKNDQSVLLGMA</p> <p>c-less LAYNVAENIITGFAIYFVSIVIGDADLFPYLSYAGAANLTVLFFPRLVKLSRRILWA y257c LAYNVAENIITGFAIYFVSIVIGDADLFPYLSYAGAANLTVLFFPRLVKLSRRILWA</p> | <p>c-less ALIYKNDQSVLLGMAIYVNASNIITGFAIYFVSIVIGDADLFPYLSYAGAANLTVL y257c ALIYKNDQSVLLGMAIYVNASNIITGFAIYFVSIVIGDADLFPYLSYAGAANLTVL</p> <p>c-less FFPRLVKLSRRILWAGASILPVLSSGVLLMALMSYHNVLIVIAGILLNVGTALFWLV y257c FFPRLVKLSRRILWAGASILPVLSSGVLLMALMSYHNVLIVIAGILLNVGTALFWLV</p> <p>c-less QVIMVADIVDYGKLVHRSSEIAYSQVTMVKGGSAFAAFFIAVVLGMIGYVFNVEQST y257c QVIMVADIVDYGKLVHRSSEIAYSQVTMVKGGSAFAAFFIAVVLGMIGYVFNVEQST</p> <p>c-less QALLGMQFIMIALPTLFFMVTLLIYFRFRYRNGDTRRIQIHLDRKRVPEPVPVHADIP y257c QALLGMQFIMIALPTLFFMVTLLIYFRFRYRNGDTRRIQIHLDRKRVPEPVPVHADIP</p> <p>c-less VGVASDVKAHHHHHH y257c VGVASDVKAHHHHHH</p> |
|--|--|

F258C

| | |
|---|---|
| <p>c-less MSISMTTKLSYGFAGKDFAIIVMYMLYYTDDVGLSVGLVSTLFLVARINDAINDP 4-f258 MSISMTTKLSYGFAGKDFAIIVMYMLYYTDDVGLSVGLVSTLFLVARINDAINDP</p> <p>c-less IMGWIVNATRSRWGKFKPFWILIGTLANSVILFLFSAHLEFEGTQIVFVSVTYILWGNTY 4-f258 IMGWIVNATRSRWGKFKPFWILIGTLANSVILFLFSAHLEFEGTQIVFVSVTYILWGNTY</p> <p>c-less TIMDIPFWSLVPTIILDKREREQLVYPRFFASLAGFVTAGVTLFPVNVYGGGDRGFGFQ 4-f258 TIMDIPFWSLVPTIILDKREREQLVYPRFFASLAGFVTAGVTLFPVNVYGGGDRGFGFQ</p> <p>c-less MFTLVLIAFFIVSTIILNVEHFSSDQPSAEGSHLTKAIVALIYKNDQSVLLGMA 4-f258 MFTLVLIAFFIVSTIILNVEHFSSDQPSAEGSHLTKAIVALIYKNDQSVLLGMA</p> <p>c-less LAYNVAENIITGFAIYFVSIVIGDADLFPYLSYAGAANLTVLFFPRLVKLSRRILWA 4-f258 LAYNVAENIITGFAIYFVSIVIGDADLFPYLSYAGAANLTVLFFPRLVKLSRRILWA</p> | <p>c-less VHEVFSNDQPSAEGSHLTKAIVALIYKNDQSVLLGMAIYVNASNIITGFAIYFVS 4-f258 LHEVFSNDQPSAEGSHLTKAIVALIYKNDQSVLLGMAIYVNASNIITGFAIYFVS</p> <p>c-less VIGDADLFPYLSYAGAANLTVLFFPRLVKLSRRILWAGASILPVLSSGVLLMALMS 4-f258 VIGDADLFPYLSYAGAANLTVLFFPRLVKLSRRILWAGASILPVLSSGVLLMALMS</p> <p>c-less YHNVVLIIVAGILLNVGTALFWLVQIMVADIVDYGKLVHRSSEIAYSQVTMVKGG 4-f258 YHNVVLIIVAGILLNVGTALFWLVQIMVADIVDYGKLVHRSSEIAYSQVTMVKGG</p> <p>c-less AFAAFFIAVVLGMIGYVFNVEQSTQALLGMQFIMIALPTLFFMVTLLIYFRFRYRNGD 4-f258 AFAAFFIAVVLGMIGYVFNVEQSTQALLGMQFIMIALPTLFFMVTLLIYFRFRYRNGD</p> <p>c-less RRIQIHLDRKRVPEPVPVHADIPVGVASDVKAHHHHHH 4-f258 RRIQIHLDRKRVPEPVPVHADIPVGVASDVKAHHHHHH</p> |
|---|---|

S259A

```

Cless 10 20 30 40 50 60 210 220 230 240 250 260
MSISMTKLSYGFAGKDFAIgIVMYLMYYTDDVGLSVGLVGTFLVARIWDAINDP Cless NQPSAEGSHLTKAIVALIYKNDQLSVLLGMALAYNVASNIITGFAYIYFVSIVIGDADLF
S259A- MSISMTKLSYGFAGKDFAIgIVMYLMYYTDDVGLSVGLVGTFLVARIWDAINDP S259A- HQPSAEGSHLTKAIVALIYKNDQLSVLLGMALAYNVASNIITGFAYIYFVSIVIGDADLF
30 40 50 60 70 80 10 20 30 40 50 60
Cless 70 80 90 100 110 120 Cless 270 280 290 300 310 320
IMGWIVNATRSRWGKFKFWILIGTLANSVILFLLSAHLFEGTQIVFVSVTYILWGMTY Cless PYYLSYAGAANLVTLVFFPRLVKLSRRILMAGASILPVLSSGVLLMALMSYHNVVLLIV
S259A- IMGWIVNATRSRWGKFKFWILIGTLANSVILFLLSAHLFEGTQIVFVSVTYILWGMTY S259A- PYYLSYAGAANLVTLVFFPRLVKLSRRILMAGASILPVLSSGVLLMALMSYHNVVLLIV
90 100 110 120 130 140 70 80 90 100 110 120
Cless 130 140 150 160 170 180 Cless 330 340 350 360 370 380
TIMDIPFWSLVPTITLTKREREQLVYPPFFASLAGFVITAGVTLFFVNYVGGGDRGFGFQ Cless IAGILLNVGTALFWLQVIMVADIVDYGKYLHVRSSEIAYSQVTMVVKGGSFAFAFFIA
S259A- TIMDIPFWSLVPTITLTKREREQLVYPPFFASLAGFVITAGVTLFFVNYVGGGDRGFGFQ S259A- IAGILLNVGTALFWLQVIMVADIVDYGKYLHVRSSEIAYSQVTMVVKGGSFAFAFFIA
150 160 170 180 190 200 130 140 150 160 170 180
Cless 190 200 210 220 230 240 Cless 390 400 410 420 430 440
MFTLVLIAFFIVSTIITLNRVHEVFSSDNQPSAEGSHLTKAIVALIYKNDQLSVLLGMA Cless VVLGMIGYVFNVEQSTQALLGMQFIMIALPTLFFMVTLLIYFRYRLNGDTLRRIQIHL
S259A- MFTLVLIAFFIVSTIITLNRVHEVFSSDNQPSAEGSHLTKAIVALIYKNDQLSVLLGMA S259A- VVLGMIGYVFNVEQSTQALLGMQFIMIALPTLFFMVTLLIYFRYRLNGDTLRRIQIHL
210 220 230 240 250 260 190 200 210 220 230 240
Cless 250 260 270 280 290 300 Cless 450 460 470
LAYNVASNIITGFAYIYFVSIVIGDADLFYLYLSYAGAANLVTLVFFPRLVKLSRRILWA Cless DKYRKVPPEPVHADIPVGVASDVKAHHHHHH
S259A- LAYNVASNIITGFAYIYFVSIVIGDADLFYLYLSYAGAANLVTLVFFPRLVKLSRRILWA S259A- DKYRKVPPEPVHADIPVGVASDVKAHHHHHH
270 280 290 300 310 320 250 260 270

```

S259C

```

cless 10 20 30 40 50 60 230 240 250 260 270 280
MSISMTKLSYGFAGKDFAIgIVMYLMYYTDDVGLSVGLVGTFLVARIWDAINDP cless IYKNDQLSVLLGMALAYNVASNIITGFAYIYFVSIVIGDADLFYLYLSYAGAANLVTLVFF
S259C- MSISMTKLSYGFAGKDFAIgIVMYLMYYTDDVGLSVGLVGTFLVARIWDAINDP S259C- IYKNDQLSVLLGMALAYNVASNIITGFAYIYFVSIVIGDADLFYLYLSYAGAANLVTLVFF
30 40 50 60 70 80 20 30 40 50 60 70
cless 70 80 90 100 110 120 cless 290 300 310 320 330 340
IMGWIVNATRSRWGKFKFWILIGTLANSVILFLLSAHLFEGTQIVFVSVTYILWGMTY cless PRLVKLSRRILMAGASILPVLSSGVLLMALMSYHNVVLLIVIAIGILLNVGTALFWLQV
S259C- IMGWIVNATRSRWGKFKFWILIGTLANSVILFLLSAHLFEGTQIVFVSVTYILWGMTY S259C- PRLVKLSRRILMAGASILPVLSSGVLLMALMSYHNVVLLIVIAIGILLNVGTALFWLQV
90 100 110 120 130 140 80 90 100 110 120 130
cless 130 140 150 160 170 180 cless 350 360 370 380 390 400
TIMDIPFWSLVPTITLTKREREQLVYPPFFASLAGFVITAGVTLFFVNYVGGGDRGFGFQ cless IMVADIVDYGKYLHVRSSEIAYSQVTMVVKGGSFAFAFFIAVVLGMIGYVFNVEQSTQA
S259C- TIMDIPFWSLVPTITLTKREREQLVYPPFFASLAGFVITAGVTLFFVNYVGGGDRGFGFQ S259C- IMVADIVDYGKYLHVRSSEIAYSQVTMVVKGGSFAFAFFIAVVLGMIGYVFNVEQSTQA
150 160 170 180 190 200 140 150 160 170 180 190
cless 190 200 210 220 230 240 cless 410 420 430 440 450 460
MFTLVLIAFFIVSTIITLNRVHEVFSSDNQPSAEGSHLTKAIVALIYKNDQLSVLLGMA cless LLGMQFIMIALPTLFFMVTLLIYFRYRLNGDTLRRIQIHLDKYRKVPPEPVHADIPV
S259C- MFTLVLIAFFIVSTIITLNRVHEVFSSDNQPSAEGSHLTKAIVALIYKNDQLSVLLGMA S259C- LLGMQFIMIALPTLFFMVTLLIYFRYRLNGDTLRRIQIHLDKYRKVPPEPVHADIPV
210 220 230 240 250 260 200 210 220 230 240 250
cless 250 260 270 280 290 cless 470
LAYNVASNIITGFAYIYFVSIVIGDADLFYLYLSYAGAANLVTLVFFPRLVKLSRRIL cless AVSIVKAHHHHHH
S259C- LAYNVASNIITGFAYIYFVSIVIGDADLFYLYLSYAGAANLVTLVFFPRLVKLSRRIL S259C- AVSIVKAHHHHHH
270 280 290 300 310 320 260

```

Y260C

```

c-less 10 20 30 40 50 60 240 250 260 270 280 290
MSISMTKLSYGFAGKDFAIgIVMYLMYYTDDVGLSVGLVGTFLVARIWDAINDP c-less SVLLGMALAYNVASNIITGFAYIYFVSIVIGDADLFYLYLSYAGAANLVTLVFFPRLVKSL
Y260c MSISMTKLSYGFAGKDFAIgIVMYLMYYTDDVGLSVGLVGTFLVARIWDAINDP Y260c SVLLGMALAYNVASNIITGFAYIYFVSIVIGDADLFYLYLSYAGAANLVTLVFFPRLVKSL
30 40 50 60 70 80 30 40 50 60 70 80
c-less 70 80 90 100 110 120 c-less 300 310 320 330 340 350
IMGWIVNATRSRWGKFKFWILIGTLANSVILFLLSAHLFEGTQIVFVSVTYILWGMTY c-less SRRILMAGASILPVLSSGVLLMALMSYHNVVLLIVIAIGILLNVGTALFWLQVIMVADIV
Y260c IMGWIVNATRSRWGKFKFWILIGTLANSVILFLLSAHLFEGTQIVFVSVTYILWGMTY Y260c SRRILMAGASILPVLSSGVLLMALMSYHNVVLLIVIAIGILLNVGTALFWLQVIMVADIV
90 100 110 120 130 140 90 100 110 120 130 140
c-less 130 140 150 160 170 180 c-less 360 370 380 390 400 410
TIMDIPFWSLVPTITLTKREREQLVYPPFFASLAGFVITAGVTLFFVNYVGGGDRGFGFQ c-less DYGEYKLVHRSSEIAYSQVTMVVKGGSFAFAFFIAVVLGMIGYVFNVEQSTQALLGMQFI
Y260c TIMDIPFWSLVPTITLTKREREQLVYPPFFASLAGFVITAGVTLFFVNYVGGGDRGFGFQ Y260c DYGEYKLVHRSSEIAYSQVTMVVKGGSFAFAFFIAVVLGMIGYVFNVEQSTQALLGMQFI
150 160 170 180 190 200 150 160 170 180 190 200
c-less 190 200 210 220 230 240 c-less 420 430 440 450 460 470
MFTLVLIAFFIVSTIITLNRVHEVFSSDNQPSAEGSHLTKAIVALIYKNDQLSVLLGMA c-less MIALPTLFFMVTLLIYFRYRLNGDTLRRIQIHLDKYRKVPPEPVHADIPVGVASDVKA
Y260c MFTLVLIAFFIVSTIITLNRVHEVFSSDNQPSAEGSHLTKAIVALIYKNDQLSVLLGMA Y260c MIALPTLFFMVTLLIYFRYRLNGDTLRRIQIHLDKYRKVPPEPVHADIPVGVASDVKA
210 220 230 240 250 260 210 220 230 240 250 260
c-less 250 260 270 280 290 c-less HHHHHH
LAYNVASNIITGFAYIYFVSIVIGDADLFYLYLSYAGAANLVTLVFFPRLVKLSRRIL c-less HHHHHH
Y260c LAYNVASNIITGFAYIYFVSIVIGDADLFYLYLSYAGAANLVTLVFFPRLVKLSRRIF Y260c HHHHHH
270 280 290 300 310 320 270

```

V261C

```

10      20      30      40      50      60      210      220      230      240      250      260
Cless  MSISMTKLSYGFAGKDFAIQIVVMYLMYYTDDVGLSVGLVGTFLVARIWDAINDP Cless  EVFSSDNQPSAEGSHLTKAIVALIYKNDQLSVLLGMALAYNVASNIITGFAYIYFSYVI
V261C- MSISMTKLSYGFAGKDFAIQIVVMYLMYYTDDVGLSVGLVGTFLVARIWDAINDP V261C- EVFSSDNQPSAEGSHLTKAIVALIYKNDQLSVLLGMALAYNVASNIITGFAYIYFSYVI
30      40      50      60      70      80      10      20      30      40      50      60
Cless  70      80      90      100     110     120 Cless  270     280     290     300     310     320
V261C- 70      80      90      100     110     120 V261C- 270     280     290     300     310     320
90     100     110     120     130     140 Cless  330     340     350     360     370     380
Cless  TIMDIPFWSLVPTITLDREREQLVYPRFFASLAGFVTAGVTLFPVNVYGGGDRGFGFQ Cless  NVVLIIVAGILLNVGTALFWVLQVIMVADIVDYGEYKLVHVRSESIAYSVQTMVVKGGSF
V261C- TIMDIPFWSLVPTITLDREREQLVYPRFFASLAGFVTAGVTLFPVNVYGGGDRGFGFQ V261C- NVVLIIVAGILLNVGTALFWVLQVIMVADIVDYGEYKLVHVRSESIAYSVQTMVVKGGSF
150    160    170    180    190    200 Cless  390     400     410     420     430     440
Cless  MFTLVLIAPFIVSTIITLRNVHEVSSDNQPSAEGSHLTKAIVALIYKNDQLSVLLGMA Cless  AAFPIAVLGMIGYVFNVEQSTQALLGMQFIMIALPTLFFMVTLLIYFRYRLMGDTLRR
V261C- MFTLVLIAPFIVSTIITLRNVHEVSSDNQPSAEGSHLTKAIVALIYKNDQLSVLLGMA V261C- AAFPIAVLGMIGYVFNVEQSTQALLGMQFIMIALPTLFFMVTLLIYFRYRLMGDTLRR
210    220    230    240    250    260 Cless  450     460     470
Cless  LAYNVASNIITGFAYIYFSYVIGDADLFPYVLSYAGAANLVTLVFFPRLVKLSRRLIWA Cless  IQIHLLDKRYKVPPEFVHADIPVGAUSDVKAHHHHHH
V261C- LAYNVASNIITGFAYIYFSYVIGDADLFPYVLSYAGAANLVTLVFFPRLVKLSRRLIWA V261C- IQIHLLDKRYKVPPEFVHADIPVGAUSDVKAHHHHHH
270    280    290    300    310    320 Cless  250     260     270

```

G263C

```

10      20      30      40      50      60      200      210      220      230      240      250
cless  MSISMTKLSYGFAGKDFAIQIVVMYLMYYTDDVGLSVGLVGTFLVARIWDAINDP cless  STIITLRNVHEVSSDNQPSAEGSHLTKAIVALIYKNDQLSVLLGMALAYNVASNIITG
1-G263 MSISMTKLSYGFAGKDFAIQIVVMYLMYYTDDVGLSVGLVGTFLVARIWDAINDP 1-G263 STIITLRNVHEVSSDNQPSAEGSHLTKAIVALIYKNDQLSVLLGMALAYNVASNIITG
30      40      50      60      70      80      10      20      30      40      50      60
cless  70      80      90      100     110     120 cless  260     270     280     290     300     310
1-G263 70      80      90      100     110     120 1-G263 260     270     280     290     300     310
90     100     110     120     130     140 cless  320     330     340     350     360     370
cless  TIMDIPFWSLVPTITLDREREQLVYPRFFASLAGFVTAGVTLFPVNVYGGGDRGFGFQ cless  LLLMALMSYHNVVLIIVAGILLNVGTALFWVLQVIMVADIVDYGEYKLVHVRSESIAYSVQ
1-G263 TIMDIPFWSLVPTITLDREREQLVYPRFFASLAGFVTAGVTLFPVNVYGGGDRGFGFQ 1-G263 LLLMALMSYHNVVLIIVAGILLNVGTALFWVLQVIMVADIVDYGEYKLVHVRSESIAYSVQ
150    160    170    180    190    200 cless  380     390     400     410     420     430
cless  MFTLVLIAPFIVSTIITLRNVHEVSSDNQPSAEGSHLTKAIVALIYKNDQLSVLLGMA cless  TMVVKGGSFAFAFFIAVVLGMIGYVFNVEQSTQALLGMQFIMIALPTLFFMVTLLIYFRF
1-G263 MFTLVLIAPFIVSTIITLRNVHEVSSDNQPSAEGSHLTKAIVALIYKNDQLSVLLGMA 1-G263 TMVVKGGSFAFAFFIAVVLGMIGYVFNVEQSTQALLGMQFIMIALPTLFFMVTLLIYFRF
210    220    230    240    250    260 cless  440     450     460     470
cless  LAYNVASNIITGFAYIYFSYVIGDADLFPYVLSYAGAANLVTLVFFPRLVKLSRRLIWA cless  YRLNGDTLRRIQIHLLDKRYKVPPEFVHADIPVGAUSDVKAHHHHHH
1-G263 LAYNVASNIITGFAYIYFSYVIGDADLFPYVLSYAGAANLVTLVFFPRLVKLSRRLIWA 1-G263 YRLNGDTLRRIQIHLLDKRYKVPPEFVHADIPVGAUSDVKAHHHHHH
270    280    290    300    310    320 cless  250     260     270     280

```

A265C

```

10      20      30      40      50      60      200      210      220      230      240      250
Cless  MSISMTKLSYGFAGKDFAIQIVVMYLMYYTDDVGLSVGLVGTFLVARIWDAINDP Cless  TITTLRNVHEVSSDNQPSAEGSHLTKAIVALIYKNDQLSVLLGMALAYNVASNIITGF
A265C- MSISMTKLSYGFAGKDFAIQIVVMYLMYYTDDVGLSVGLVGTFLVARIWDAINDP A265C- TITTLRNVHEVSSDNQPSAEGSHLTKAIVALIYKNDQLSVLLGMALAYNVASNIITGF
30      40      50      60      70      80      10      20      30      40      50      60
Cless  70      80      90      100     110     120 Cless  260     270     280     290     300     310
A265C- 70      80      90      100     110     120 A265C- 260     270     280     290     300     310
90     100     110     120     130     140 Cless  320     330     340     350     360     370
Cless  TIMDIPFWSLVPTITLDREREQLVYPRFFASLAGFVTAGVTLFPVNVYGGGDRGFGFQ Cless  LLLMALMSYHNVVLIIVAGILLNVGTALFWVLQVIMVADIVDYGEYKLVHVRSESIAYSVQ
A265C- TIMDIPFWSLVPTITLDREREQLVYPRFFASLAGFVTAGVTLFPVNVYGGGDRGFGFQ A265C- LLLMALMSYHNVVLIIVAGILLNVGTALFWVLQVIMVADIVDYGEYKLVHVRSESIAYSVQ
150    160    170    180    190    200 Cless  380     390     400     410     420     430
Cless  MFTLVLIAPFIVSTIITLRNVHEVSSDNQPSAEGSHLTKAIVALIYKNDQLSVLLGMA Cless  MVVKGGSFAFAFFIAVVLGMIGYVFNVEQSTQALLGMQFIMIALPTLFFMVTLLIYFRY
A265C- MFTLVLIAPFIVSTIITLRNVHEVSSDNQPSAEGSHLTKAIVALIYKNDQLSVLLGMA A265C- MVVKGGSFAFAFFIAVVLGMIGYVFNVEQSTQALLGMQFIMIALPTLFFMVTLLIYFRY
210    220    230    240    250    260 Cless  440     450     460     470
Cless  LAYNVASNIITGFAYIYFSYVIGDADLFPYVLSYAGAANLVTLVFFPRLVKLSRRLIWA Cless  RLNGDTLRRIQIHLLDKRYKVPPEFVHADIPVGAUSDVKAHHHHHH
A265C- LAYNVASNIITGFAYIYFSYVIGDADLFPYVLSYAGAANLVTLVFFPRLVKLSRRLIWA A265C- RLNGDTLRRIQIHLLDKRYKVPPEFVHADIPVGAUSDVKAHHHHHH
270    280    290    300    310    320 Cless  250     260     270     280

```

D266C

| | |
|--|--|
| <p>Cless MSISMTKLSYGFAGKDFAIQIVMYLMYYTDDVGLSVGLVGTFLVARIWDAINDP D266C- MSISMTKLSYGFAGKDFAIQIVMYLMYYTDDVGLSVGLVGTFLVARIWDAINDP</p> <p>Cless IMGWIVNATRSRWGKFKPWILIGTLANSVILFLLSAHLFEGTTQIVFVSVTYILWGMTY D266C- IMGWIVNATRSRWGKFKPWILIGTLANSVILFLLSAHLFEGTTQIVFVSVTYILWGMTY</p> <p>Cless TIMDIPFWSLVPTITLTKREREQLVYPRFFASLAGFVTAGVTLFFVNYVGGGDRGFGFQ D266C- TIMDIPFWSLVPTITLTKREREQLVYPRFFASLAGFVTAGVTLFFVNYVGGGDRGFGFQ</p> <p>Cless MFTLVLIAPFVSTIITLNRNVEVFSSDNQPSAEGSHLTKAIVALIYKNDQLSVLLGMA D266C- MFTLVLIAPFVSTIITLNRNVEVFSSDNQPSAEGSHLTKAIVALIYKNDQLSVLLGMA</p> <p>Cless LAYNVAENIITGFAYIYFSYVIGDADLFYYLSYAGAANLVTLVFFPRLVKLSRRLIWA D266C- LAYNVAENIITGFAYIYFSYVIGDADLFYYLSYAGAANLVTLVFFPRLVKLSRRLIWA</p> | <p>Cless IAPFVSTIITLNRNVEVFSSDNQPSAEGSHLTKAIVALIYKNDQLSVLLGMAIYNVA D266C- IAPFVSTIITLNRNVEVFSSDNQPSAEGSHLTKAIVALIYKNDQLSVLLGMAIYNVA</p> <p>Cless SNIITGFAYIYFSYVIGDADLFYYLSYAGAANLVTLVFFPRLVKLSRRLIWA D266C- SNIITGFAYIYFSYVIGDADLFYYLSYAGAANLVTLVFFPRLVKLSRRLIWA</p> <p>Cless VLSGVLMLMMSYHNVVLIAGILLNVGTALFWLQVIMVADIVDYGEXKLVHRSSES D266C- VLSGVLMLMMSYHNVVLIAGILLNVGTALFWLQVIMVADIVDYGEXKLVHRSSES</p> <p>Cless IAYSQTMVVRKGSAPFAFFIAVLMIGYVNVVEQSTQALLGMQFIMIALPTLFFMVTLL D266C- IAYSQTMVVRKGSAPFAFFIAVLMIGYVNVVEQSTQALLGMQFIMIALPTLFFMVTLL</p> <p>Cless ILYFRYRLNGDTLRRIQIHLKDKYRKPVEPVHADIPVGAVSQVKAHHHHHH D266C- ILYFRYRLNGDTLRRIQIHLKDKYRKPVEPVHADIPVGAVSQVKAHHHHHH</p> |
|--|--|

L267C

| | |
|--|--|
| <p>cless MSISMTKLSYGFAGKDFAIQIVMYLMYYTDDVGLSVGLVGTFLVARIWDAINDP L267C- MSISMTKLSYGFAGKDFAIQIVMYLMYYTDDVGLSVGLVGTFLVARIWDAINDP</p> <p>cless IMGWIVNATRSRWGKFKPWILIGTLANSVILFLLSAHLFEGTTQIVFVSVTYILWGMTY L267C- IMGWIVNATRSRWGKFKPWILIGTLANSVILFLLSAHLFEGTTQIVFVSVTYILWGMTY</p> <p>cless TIMDIPFWSLVPTITLTKREREQLVYPRFFASLAGFVTAGVTLFFVNYVGGGDRGFGFQ L267C- TIMDIPFWSLVPTITLTKREREQLVYPRFFASLAGFVTAGVTLFFVNYVGGGDRGFGFQ</p> <p>cless MFTLVLIAPFVSTIITLNRNVEVFSSDNQPSAEGSHLTKAIVALIYKNDQLSVLLGMA L267C- MFTLVLIAPFVSTIITLNRNVEVFSSDNQPSAEGSHLTKAIVALIYKNDQLSVLLGMA</p> <p>cless LAYNVAENIITGFAYIYFSYVIGDADLFYYLSYAGAANLVTLVFFPRLVKLSRRLIWA L267C- LAYNVAENIITGFAYIYFSYVIGDADLFYYLSYAGAANLVTLVFFPRLVKLSRRLIWA</p> | <p>cless FFIIVSTIITLNRNVEVFSSDNQPSAEGSHLTKAIVALIYKNDQLSVLLGMAIYNVASN L267C- FFIIVSTIITLNRNVEVFSSDNQPSAEGSHLTKAIVALIYKNDQLSVLLGMAIYNVASN</p> <p>cless IITGFAYIYFSYVIGDADLFYYLSYAGAANLVTLVFFPRLVKLSRRLIWA L267C- IITGFAYIYFSYVIGDADLFYYLSYAGAANLVTLVFFPRLVKLSRRLIWA</p> <p>cless SSGVLLMMSYHNVVLIAGILLNVGTALFWLQVIMVADIVDYGEXKLVHRSSESIA L267C- SSGVLLMMSYHNVVLIAGILLNVGTALFWLQVIMVADIVDYGEXKLVHRSSESIA</p> <p>cless YSVQTMVVRKGSAPFAFFIAVLMIGYVNVVEQSTQALLGMQFIMIALPTLFFMVTLL L267C- YSVQTMVVRKGSAPFAFFIAVLMIGYVNVVEQSTQALLGMQFIMIALPTLFFMVTLL</p> <p>cless YFRYRLNGDTLRRIQIHLKDKYRKPVEPVHADIPVGAVSQVKAHHHHHH L267C- YFRYRLNGDTLRRIQIHLKDKYRKPVEPVHADIPVGAVSQVKAHHHHHH</p> |
|--|--|

F268C

| | |
|--|--|
| <p>Cless MSISMTKLSYGFAGKDFAIQIVMYLMYYTDDVGLSVGLVGTFLVARIWDAINDP F268C- MSISMTKLSYGFAGKDFAIQIVMYLMYYTDDVGLSVGLVGTFLVARIWDAINDP</p> <p>Cless IMGWIVNATRSRWGKFKPWILIGTLANSVILFLLSAHLFEGTTQIVFVSVTYILWGMTY F268C- IMGWIVNATRSRWGKFKPWILIGTLANSVILFLLSAHLFEGTTQIVFVSVTYILWGMTY</p> <p>Cless TIMDIPFWSLVPTITLTKREREQLVYPRFFASLAGFVTAGVTLFFVNYVGGGDRGFGFQ F268C- TIMDIPFWSLVPTITLTKREREQLVYPRFFASLAGFVTAGVTLFFVNYVGGGDRGFGFQ</p> <p>Cless MFTLVLIAPFVSTIITLNRNVEVFSSDNQPSAEGSHLTKAIVALIYKNDQLSVLLGMA F268C- MFTLVLIAPFVSTIITLNRNVEVFSSDNQPSAEGSHLTKAIVALIYKNDQLSVLLGMA</p> <p>Cless LAYNVAENIITGFAYIYFSYVIGDADLFYYLSYAGAANLVTLVFFPRLVKLSRRLIWA F268C- LAYNVAENIITGFAYIYFSYVIGDADLFYYLSYAGAANLVTLVFFPRLVKLSRRLIWA</p> | <p>Cless QPSAEGSHLTKAIVALIYKNDQLSVLLGMAIYNVASNIIITGFAYIYFSYVIGDADLF F268C- QPSAEGSHLTKAIVALIYKNDQLSVLLGMAIYNVASNIIITGFAYIYFSYVIGDADLF</p> <p>Cless YLSYAGAANLVTLVFFPRLVKLSRRLIWA F268C- YLSYAGAANLVTLVFFPRLVKLSRRLIWA</p> <p>Cless AGILLNVGTALFWLQVIMVADIVDYGEXKLVHRSSESIAYSVQTMVVRKGSAPFAFFIAV F268C- AGILLNVGTALFWLQVIMVADIVDYGEXKLVHRSSESIAYSVQTMVVRKGSAPFAFFIAV</p> <p>Cless VLMIGYVNVVEQSTQALLGMQFIMIALPTLFFMVTLLIYFRYRLNGDTLRRIQIHLK F268C- VLMIGYVNVVEQSTQALLGMQFIMIALPTLFFMVTLLIYFRYRLNGDTLRRIQIHLK</p> <p>Cless KYRKPVEPVHADIPVGAVSQVKAHHHHHH F268C- KYRKPVEPVHADIPVGAVSQVKAHHHHHH</p> |
|--|--|

Appendix 2 The files used in the MDS

CONFIGURATION FILES

1. Minimization

```

# minimization with NAMD

# Periodic conditions. 100 ps.

coordinates      ionized.pdb
structure        ionized.psf
parameters       par_all36_lipid.prm
parameters       par_all36_prot.prm
parameters       toppar_water_ions.mod.str
paratypecharmm  on
set output       minimized
outputname       $output
dcdfile          ${output}.dcd
xstFile          ${output}.xst
dcdfreq          500
xstFreq          500
binaryoutput     no
binaryrestart     no
outputEnergies   200
restartfreq      1000
rigidbonds all
rigidTolerance 0. 5
exclude          scaled1-4
1-4scaling       1
COMmotion        no
dielectric        1.0
switching        on
switchdist       8
cutoff           10
pairlistdist     12
firsttimestep    0
stepspercycle    20
timestep         1.0
nonbondedFreq    1
fullElectFrequency 2
set temperature   298
temperature       $temperature
cellBasisVector1 X 0 0
cellBasisVector2 0 Y 0
# according to cell dimensions.

```

```

cellBasisVector3    0 0 Z
cellOrigin          a  b  c
wrapWater           on
wrapAll             on
wrapNearest        off
PME                 yes
PMEGridSpacing     1.0
minimize            100000

```

2. Equilibration

```
# Equilibration in Windows with NAMD after minimization all free in Windows
```

```
# Periodic conditions
```

```
# 100 ps. Heating from 0K in 2K increments.
```

```
# input
```

```

set input           minimized
coordinates         ${input}.coor
extendedSystem     ${input}.xsc
structure           ionized.psf
parameters         par_all36_lipid.prm
parameters         par_all36_prot.prm
parameters         toppar_water_ions.mod.str
paratypecharmm    on

```

```
# output
```

```

set output         equilibrated
outputname        $output
dcdfile           ${output}.dcd
xstFile           ${output}.xst
dcdfreq          200
xstFreq          500
binaryoutput     no
binaryrestart    no
outputEnergies   200
restartfreq      1000

```

```
# mobile atom selection:
```

```
fixedAtoms       off
```

```
# Basic dynamics
```

```

exclude          scaled1-4
1-4scaling       1
COMmotion        no
dielectric        1.0

```

```
# Simulation spacepartitioning
```



```

switching                on
switchdist              8
cutoff                  10
pairlistdist            12
# Multiple timeste      pping
firsttimestep           0
stepspercycle           20
timestep                1.0  ;# 1fs/step
rigidBonds              all  ;# needed if 2fs steps
nonbondedFreq           1    ;# nonbonded forces every step
fullElectFrequency      2    ;# PME only every other step
wrapWater               on          ;# wrap water to central cell
wrapAll                 on          ;# wrap other molecules too
wrapNearest             off         ;# use for non-rectangular cells
#PME (for full-system periodic electrostatics)
PME                     yes
# let NAMD determi      ne grid
PMEGridSpacing          1.0
# Scripting
temperature              0        # starting at 0 K
reassignFreq            500
reassignIncr            2
reassignHold            298      # target T: 298 K
numsteps                100000

```

3. Molecular Dynamics (production)

```

# Production in linux with ACEMD (250 ns) after equilibration with NAMD in Win.

# Periodic conditions. Equilibration started at 0 K, 2K incr.

# input
set input                equilibrated
coordinates              ${input}.coor
extendedsystem           ${input}.xsc
velocities               ${input}.vel
structure                ionized.psf
parameters               par_all36_prot_lipids_na_carb_ethers_water_ions.prm
# output
restart                  on
set output               Melbec-250
outputname               $output
dcdfile                  ${output}.dcd
dcdfreq                  25000
restartfreq              1000000

```

```

restartname                ${output}
restartsave                on
energyfreq                10000
# Basic dynamics
exclude                    scaled1-4
1-4scaling                1
dielectric                1.0
# Simulation space partitioning
switching                 on
switchdist                8
cutoff                    10
pairlistdist              12
# Multiple time stepping
timestep                  4.0                ;# 4fs/step
rigidbonds                all                ;# needed for 4fs steps
fullelectfrequency        2                ;# PME only every other step
hydrogenscale             4                ;# needed for 4fs steps
# Constant Temperature Control
langevin                  on                ;# langevin dynamics
langevindamping           2                ;# damping coefficient of 2/ps
langevintemp              298               ;# random noise at this level
berendsenpressure         on
berendsenpressurerelease  101.325
berendsenpressurerelease  400
useconstantratio         on
#PME (for full-system periodic electrostatics)
pme                       on
wrap                      on                ;# wrap all to central cell
pmegridspacing            1.0
# Scripting
run                       62500000        ;# 250 ns (because 4 fs/step)

```

Appendix 3 The changed amino acids*Salmonella typhimurium* to *Escherichia coli*

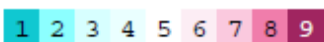
| No. | RESID | Amino acid | Mutant |
|-----|-------|------------|--------|
| 1 | 86 | THR | ALA |
| 2 | 89 | LEU | VAL |
| 3 | 90 | VAL | ILE |
| 4 | 104 | ALA | THR |
| 5 | 106 | VAL | ILE |
| 6 | 147 | PHE | TYR |
| 7 | 162 | ILE | VAL |
| 8 | 168 | SER | ASN |
| 9 | 173 | ALA | GLY |
| 10 | 192 | ALA | VAL |
| 11 | 196 | VAL | ILE |
| 12 | 205 | TYR | PHE |
| 13 | 210 | GLY | GLN |
| 14 | 211 | VAL | PRO |
| 15 | 212 | THR | SER |
| 16 | 214 | GLY | GLU |
| 17 | 215 | ARG | GLY |
| 18 | 216 | PRO | SER |
| 19 | 222 | THR | ALA |
| 20 | 225 | GLY | ALA |
| 21 | 245 | ILE | VAL |
| 22 | 251 | ASN | THR |
| 23 | 259 | THR | SER |
| 24 | 281 | LEU | VAL |
| 25 | 284 | ILE | VAL |
| 26 | 285 | VAL | PHE |
| 27 | 292 | MET | SER |
| 28 | 304 | VAL | ILE |
| 29 | 305 | MET | LEU |
| 30 | 311 | ALA | GLY |
| 31 | 312 | GLY | VAL |
| 32 | 314 | PHE | LEU |
| 33 | 315 | ALA | LEU |
| 34 | 319 | ALA | MET |
| 35 | 320 | ASP | SER |
| 36 | 321 | ILE | TYR |
| 37 | 324 | ALA | VAL |

| | | | |
|----|-----|-----|-----|
| 38 | 325 | ALA | VAL |
| 39 | 329 | ALA | ILE |
| 40 | 333 | PHE | LEU |
| 41 | 336 | ILE | VAL |
| 42 | 352 | THR | ILE |
| 43 | 358 | PHE | TYR |
| 44 | 361 | ASN | HSD |
| 45 | 362 | ILE | VAL |
| 46 | 389 | LEU | VAL |
| 47 | 393 | LEU | MET |
| 48 | 397 | THR | VAL |
| 49 | 401 | ALA | GLU |
| 50 | 404 | ALA | THR |
| 51 | 406 | THR | ALA |
| 52 | 408 | GLN | LEU |
| 53 | 416 | VAL | ALA |
| 54 | 419 | VAL | THR |
| 55 | 424 | MET | VAL |
| 56 | 427 | VAL | ILE |
| 57 | 432 | TYR | PHE |
| 58 | 439 | MET | THR |
| 59 | 442 | LYS | ARG |

Appendix 4 The result from ConSurf



The conservation scale:



Variable Average Conserved

- e - An exposed residue according to the neural-network algorithm.
- b - A buried residue according to the neural-network algorithm.
- f - A predicted functional residue (highly conserved and exposed).
- s - A predicted structural residue (highly conserved and buried).
- x - Insufficient data - the calculation for this site was performed on less than 10% of the sequences.